UNIVERSITY OF OSLO

Master thesis

UNIVERSITY OF OSLO

May / 2023

Quantification of wildfires in North American permafrost domain, based on the MODIS Fire product

Milot Malaj

Geomorphology and Geomatics
60 ECTS

Department of Geosciences
Faculty of Mathematics and Natural Sciences

II

IV

Abstract

A number of studies have shown that the boreal forest in North America has experienced a nearly two-fold increase in burned area over the past 60 years, with a corresponding rise in the number of large fires. Permafrost is the dominant ground cover for most of the boreal forest, and forested areas experience greater fire impacts that may decrease permafrost by up to 9-16% by 2100. Modern fire regimes rely on remotely sensed satellite data, including the active fire product from the Moderate Resolution Imaging Spectrometer (MODIS), which has been gathering data since 2000. This study uses the MODIS Active Fire product to quantify the area that experienced fires in permafrost areas, covering a study area between 50 and 70 degrees in North America divided into four subregions, over a 20-year period from 2001 to 2021. The results show that more than 75% of fires occur in central and western Canada, compared to 20% in Alaska and only 5% in Quebec and the Labrador Peninsula. Furthermore, the results indicate that fires occur in all types of permafrost, regardless of ground type, where Alaska has the highest number of fires occurring on permafrost ground, with 96% of all fires occurring in that region. Fires are highly influenced by climate as it determines the tree line of the boreal forest. Additional spatial distribution analyses support these findings. The study also examines trends in the spatial and temporal distribution of fires and finds that 20 years is a short period for analysis, given the significant variation in fire occurrence between years. Finally, the study concludes that while the active fire product has limitations, it is a valuable tool when used in conjunction with other sources of wildfire information such as the Burned Area product and Fire Radiative Power (FRP), as well as other wildfire databases prior to the year 2000.

Acknowledgments

I would like to express my gratitude toward all involved in my master's thesis. A special thanks to my supervisor Assoc. Prof Sebastian Westermann for his guidance within remote sensing, MODIS Fire products, MATLAB scripts and critical assessment of various drafts.

In addition, I would also like to thank the other geoscience and especially geomatic students for their helpful discussions, collaboration, friendship including the good and the bad jokes during our daily lunch breaks.

Last but not least, I want to thank my partner for the love, support and understanding she has shown to me throughout this process.

Preface

This master's thesis (ECTS 60) is submitted to the Department of Geosciences, University of Oslo (UiO), in the candidacy of the Master of Science in Geosciences (ECTS 120) following the Geomorphology and Geomatics program. The main supervisor of the thesis is Assoc. Prof Sebastian Westermann.

Contents

Table of Figures

1   Introduction

Fires have always been an integral part of the boreal forest, ignited by lightning just as they are today (Rowe & Scotter, 1973). However, boreal forest of North American territories have witnessed almost twice as many burnt areas during last sixty years with frequency and intensity for large sized fire occurrences increasing, particularly in western North America (Hanes et al., 2019; Kasischke & Turetsky, 2006; Veraverbeke et al., 2017). The burning of boreal forests generates significant carbon emissions that accelerate global warming through the combustion of organic soil and biomass (Turetsky et al., 2011). In the context of a warming climate, significant changes in fire regime and frequency have been observed. Fire data analysis indicates that the 1980s-1990s experienced a doubling of annual burned area and more than a doubling of the frequency of larger fire years compared to the 1960s-1970s. Additionally, the proportion of total burned area from human-ignited fires decreased during this period, while the burned area from lightning-ignited fires increased. Furthermore, there was an increase in the proportion of burning during both the early and late growing seasons (Kasischke & Turetsky, 2006). In the Alaskan boreal forest, the burned area during the 2000s was 50% greater than any previous decade since the 1940s. Moreover, recent studies reported that the frequency of fire has increased from 1920-2009 compared to 1860-1919, and there has been an increase in the amount of area burned during the late-growing-season fires over the past two decades (Kasischke et al., 2010).

The devastating forest fires have severely damaged human life and infrastructure, drastically altered forest ecosystems, and altered the environment of the permafrost. For instance, from 1950 to 2005, Alaska burnt an average of 3920 km^2 of forest per year. In 2004, 123 fires (> 0.405 km^2) occurred, and 40 of them burned an area larger than 80 km^2 (Harden et al., 2006).

Permafrost was first defined as "Earth material that remains below 0 °C for at least two years" by Sumgin (1927) (Vincent et al., 2017). Meanwhile the term "permafrost" was first used from Muller (Muller, 1947), which was later modified and adopted by International Permafrost Association (IPA) as "ground that remains at or below 0 °C for at least two consecutive years". The base of the active layer is on the top of permafrost. When the environment allows for frozen ground, such as in the far norths of Canada, Alaska, and Siberia, is where one can find continental permafrost. Plateau or alpine permafrost, on the other hand, is found at high elevations where continental permafrost is absent. The majority of

the world's mountains have permafrost patches, and the Tibetan Plateau has a particularly wide distribution. The Northern Hemisphere's permafrost covers around 15% of its entire land area (Zhang et al., 2000).

Permafrost is categorized according to the percentage of an area's exposed land that is made up of permanently frozen ground. Permafrost is by definition regarded as continuous where it covers more than 90% of the land. Just a few localities in these regions have a microclimate that does not sustain permafrost, and the spatial mean ground temperature is typically below -5 °C in these regions. The proportions of perennially frozen ground in the discontinuous and sporadic permafrost zones are 90-50% and 50-10%, respectively, due to an increase in the amount of unfrozen ground in these zones (Zhang et al., 2000). Meanwhile isolated patches of permafrost occur where less than 10% of the ground supports permafrost.

By 2100, the amount of permafrost in the Canadian subarctic region is predicted to drop from 67% at present to 2%, with an increase in air temperature by 4.5 °C (2.0°C to 5.8°C from the low- and high-warming scenarios) during the 21th century (Zhang et al., 2015). The impacts of fire on permafrost are far greater in forested areas than in tundra, bogs, and fens on average, forest fires reduce the extent of permafrost by up to 9%-16% and speed up permafrost thaw by five years (Zhang et al., 2015). Fires reduce the depth of organic soil, which functions as an insulator of permafrost, leading to permafrost degradation and thaw, exposing large ancient carbon stores at risk of release to the atmosphere (Brown et al., 2015), from which permafrost stores roughly 50% of the estimated belowground organic carbon globally (Tarnocai et al., 2009). The active layer thickness has increased in the recent decades due to global warming (Overland et al., 2014).

In the coldest regions of the world, trees are absent and instead, dwarf shrubs dominate at high latitudes. This transition from forest to shrub-dominated terrain is referred to as the tree line, although it is not always a clearly defined boundary. It is common to observe a mix of immature trees and old dwarf trees scattered above a rough "line" (Grace et al., 2002). Currently, there is substantial proof of regeneration occurring beyond the northern tree line during periods of warm summers (Grace et al., 2002).

Fire seasonality has changed over the last years in Canada. For instance, compared to 1959-2000, interior British Columbia, Alberta, and northern Ontario have longer fire seasons (Albert-Green et al., 2013; Hanes et al., 2019). Gillett et al. (2004) attribute the increase in

2

area burned over the past four decades in Canada to human-induced temperature rises. Recent studies have found that extreme burning conditions in western Canada have increased by 1.5 to 6 times over the last decade as a result of climate change (Kirchmeier-Young et al., 2017), and during extreme fire seasons, anthropogenic climate change is believed to have increased the burned area by a factor of 7 to 11 (Kirchmeier-Young et al., 2017).

Current modern fire regimes rely on remotely sensed satellite images, such as The Moderate Resolution Imaging Spectrometer (MODIS), which is an instrument onboard Terra and Aqua satellites launched in late 1999 and 2002, respectively (Giglio et al., 2016). The instrument relies on 36 sensors that are used to acquire data in a moderate spatial resolution of ~1km. MODIS has an Active Fire and a Burned Area fire product, which are designed to provide information for both climate change and practical applications (Justice et al., 2002b). Since the first data acquired in early 2000, fire products have been used in a broad range of scientific questions concerning the role of biomass burning within the Earth system and other operational applications (D. Chen et al., 2017; Y. Chen et al., 2013; Fusco et al., 2019; Peterson et al., 2014; Vadrevu et al., 2012). These products are widely used to understand the interaction between fire and climate.

The aim of this thesis is to quantify the frequency of wildfires and fire patterns in areas of Northern America with permafrost, using 20 years of data collected by NASA's Terra satellite's MODIS. Furthermore, the study examines the incidence of wildfires across various types of permafrost, including non-permafrost areas and those categorized by percentage according to Shur & Jorgenson (2007) classification system, and evaluates the trends across these ground types. The study also analyses changes in mean latitudinal and seasonality, as well as the seasonality of the 20-year period.

2   Study area

The research was carried out across a latitudinal range of 50 to 70 degrees north in the Northern American regions. The study area was segmented into four subregions, namely, Quebec and Labrador Peninsula (QLP), which extended to 80 degrees west, Central Canada (CC) covering the region between 80 to 115 degrees west and dividing the Great Slave Lake into two, Western Cordillera encompassing the geographic area from 115 degrees to 140 degrees near the Alaska border (141 degrees west), and Alaska (AL) spanning from 140 degrees to 170 degrees west. However, some portions of Alaska, including the northern and southwestern parts (figure 1), were not included in the study (more in section 3.2).
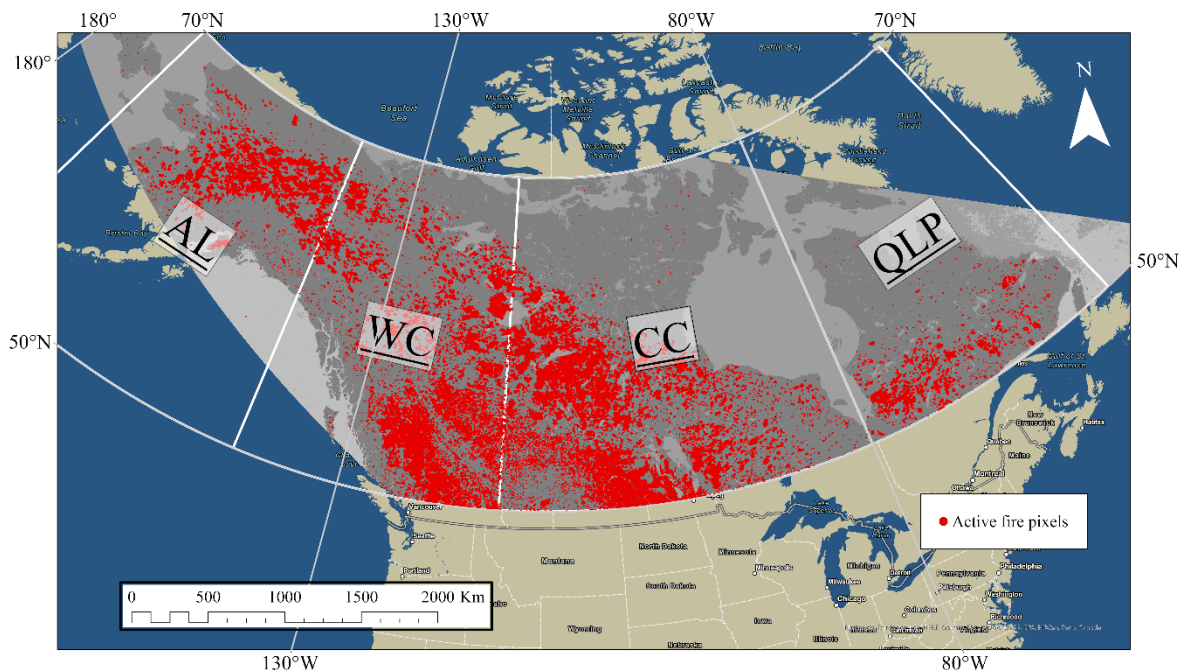
Figure 1. Map of study area with four subregions: Alaska (AL), Western Cordillera (WC), Central Canada (CC) and Quebec and Labrador Peninsula (QLP). Active fire pixels as detected by the MODIS Fire product between 2001 and 2021 shown in red.

The geological chronology of Canada reveals the presence of six distinct regions, each characterized by unique landscape features. These regions, namely the Canadian Shield, Interior Platform, Appalachian Orogen, Innuitian Orogen, Cordillera and Western Canada Sedimentary Basin, and the Eastern Continental Margin, have been identified in previous research (Eyles & Miall, 2018). Additionally, Canada can be divided into seven physiographic regions, with the Canadian Shield being the largest and oldest among them.

The remaining six physiographic regions are comparatively younger and form two concentric rings around the Canadian Shield. The outer ring, which is older, contains the Western Cordillera, Canadian Arctic, and Appalachian Region, while the second, younger ring includes the Interior Plains, Hudson Bay Lowlands, and St. Lawrence Lowlands (Slaymaker et al., 2023).
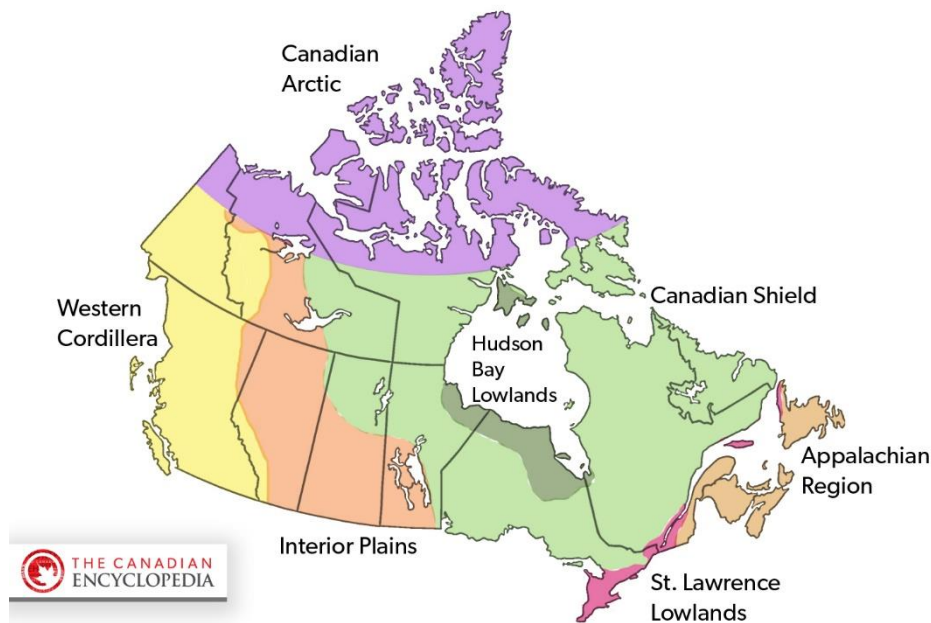
Figure 2. Map of Canada showing seven physiographic regions: the Canadian Shield, the Western Cordillera, the Canadian Arctic, the Appalachian Region, the Interior Plains, the Hudson Bay Lowlands and the St. Lawrence Lowlands (map by The Canadian Encyclopedia).

Canadian Shield covers half of Canada land surface, which contains vast portions of Quebec, Ontario, Manitoba, north-eastern Saskatchewan, Northwest Territories, and Nunavut, including south-eastern Ellesmere Island and much of Baffin Island.

North America accounts for 30% of the world's permafrost, whereas around 40% of Canada and as much as 80% of Alaska are covered in permafrost (Obu et al., 2019; Jorgenson et al., 2008). The ecoclimates of these regions vary from high arctic tundra in the north to boreal forest in the south, reflecting the latitudinal and altitudinal gradients that exist across the continent. Permafrost is generally continuous in the north and in higher elevations, but becomes patchy in more southerly regions where its thickness exceeds only a few meters deep (Smith et al., 2010).

The distribution of permafrost reflects the climate variation in North America. Canada has a wide range of climatic conditions: Canada's Pacific coast is relatively mild year-round, while the Prairie Provinces (in the central western portion of the country) have greater extremes (cold winters and warm summers).
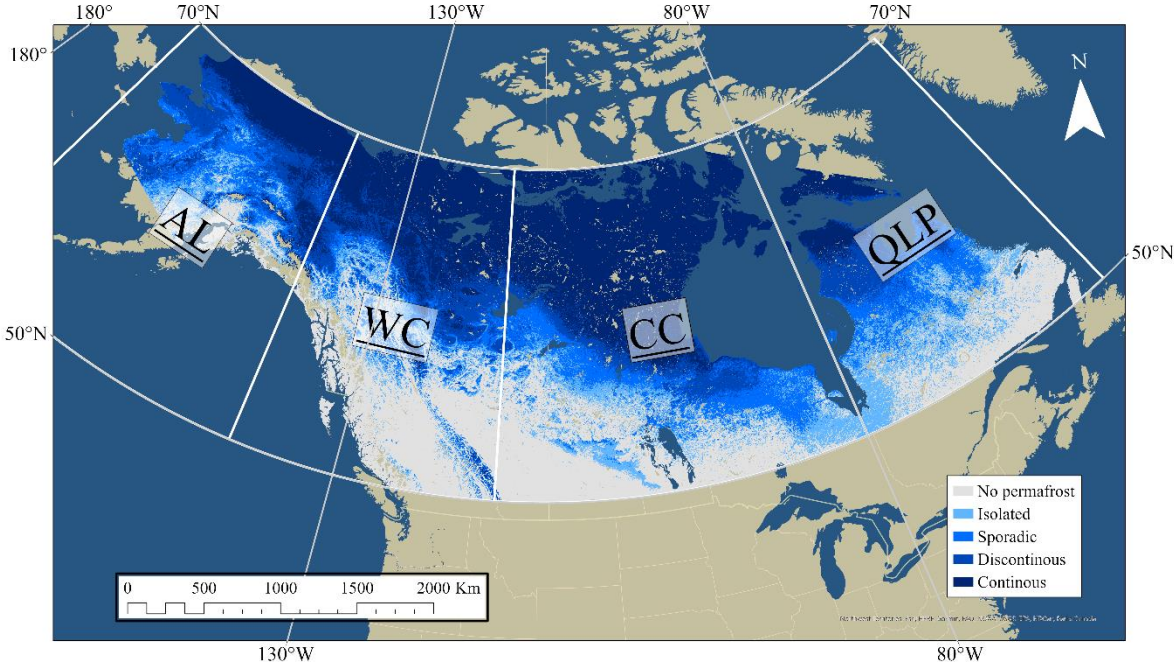
Figure 3. TTOP map over North America that covers our study areas of QLP, CC, WC and AL. The map shows no permafrost, isolated, sporadic, discontinuous and continuous permafrost zones. Glaciers and ice sheets are not included in this map.

2.1 Quebec and Labrador Peninsula

2.1.1 Topography

The Canadian Shield

Located in eastern and south-eastern regions, has been uplifted due to tectonic movements associated with the creation of the Atlantic Ocean (Slaymaker et al., 2023). About half of the Shield is classified as upland, extending from north-western Quebec to Nunavut and the Northwest Territories. The terrain is elevated, ranging from 200-500 masl, and is

characterized by glacial till and sediment deposits. Hudson Bay and the Gulf of St. Lawrence dominate the eastern part of the Shield, with elevations increasing from 300 to 900 masl. Valleys and hills are formed due to differential erosion, with highlands reaching up to 800-1,500 masl in Baffin Island and northern Labrador. The central parts of the Shield show unorganized terrain covered in till and lake basins, while eskers and moraines indicate past glacial activity. The periphery of the Shield is marked by more level terrain that was flooded during ice retreat (Slaymaker et al., 2023).

The boreal forest ecosystem dominates the Canadian Shield in QLP and is home to a variety of coniferous trees, such as white and black spruce, jack, red, white and eastern white pine, balsam fir, tamarack, eastern hemlock, and eastern red cedar. The QLP study zone is identified as the area located from 50° north and above and which contains the northern parts of boreal shield ecozone, taiga shield (Mahdianpari et al., 2020), that does not surpass 58° (Saucier, 2007) because of its maritime climate with cold summers. This zone can be further classified into three subzones: continuous forest, taiga, and forest tundra (Saucier, 2007).

Moving north in taiga shield, the open forest gradually gives way to shrub and tundra. Wetlands constitute approximately 13% of the area, but current trends suggest that they are expanding due to changes in weather and permafrost (Mahdianpari et al., 2020).

Above the boreal forest lies the Arctic tundra ecozone, which is identified by low vegetation and a scarcity of trees. Because the majority of the tundra is built upon permafrost, the vegetation is not capable of developing deep roots, which ultimately stunts its growth (Saucier, 2007).

2.1.2 Climate

Quebec and Labrador Peninsula climates are categorized as cold, no dry season and cold summer, although northmost part of peninsula have dry summers and polar climate (Beck et al., 2018). Although extremes of heat and cold are a more common feature of Quebec's climate compared to Labrador, and sometimes weather can be very severe. Major continental air masses that are coming in from the northwest have an impact on it. The north-eastern regions have cool summers as a result of these air masses colliding with the chilly Labrador Current. Heat waves are caused by humid hot air rising from the Gulf of Mexico in the summer, and a lot of snow falls in the winter. The mean annual precipitation varies from 1000

mm per year in the south and south-east to 375 mm per year in the north-west (Wang et al., 2013). Summer mean temperatures are milder in the Atlantic coast in the east and hotter inland and west of peninsula with mean annual for summer month of 10 degrees. Meanwhile the mean number of dry days and dry spells are most common in north-west and least in the central of peninsula (Sushama et al., 2010).

2.1.3 Permafrost

In QLP, where the climate conditions are such that 50° north and above, permafrost can be found in over 65% of its territory. However, only 10% of the area has continuous permafrost and is situated above the 60° north in the arctic tundra of Quebec, where the depth of permafrost can reach as much as 540m deep (Taylor & Judge, 1979). Similar, The Torngat Mountains in northern Labrador support continuous permafrost, but only at high elevations.
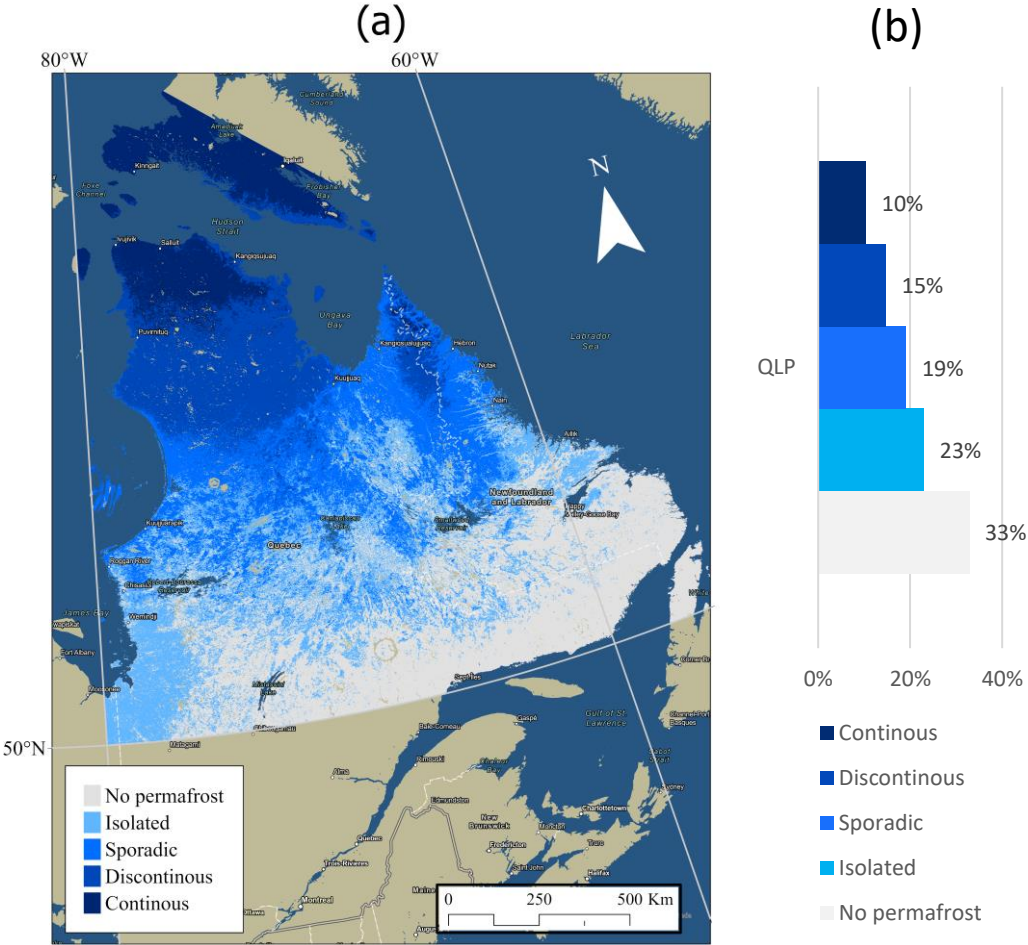
Figure 4. (a) TTOP map showing the different permafrost zones for Quebec and Labrador Peninsula (QLP). (b) Areal coverage of the different permafrost zones for QLP.

8

Climatic and terrain factors affect the distribution of permafrost in the southern part of the discontinuous zone in Quebec and Labrador. Among these factors, climate plays the most significant role in determining the presence of permafrost. Regional snowfall conditions are considered a significant factor (Brown, 1979).

2.2 Central Canada

2.2.1 Topography

The Canadian shield

The Canadian shield located in the Central Canada (CC) study zone is divided into same ecozones as QLP, boreal shield and taiga shield, but because of its continental climate, it stretches much further north that the QLP subregion (Mahdianpari et al., 2020).

Boreal shield is a region that experiences moderate temperatures in both summer and winter and is part of the largest ecozone in Canada. The low-lying areas are predominantly covered by forests and shrubs with minimal human interference (Mahdianpari et al., 2020).

Hudson Bay Lowlands

Close to the coast of Hudson Bay lies Hudson Bay Lowlands, 40% of which lies down on land and the other 60% beneath the waters in Hudson Bay and James Bay (Slaymaker et al., 2023). Apart from the Sutton Ridges in the northeast of the lowland, the bedrock terrain is completely masked by a mantle of glacial and marine sediments associated with the advance and retreat of ice during the last glaciation. The inland edge of the lowland which are about 180 masl, coincides approximately with the highest level of marine inundation that followed the disappearance of glacial ice from Hudson Bay. Nearer the Canadian Shield adjacent to the lowlands are streamlined hills of glacial till, which were formed beneath ice moving southwest from Hudson Bay toward Manitoba, and south and southeast out of James Bay. These have not been totally masked by younger marine deposits and therefore give the surface a corrugated appearance (Slaymaker et al., 2023).

The region has a maritime climate and is characterized by vast wetlands, including peatlands, with marshes being a common feature in the north. This area is recognized as Canada's largest

wetland complex and has a relatively low presence of forests (Abraham & Keddy, 2005; Slaymaker et al., 2023).

The coastal areas of the Hudson Bay Lowlands are characterized by vast plains of muskeg with thick peat accumulations and numerous ponds, due to the thicker marine mantle. Inland, about 50-80 kilometres from the coast, there are parallel gravel beach ridges that formed over the last 5,000-6,000 years as sea levels fell in response to rapid crustal uplift. This zone is marked by dry, forested, low ridges separated by boggy depressions, presenting a distinct contrast to the coastal plains (Slaymaker et al., 2023).

The Interior Plains

The Interior Plains area of Canada, covering 18% of Canada's land surface, lies between the Canadian Shield and the Western Cordillera. The region's topography is characterized by high and low areas resulting from various geological processes (Slaymaker et al., 2023).

High topography is found in the western part of the region, where erosion of non-marine sediments has resulted in isolated uplands. The Manitoba Escarpment and the Missouri Coteau break the relatively uniform slope of the southern portion of the region into three steps. The Manitoba Plain is the lowest and flattest of the three steps, with elevations under 400 masl. The Saskatchewan Plain, which is lower and smoother than the plains to the west, has elevations ranging from 460 to 790 masl, reaching 915 masl in hillier areas. Beyond the Saskatchewan Plain lies the Missouri Coteau, a gradual slope upward to the Rocky Mountains (Slaymaker et al., 2023).

The third step of the region, the Eastern Alberta Plains, extends to the Western Alberta Plains, with elevations reaching 1,100 masl, except for the Cypress Hills which are isolated. The Southern Alberta Uplands, acting as a buffer between the plains and the mountains, have elevations approaching 1,650 masl and exhibit a bolder, more varied relief due to erosion-resistant bedrock. The Northern Alberta Uplands, north of Lesser Slave Lake, are disconnected plateaus rising 250-700 masl from the surrounding Northern Alberta Lowlands (Slaymaker et al., 2023).

Low topography is found in the lowlands of the region, where elevations generally decrease northward along the drainage of the Mackenzie River Valley, with a gentle rise eastward to the Canadian Shield and a sharp rise westward to the Rocky Mountains. Glacial lake deposits

and till plains are widespread in the lowlands, and peat-covered areas are common. The Arctic Coastal Plain and Arctic Lowlands bound the region in the north (Slaymaker et al., 2023).

The vegetation in the southern Interior Plains is mostly characterized by grasslands under semiarid climatic conditions, transitioning to aspen parkland to the north and east under slightly cooler temperatures and higher precipitation. Further northward, the dominant vegetation changes to mixed-wood forest, and finally to treeless tundra and polar deserts at the northern extension of the Interior Plains (Slaymaker et al., 2023).

2.2.2 Climate

The Central Canada from Hudson Bay to the mountain chains of Canadian Rockies have a climate categorized as cold, no dry season and warm summers in the southern part, meanwhile the northern part is similar to QLP, although it stretches much further north (Beck et al., 2018). Precipitation is most in the south-east up to 1000 mm per year, meanwhile least is in the south-west and northern parts with 250 mm per year and as little as 125 mm per year respectively (Wang et al., 2013). Mean number of dry days and dry spells are more common as well, with most in northern and western parts (Sushama et al., 2010).

2.2.3 Permafrost

This extensive study zone displays a varied distribution of permafrost, with the greatest concentration at lower latitudes observed in the eastern region. However, permafrost decreases as one moves towards the west due to the continental warm climate which maintains mean annual temperatures above 0 °C. Nevertheless, the region covers a vast expanse including the Canadian Arctic, which is known for its abundant permafrost.

The Hudson Bay Lowlands in northern Ontario and Manitoba is home to the southernmost continuous expanse of permafrost in North America, according to the TTOP map. In Saskatchewan, permafrost can be found in scattered areas within peatlands, with its prevalence being higher in the northeastern region (R. Brown, 2010). In Manitoba, discontinuous permafrost is present to the north of the isotherm that corresponds to a current mean annual air temperature of about 0°C, which translates to an air freezing index of approximately 2,500 °C-days (Batenipour et al., 2009). Further north, near the Hudson Bay coast, the permafrost transitions to being continuous.
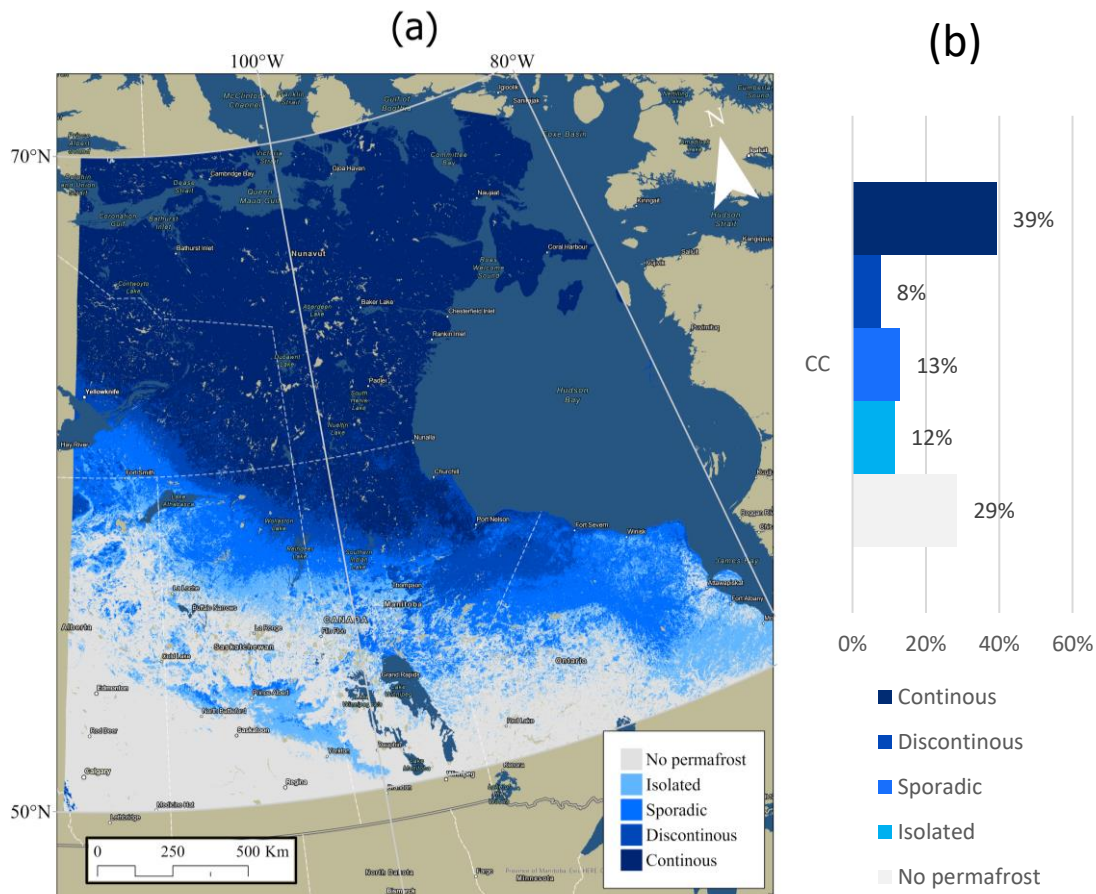
Figure 5. (a) TTOP map showing the different permafrost zones for Central Canada (CC). (b) Areal coverage of the different permafrost zones for CC.

2.3 Western Cordillera

2.3.1 Topography

Besides the Interior Plains, this region includes Western Cordillera which is characterized by diverse topography and land cover. It extends from southern British Columbia to the Yukon and the Beaufort Sea, with some parts also extending into southwestern Alberta and the Northwest Territories.

Western Cordillera

The Western Cordillera includes plateaus, valleys, plains, and rugged mountains, with the Coast and Rocky Mountains forming continuous mountain chains along the southwestern and south-eastern sides. There are three distinct mountain systems within the region: the Eastern

system with tilted, faulted, and folded sedimentary rocks, the Interior system with folded sedimentary and volcanic rocks, and the Western system with interlocking igneous intrusions and metamorphic rocks (Slaymaker et al., 2023).

The Rocky Mountains System, located in the western part of the Northern Cordillera, is known for its numerous summits that exceed 2000 masl in elevation. The highest peak in this system is Mount Robson, reaching an elevation of 3954 masl near latitude 53°N. Notably, the Rocky Mountain Trench, a vast valley, runs longitudinally between latitudes 48° and 60°N, dividing the system. Another trench, known as the Tintina Trench, continues north of the Rocky Mountain Trench, extending into the Intermontane Plateaus System in east-central Alaska (Colpron & Nelson, 2021).

Figure 6. Map showing Northern Cordillera divided into three major physiographic divisions the Rocky Mountains System, the Intermontane Plateaus System, and the Pacific Mountains System (Colpron & Nelson, 2021).

The oldest recognizable feature of the Western Cordillera is the gently rolling upland of its interior plateaus, which has been uplifted, buried by lava flows, dissected by river erosion, and modified by the Cordilleran ice sheet (Colpron & Nelson, 2021). Glacial activity has shaped much of the landscape, with features such as cirques, U-shaped valleys, striations, drumlins, eskers, till plains, and deposits from ice-dammed lakes and meltwater streams being widespread.

Postglacial rivers have formed terraces, alluvial fans, floodplains, and deltas, while periglacial landforms are present above the treeline, with permafrost occurring at higher elevations in the north.

This region encompasses two mains distinct ecozones. The first one, Montane Cordillera, has the most diverse topography and climate among all ecozones, with a significant portion covered by forests and limited wetlands mostly situated in valleys. The second ecozone, Boreal and Taiga Cordillera, experiences short and cool summers, and its land cover comprises mountains and tundra in the north and forests in the south. Same as Montane Cordillera, the majority of wetlands are located in valleys (Mahdianpari et al., 2020).

2.3.2 Climate

Due to its location between the Pacific Ocean and continental interior, as well as its rugged terrain and latitudinal extent, the Western Cordillera experiences a range of climates. The impact of climate on the natural landscape is notable, as seen in the Coast Mountains where heavy rainfall and snowfall have led to the formation of dense forests, snowfields, and glaciers. Unfortunately, climate change has caused a decrease in these features in recent years. Altitudinal vegetation zones, such as alpine tundra and grasslands, reflect changes in climate based on elevation. As a result of climate change, the boundaries of these zones are also being altered, particularly in the semiarid valleys of the Interior system (Colpron & Nelson, 2021).

The Canadian Cordillera has a diverse geography, spanning from polar tundra environments in the highest mountain peaks to coastal districts with mild winters that rarely see temperatures below freezing. The region's climate is greatly influenced by this range of geographical features (Beck et al., 2018). The mountainous and coastal areas receive high levels of precipitation, while the coastal regions in the west experience fewer dry days and dry spells (Sushama et al., 2010).

2.3.3 Permafrost

The occurrence of permafrost in a region is influenced by its topography and climate. In the southern areas of the Canadian Rockies Mountain range, permafrost is present at high elevations, which is classified as mountains permafrost, owing to the diverse topography and climate of the region. Additionally, the TTOP map in Obu et al. (2019) has identified the presence of isolated patches and sporadic permafrost in the Coast Mountains. Surprisingly, over half of the permafrost in British Columbia can be found in the mountains (Hasler et al., 2015).
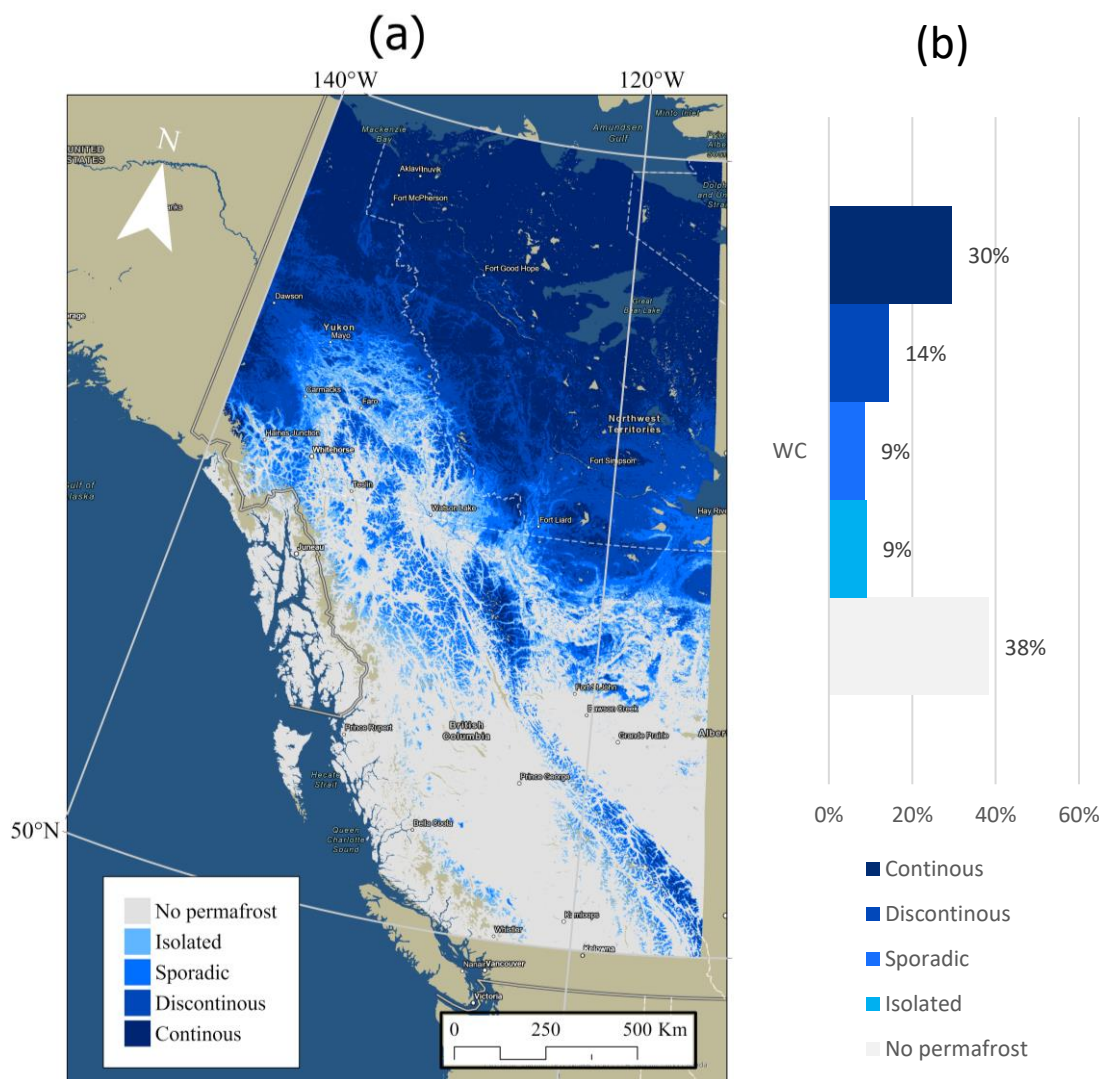
Figure 7. (a) TTOP map showing permafrost zones for the Western Cordillera (WC). (b) Areal coverage of different permafrost zones for WC.

Meanwhile, the regions in northeastern British Columbia and southwestern Northwest Territories are characterized by permafrost ecosystems in transition, where permafrost thaw is widespread. According to estimates by another TTOP model from Bevington & Lewkowicz (2015), permafrost covers nearly 88% of the area in Yukon and British Columbia.

2.4 Alaska

2.4.1 Topography

Alaska's topography is also characterized by the Western Cordillera, which includes three major physiographic divisions: the Rocky Mountains System, the Intermontane Plateaus System, and the Pacific Mountains System (Colpron & Nelson, 2021).

The Rocky Mountains System in Alaska contains many summits exceeding 2000 m in elevation. Between latitudes 48° and 60°N, the great valley called the Rocky Mountain Trench divides the system longitudinally, and its continuation northward is called the Tintina Trench, extending into the Intermontane Plateaus System in east-central Alaska (Colpron & Nelson, 2021).
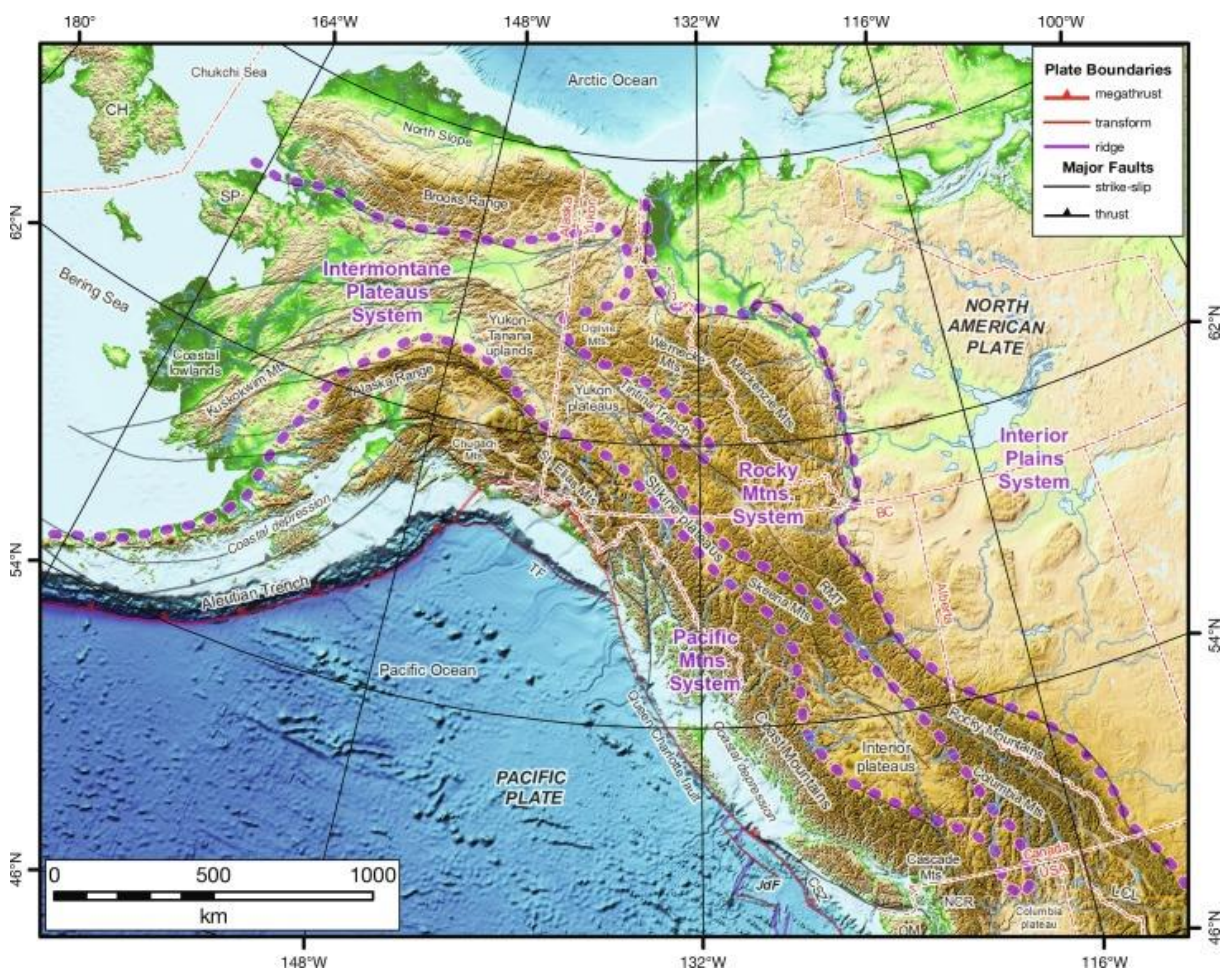
The Intermontane Plateaus System in Alaska exhibits lower relief compared to the flanking mountain systems, with elevations mostly ranging between 1000 and 2000 masl, and includes extensive lowlands under 300 masl.

The Pacific Mountains System in Alaska has summit elevations primarily between 2000 and 3000 masl, except for the Alaska Range in southern Alaska and the Saint Elias Mountains in southwestern Yukon. Denali (or Mount McKinley) at 6190 masl in the Alaska Range and Mount Logan at 5959 masl in the Saint Elias Mountains are the highest peaks on the continent. The Pacific Mountains System also features a longitudinal but discontinuous coastal depression, with many islands, and is bounded by the Olympic Mountains in the south and the Alaska Range in the north (Colpron & Nelson, 2021).

2.4.2 Climate

The climate of Alaska is hugely influenced by its wide latitudinal range topography including its mountain ranges and its proximity to the ocean (Shulski & Wendler, 2007). Alaska

experiences predominantly freezing temperatures throughout the year, with the Arctic region recording the lowest mean annual temperature of -12 °C. As you move towards the southern parts of the state, temperatures show a gradient of increase, culminating in the Southwest Islands and Southeast Panhandle region, where the highest mean annual temperature ranging from 4-7 °C. Despite the frigid climate, some parts of Alaska experience a strong continental climate, with the Tanana Valley and Yukon flats in the central and eastern Interior region having average highs for summer months of around 21°C. Similar to temperature, precipitation exhibits regional variation across the north-south axis. Annual precipitation levels range from 200 mm in the Arctic region, to over 1000 mm in the south along the coastal areas, where a maritime climate predominates. In the Southeast Panhandle, precipitation can exceed 5,000 mm per year (Stafford et al., 2000). Warm days and spells during summer months are particularly common in the Interior of Alaska (Sulikowska et al., 2019).

2.4.3 Permafrost

The distribution of permafrost in Alaska is primarily influenced by the temperature gradient, resulting in a higher concentration of permafrost compared to other study zones, due to its more northern location. Permafrost is a widespread geological feature in Alaska, occupying approximately 80% of the region. In the Arctic Alaska north of the Brooks Range, it is found extensively, reaching depths of up to 600 meters below the surface of the Arctic Coastal Plain. Recent estimates suggest that near-surface permafrost exists on 34% of Alaska with a mean spatial probability of 0.63 and an active-layer thickness of 0.8 meters. Current models indicate that 38% of mainland Alaska is underlain by near-surface permafrost, and it is projected to disappear on 16-24% of the landscape by the end of the 21st century (Pastick et al., 2015). In light of this, a new permafrost map of Alaska has been developed, utilizing a terrain-unit approach to map permafrost distribution based on climate and surficial geology. Additionally, the distribution of lakes and changes in permafrost regions in western Alaska have been studied using Landsat imagery spanning the period between the 1970s and 2010s (Lindgren et al., 2021).

The TTOP map developed by Obu et al. (2019) and used in this study, revealed that about 28% of Alaska is characterized by continuous permafrost. It is worth noting that this percentage would have been greater if the northern regions above 70° north had been

included. This type of permafrost is mostly found in the northern parts of Arctic Alaska, situated north of the Brooks Range, as well as in the eastern areas of Interior Alaska. On the other hand, the southern regions, which are affected by a maritime climate, do not exhibit as much permafrost. Furthermore, like the unaccounted northern parts, the unrepresented southern parts of Alaska may have had an impact on the percentage of non-permafrost and various types of permafrost zones, including those in the missing southwestern region.
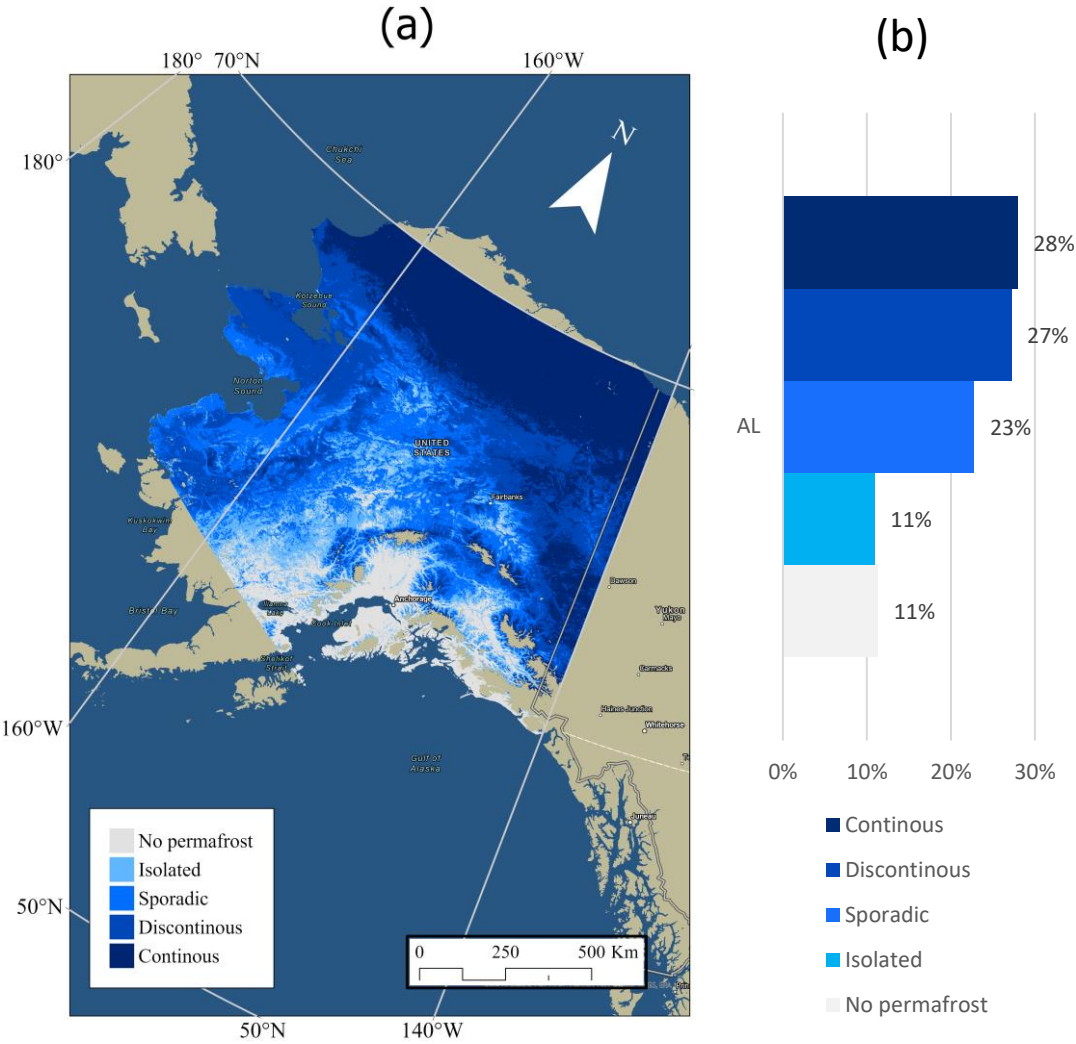
Figure 8. (a) TTOP map showing the different permafrost zones for Alaska (AL). (b) Areal coverage of the different permafrost zones for AL. Notice that TTOP map does not cover over 70° north, and parts of southwestern part such as Alaska Peninsula and parts of Dillingham, Bethel and Kusilvak.

3 Data and Methods

3.1 MODIS

The Moderate Resolution Imaging Spectroradiometer (MODIS) is an instrument designed to collect data on a wide range of environmental variables. There are two MODIS instruments, one on board the Terra satellite and the other on board the Aqua satellite. Both of these instruments have been collecting data since the early 2000s (Justice et al., 2002a).

The Terra satellite was launched in 1999 and carries the first MODIS instrument. This instrument has 36 spectral bands and a resolution of 250 meters to 1 kilometer. It is capable of capturing data in visible, near-infrared, and thermal infrared bands, which allows it to collect information on variables such as land and ocean surface temperature, vegetation cover, atmospheric aerosols, and cloud properties (Justice et al., 2002a). The Terra MODIS instrument orbits the Earth in a sun-synchronous polar orbit, passing over the equator at approximately 10:30 am local time (Erives et al., 2004).

The Aqua satellite was launched in 2002 and carries the second MODIS instrument. This instrument is similar to the one on board Terra but has a few modifications that allow it to better collect data on the Earth's oceans. For example, Aqua MODIS has a wider field of view and a different scan angle, which helps it to capture data on the ocean's surface more effectively. The Aqua MODIS instrument also has 36 spectral bands, with a resolution of 250 meters to 1 kilometer. Like Terra MODIS, it can collect data in visible, near-infrared, and thermal infrared bands, and can provide information on variables such as land and ocean surface temperature, vegetation cover, atmospheric aerosols, and cloud properties (Justice et al., 2002a). The Aqua MODIS instrument orbits the Earth in a sun-synchronous polar orbit, passing over the equator at approximately 1:30 pm local time (NASA, 2009).

MODIS data are used to generate a wide range of products, including vegetation indices, land surface temperature maps, and cloud properties. The data are also used to monitor events such as wildfires, floods, and volcanic eruptions, and to track changes in the Earth's climate over time. MODIS data are freely available to researchers and the public, and are widely used in environmental and climate studies (Salomonson et al., 2006).

Main data products from MODIS are (NASA MODIS Web, 2023):

- Level 1 products (3 products)
- MODIS atmosphere products (7 products)
- MODIS Land products (14 products, one of which is MODIS thermal anomalies - Active Fires)
- MODIS Cryosphere products (2 products)
- MODIS Ocean products (12 products)

3.1.1 MODIS fire products

One of the important applications of the MODIS instruments is the detection and monitoring of fires. The instruments' thermal sensors are particularly well-suited for this task, as they can detect the heat signatures of fires even through smoke and cloud cover. MODIS provides several fire products that are widely used for fire management and research purposes (Justice et al., 2002b).

One such product is the MODIS Active Fire and Burned Area Product, which provides near real-time information on the location and intensity of fires. The product uses a combination of the thermal sensors and contextual information, such as land cover and topography, to identify and map active fires. The product also includes information on the burned area and the severity of the burn, which can help in post-fire recovery efforts (Justice et al., 2002b).

3.1.2 The MODIS Active Fire product

Active fire products are categorized into two levels, namely level 2 and level 3 products. The level 2 product is the most fundamental type and is utilized to identify active fires and thermal anomalies like volcanoes. In the MODIS orbit geometry, the level 2 product covers an area of roughly 2340 km and 2030 km in the across- and along-track directions, respectively. This product serves as the basis for all other higher-level fire products (Giglio et al., 2020b).

Product	Source

Level-2 and Level-3 fire products:
    MOD14, MYD14
    MOD14A1, MYD14A1
    MOD14A2, MYD14A2
	LAADS (Section 4.1) and LP-DAAC
	(Section 4.2)

CMG fire products:
    MOD14CMQ, MYD14CMQ
    MOD14C8Q, MYD14C8Q
	University of Maryland (Section 4.3)

Global fire location product: MCD14ML	University of Maryland (Section 4.3)
Near real-time fire and corrected reflectance im-agery.	NASA LANCE (Section 4.4)
Geographic subsets of near real-time active fire locations in various GIS-compatible formats.	NASA FIRMS (Section 4.5)

Figure 9. Table showing Active Fire products and their availability (Giglio et al., 2020b).

The active fire product used in this study is a Level 3 8-day summary fire product, generated by MODIS on a daily basis and organized by tiles. Each file of the product corresponds to one of the 460 MODIS tiles, out of which 326 consist of land pixels. The product itself is a composite of fire pixels detected in each grid cell during the 8-day period, with a 1-km resolution (Giglio et al., 2016) (Giglio et al., 2020b). To make it easier to handle, the tiles are about 10° x 10° in size and each tile is assigned a unique horizontal (H) and vertical (V) coordinate, which range from 0 to 35 and 0 to 17, respectively.
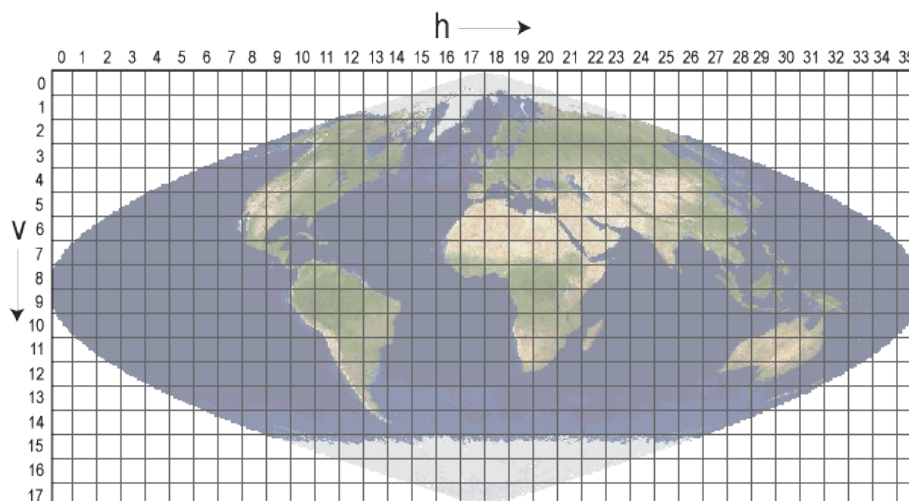
Figure 10. Map showing the MODIS tile division across the globe (NASA MODIS, 2023).

MOD14A2 data covering years from 2001 to 2021 are downloaded and used with tiles that cover this study area which are h10v02, h10v03, h11v02, h11v03, h12v02, h12v03, h13v02, h13v03, h14v02 and h14v03.

3.1.3 Fire mask

The fire mask is stored as 1200 x 1200 8-bit unsigned integer SDS named "FireMask". The SDS contains eight daily fire masks for each MODIS tile, from which each of these daily masks has a maximum value composite of the Level 2 fire product pixel classes from 7-9 (figure 11, Giglio et al., 2020b).

Class	Meaning
0	not processed (missing input data)
1	not processed (obsolete; not used since Collection 1)
2	not processed (other reason)
3	non-fire water pixel
4	cloud (land or water)
5	non-fire land pixel
6	unknown (land or water)
7	fire (low confidence, land or water)
8	fire (nominal confidence, land or water)
9	fire (high confidence, land or water)

Figure 11. Table showing the Active Fire product - MOD14 fire mask pixel classes (Giglio et al., 2020b).
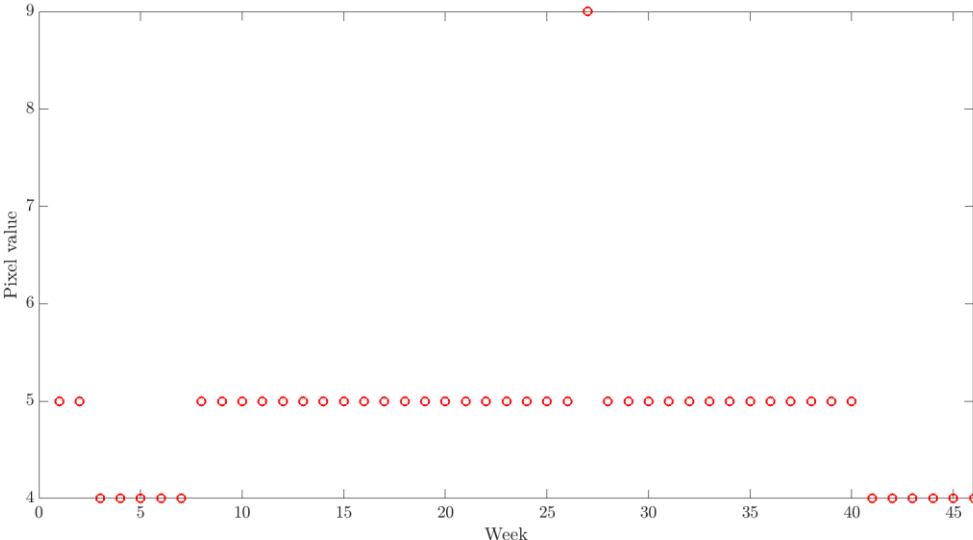
Figure 12. Figure showing an example of a pixel's fire mask throughout the year. The pixel values y-axis represents the classes from 0-9, meaning that the pixel was classified as 4

22

(cloud, land or water), 5 (non-fire land pixel) and 9 (fire high confidence, land or water). This value has varied through the year divided as an 8-day summery product MOD14A2.

3.1.4 Fire detection algorithm

The detection algorithm uses 4-, 11-, and 12- µm brightness temperatures acquired from the corresponding 1 km spatial resolution MODIS channels, evaluates to T_4, T_{11}, and T_{12}, respectively. For daytime observations, 0.65-, 0.86-, and 2.1-µm reflectance (evaluates to $\rho_{0.65}$, $\rho_{0.86}$, and $\rho_{2.1}$, respectively), aggregated to 1-km spatial resolution (Giglio et al., 2016).

Channel number	Central wavelength (µm)	Purpose
1	0.65	Sun glint and coastal false alarm rejection; cloud masking.
2	0.86	Bright surface, sun glint, and coastal false alarm rejection; cloud masking.
7	2.1	Sun glint and coastal false alarm rejection.
21	4.0	High-range channel for active fire detection.
22	4.0	Low-range channel for active fire detection.
31	11.0	Active fire detection, cloud masking, forest clearing rejection.
32	12.0	Cloud masking.

Figure 13. Table showing the channel numbers with wavelength and the purpose on the fire detection algorithm (Giglio et al., 2016).

The objective of the detection algorithm is to pick out the 'fire pixels' that contain one or more actively burning fires at the time the satellite passes over. The output for each pixel of the MODIS swath is ultimately classified as four classes: missing data, cloud, non-fire, fire or unknown (table x). The missing data class is assigned to pixels that lack valid data and are excluded from further consideration.

Land and water masking

Water, land and coastal pixels will be identified next using 1-km land/sea mask contained in the MODIS Collection 6. Coastal pixels are not processed further by the detection algorithm since any remaining fragments of unmasked land might be mistaken as a small fire due to its differences in temperature and brightness compared to the surrounding water.

Cloud masking

The next step is to filter out the pixels containing clouds by working with thresholds based on reflection and temperature.

Potential fire pixels

After the elimination of the obvious non fire pixels, the remaining ones undergo further processing and are considered as potential fire pixels. Each potential fire pixel is applied a series of 6 absolute and contextual thresholds in order to identify fire pixels.

Variable	Description
$\bar{L}_4$	Mean 4-µm radiance.
$\bar{T}_4$	Mean 4-µm brightness temperature.
$\bar{T}_{11}$	Mean 11-µm brightness temperature.
$\bar{\Delta T}$	Mean brightness temperature difference ($\equiv T_4 - T_{11}$).
δ_4	4-µm brightness temperature MAD.
δ_{11}	11-µm brightness temperature MAD.
$\delta_{\Delta T}$	Brightness temperature difference MAD.
N_v	Number of valid pixels within contextual window.
$\bar{\rho}_{0.86}$	Mean 0.86-µm reflectance (daytime pixels only).
$\bar{T}_4'$	Mean 4-µm brightness temperature of pixels rejected as background fires.
δ_4'	4-µm brightness temperature MAD of pixels rejected as background fires.
N_f	Number of pixels within contextual window rejected as background fires.
N_c	Number of coast pixels (always excluded) within the contextual window.
N_w	Number of excluded water pixels within the contextual window.
N_L	Number of excluded land pixels within the contextual window.

Figure 14. Table showing the statistical quantities computed for contextual window. The acronym MAD denotes the mean absolute deviation (Giglio et al., 2016).

Tentative fire pixels

The first criterion identifies the large and/or particularly intense active fires by applying test (1), the threshold for mean brightness temperature-T4 > 360 K (320 K at night) (Kaufman et al., 1998).

Next, more contextual tests will be used to identify smaller and/or cooler fires. These tests offer a much greater sensibility by extracting information from the immediate neighbourhood

or background characterization. During this phase, the algorithm estimates the radiometric signal of each fire pixel in the absence of fire by computing statistical summaries of neighbouring pixels (Giglio et al., 2003). For those potential fire pixels in which the background characterization is not possible due to not enough valid background pixels being available, only test (1) is applied to determine if the pixel is temporarily classified as a fire pixel or finally classified as unknown.

$$\Delta T > \bar{\Delta T} + 3.5\, \delta_{\Delta T} \tag{2}$$

$$\Delta T > \bar{\Delta T} + 6\,\text{K} \tag{3}$$

$$T_4 > \bar{T}_4 + 3\, \delta_4 \tag{4}$$

$$T_{11} > \bar{T}_{11} + \delta_{11} - 4\,\text{K} \tag{5}$$

$$\delta'_4 > 5\,\text{K} \tag{6}$$

A daytime potential fire pixel is classified as temporarily fire pixel if either test (1) is reached, or test (2) to (4) are reached and test (5) or (6) are reached. Meanwhile a night-time potential fire pixel is ultimately classified as fire pixel if either test (1) is reached or test (2) to (4) are reached. If the over mentioned tests are not reached for daytime and night-time potential fire pixels, then these pixels ultimately are classified as non-fire pixels.

Rejection tests

The final phase of the detection algorithm is to verify that the daytime temporary fire pixels are no false alarm. These false-alarm rejection tests include a sun-glint rejection test, a desert boundary rejection test, a forest clearing rejection test, a water-pixel coastal rejection test and a land-pixel coastal rejection test (Giglio et al., 2016).
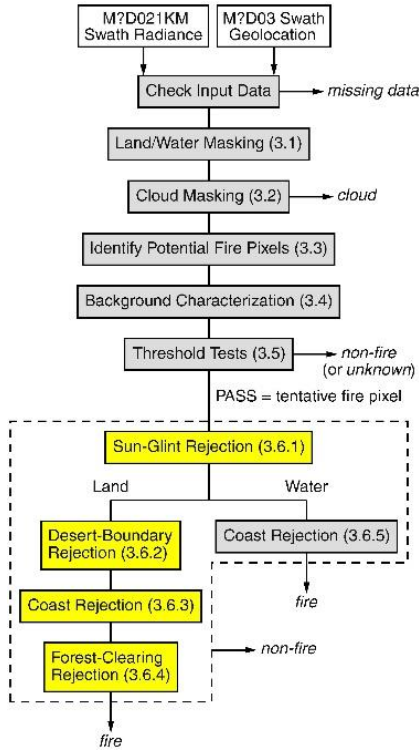
Figure 15. Figure showing the flow chart of the detection algorithm where pixels lacking valid data are summarily assigned to a class of missing data *and excluded from further consideration (Giglio et al., 2016).*

Fire detection confidence

When these tests are completed, the confidence of each detected fire pixel is calculated as the geometric mean five sub-confidence parameters, labelled C1 to C5 (Giglio et al., 2016).

$$C_1 = S\big(T_4; T_4^*, 360\text{ K}\big)$$

$$C_2 = S(z_4; 3.0, 6)$$

$$C_3 = S(z_{\Delta T}; 3.5, 6)$$

$$C_4 = 1 - S(N_{ac}; 0, 4)$$

$$C_5 = 1 - S(N_{aw}; 0, 4)$$

C_1 represents the minimum brightness temperature (less obviously a fire) and 360 K, which is a typical value (based on operational experience) that represents an obvious fire. For C_2, z_4=3 is the minimum value required for fire pixels by the detection algorithm, while z_4=3 represents a typical value for an obvious fire (again based on operational experience), and same applies to C_3. Meanwhile C_4 and C_5 reduce the detection confidence based on the increase of number of neighbouring cloud pixels and water pixels respectively. This due to the fact that fire pixels detected alongside cloud edges might trigger false alarm via reflected

26

sunlight, while fires detected alongside water pixels increase the chances that the fire is instead a costal false alarm (Giglio et al., 2003).

The confidence level varies between 0 and 100, these levels have been arranged into three classes, low ($0\% \leq C < 30\%$), nominal ($30\% \leq C < 80\%$) and high ($80\% \leq C \leq 100\%$) (Giglio et al., 2018).

In addition to the confidence level of each pixel, the fire radiative power (FRP) is calculated. The FRP is approximated as FRP $\approx Apix\sigma\, a\, \tau4(L4-\overline{L}4)$. L4 is the 4-µm radiance of the fire pixel, $\overline{L}4$ is the 4-µm background radiance, $Apix$ is the area of the MODIS pixel, which varies as a function of the scan angle, σ is the Stefan-Boltzmann constant ($5.6704 \times 10–8$ Wm–2K–4), $\tau4$is the atmospheric transmittance of the 4-µm channel and a is a sensor-specific empirical constant. Fire radiative power a unit of Megawatts (Giglio et al., 2016).

3.1.5 TTOP map

The temperature at the top of permafrost (TTOP) is a model that produces high resolution Northern Hemisphere permafrost maps up to 1 km^2 spatial resolution (Obu et al., 2019). Based on mean annual air temperature (MAAT), the model calculates mean annual ground temperature (MAGT) at the top of permafrost and uses semi-empirical adjustments factors for the effects of the snow cover and thermal offset.
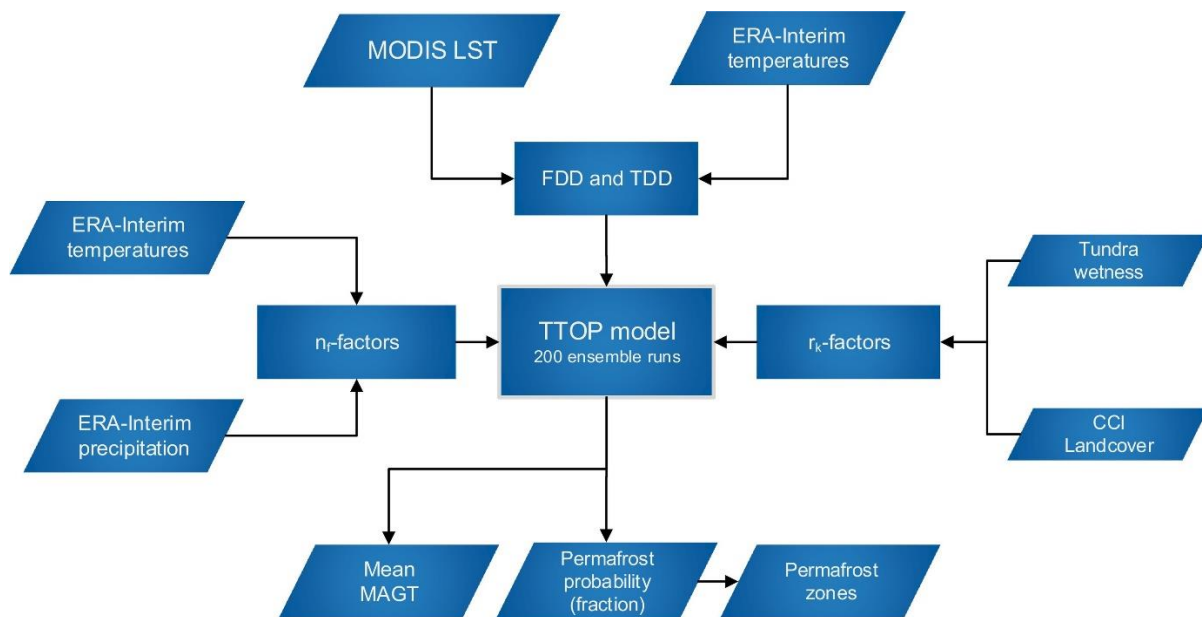
Figure 16. Flowchart of the employed methodology using for TTOP model (Obu et al., 2019).

FDD and TDD represent freezing and thawing degree days, respectively, of the surface meteorological forcing accumulated over the model period τ (in days) retrieved from MODIS LST and ERA-Interim temperatures.

The influence of the seasonal snow cover, vegetation, and ground thermal properties are taken into account by the semi-empirical adjustment factors r_k (ratio of thermal conductivity of the active layer in thawed and frozen state), n_f (scaling factor between winter air/surface and ground surface temperature) and n_t (scaling factor between summer air/surface and ground surface temperature).

The r_f factor is as a 1 km^2 dataset generated from mean annual snow depth (MASD) using a simple degree day model by ERA-interim precipitation and near-surface air temperature fields. The precipitation is adjusted according to DEM elevation differences against the ERA-Interim surface. Meanwhile, the r_k factor depends on water and organic contents, the values of which are based on the landcover and soil moisture derived from remote sensing gridded products.

3.2 Methods

The MODIS Active Fire product MOD14A2 onboard the Terra satellite, was used in this study for the years 2001 to 2021. Data from 2000 were excluded from the study due to hardware problems that MODIS suffered prior to November 2000, which affected all fire products (Giglio et al., 2020b). Additionally, data from Aqua satellite MYD14A2 were excluded from this study, since including both satellites would result in excessively large data sizes.

The MODIS tiles used in this study area are h10v02, h10v03, h11v02, h11v03, h12v02, h12v03, h13v02, h13v03, h14v02 and h14v03. Some areas of the defined study region of Alaska (AL) are not covered (same area as TTOP data for AL, section 2.4.3). The need to download two more tiles to cover relatively small areas (compared to this study scale) were considered insignificant for this study purpose. Therefore, a decision was made to exclude these two tiles from the analyses.

Analyses in this study were produced using MATLAB and ArcGIS Pro.

3.2.1 MATLAB

MATLAB is a programming platform with a matrix language which is used to analyse data, develop algorithms and create models or applications (MATLAB, 2023).

The study retrieved data from (https://e4ftl01.cr.usgs.gov/MOLT/MOD14A2.006/) the USGS website, which provides the free Active Fire data MOD14A2 from MODIS, using a MATLAB script (Appendix A). The analysis was performed in MATLAB after extracting relevant information from the Active Fire product, such as the latitude, longitude, date, day of year, month, year, and other details for all pixels with fire indexes 7, 8, and 9. Since the MODIS Fire product has the same grid as the TTOP permafrost product, it was possible to infer the permafrost fraction and other important permafrost parameters for each detected fire pixel (Appendix B). With this catalogue, it was possible to extract all detected fires in the four subregions and run temporal and spatial analyses as described in the section 3.2.2 below.

3.2.2 Analysis of annual and monthly patterns

The initial analyses conducted were annual time series analyses of wildfires, with a specific focus on different types of permafrost such as isolated, sporadic, discontinuous, and continuous as well as non-permafrost zones. The results were presented as a MATLAB figure plots, where the normalized percentage of fires for each year was displayed for different types of permafrost zones, along with a linear regression analysis for each permafrost zone, illustrating the annual trend from 2001-2021 time. Additionally, a second analysis was conducted as a subplot on the same figure, which shows the percentage of all fires that occurred in each year for the different permafrost zones. Finally, a third subplot which shows the percentage of fires that occurred in different permafrost zones for all years from 2001 to 2021, displayed side by side (Appendix C, D, E and F).

Using the same catalogue, the study performed various analyses, including the mean annual latitudes of fires from 2001 to 2021. A linear regression analysis was conducted to determine whether the trend had shifted towards higher latitudes. Similarly, the mean month of fires was presented for the same period, and a linear regression analysis was performed to determine whether the trend had changed, indicating earlier or later occurrence of fires in the year. Lastly, a temporal monthly analysis was conducted for all fires in each zone, presenting the monthly distribution of wildfires (Appendix C, D, E and F).

3.2.3 ArcGIS Pro

ArcGIS Pro is a desktop GIS application from Esri that was used in this study to conduct spatial distribution analyses, which were presented as density heat maps. These heat maps were generated using the Kernal Density distribution method (ArcGIS Pro, 2023). The process involves fitting a curved surface over every point in a smooth manner. The highest value of the surface corresponds to the location of the point and gradually decreases as distance from the point increases until it becomes zero at the distance equal to the search radius. The neighbourhood considered for this process is circular in shape, and only such a shape is permissible. The volume underneath the surface is equivalent to the population field value of the point, which defaults to 1 used in this study. The density of each output raster cell is determined by summing up the values of all the kernel surfaces that overlay the center of the raster cell. Additionally, all other maps in this study were generated with the same program ArcGIS Pro 2.8.8.

4 Results

4.1 Quebec and Labrador Peninsula

The results show that the large majority of fire pixels in Quebec and Labrador Peninsula (QLP) have not been registered in permafrost coverage. Sporadic permafrost areas had only 4% of the total fire pixels, while continuous and discontinuous permafrost areas had less than 1% of the total amount. Furthermore, the majority of fire pixels were registered in non-permafrost and isolated patches, each accounting for 48% of the total amount (figure 17c).

It is interesting to note that the occurrence of fire pixels in QLP study region varies significantly between the years, with the majority of events occurring in 2002 and 2013 (figure 17a). It is important to note that while there has been a decrease in the number of fire pixels in non-permafrost and isolated permafrost zones since 2013, fires in sporadic permafrost zone have slightly increased (figure 17b).

Figure 17. (a) Percentage of all fires that occurred in the Quebec and Labrador Peninsula (QLP) in 2001-2021 for different permafrost zones and for a given year. (b) Percentage of all fires that occurred in QLP in each year for the different permafrost zones. (c) Percentage of all fires that occurred in QLP in 2001-2021 for the different permafrost zones.

Finally, it is noteworthy that the total number of fire pixels registered in Quebec and Labrador exceeded 40,000 pixels or only 5% of the total amount of all four study zones (figure 17c).

The heat map density, derived with Kernal Density distribution, shows the composite data of wildfires occurring in the investigated area reveals that regions with lower latitudes, where permafrost is predominantly absent, particularly in the eastern Baie James region located to the east of James Bay, have exhibited the highest extent of burning. Nevertheless, it is noteworthy that fires are not infrequent in areas with similar latitudinal gradient in the central Baie James region and the Duplessis region. Furthermore, a considerable number of wildfires also occur in the western vicinity of Happy Valley-Goose Bay in central Labrador (figure 18b).

Figure 18. (a) TTOP map showing the different permafrost zones in the Quebec and Labrador Peninsula (QLP). (b) Heatmap generated with "Kernal Density estimation" where 0 shows no fires and 1 shows the most fires, for all fire pixels detected between 2001-2021 in QLP.

The analysis show that the mean latitude of fire pixels registered in Quebec has shifted approximately one-degree further north, with the highest mean latitude recorded in 2021.

However, there appears to be a high variety in mean latitudes registered between the years (figure 19a).

The mean month of fire pixels registered also exhibits significant variation across the years. The latest mean month was observed in 2004, occurring in mid-August, while the earliest mean month occurred in 2006 at the end of May (figure 19b).

The data reveals that the majority of fire pixels registered between 2001-2021 occurred in July and June, accounting for 47% and 46% of the total amount, respectively. However, fire pixels were also recorded in other months such as August and May, and late summer/early fall months such as September and October (figure 19c).

Figure 19. (a) The mean latitude of all detected fire pixels in the Quebec and Labrador Peninsula (QLP) for each year between 2001 and 2021. (b) Mean month of all detected fire pixels in QLP for each year between 2001 and 2021. (c) Monthly distribution of all detected fire pixels in QLP for the period of 2001-2021.

4.2 Central Canada

Data shows that there has been a fluctuation in the occurrence of fire pixels in the Central Canada (CC) over the years. Specifically, there were more fire events in 2021 and 2013 compared to other years. However, it is worth noting that the trend is not consistent across all

types of permafrost. While there has been an increase in the number of fire pixels in non-permafrost areas, there has been a decrease in fires in sporadic and discontinuous permafrost areas. At the same time, there has been a slight increase in fires in continuous permafrost, while the number of fires in isolated permafrost has remained relatively unchanged (figure 20a).

The fire distribution in different permafrost zones within the year varies more in CC as well, compared to QLP, with continuous, discontinuous, and sporadic permafrost dominating the percentage in some years such as 2003, 2004, 2007, 2008, 2010, 2013 and 2014 (figure 20b).

It's interesting to observe that fire pixels in CC have a more diverse distribution across different types of permafrost compared to QLP. Moreover, the majority of fire pixels detected in CC region were found in sporadic permafrost and non-permafrost areas, representing a whopping 23% and 39% of the total, respectively. Although fires do occur notably in other permafrost zones as well, such as continuous and discontinuous compared to QLP, with 7% and 9% respectively (figure 20c).

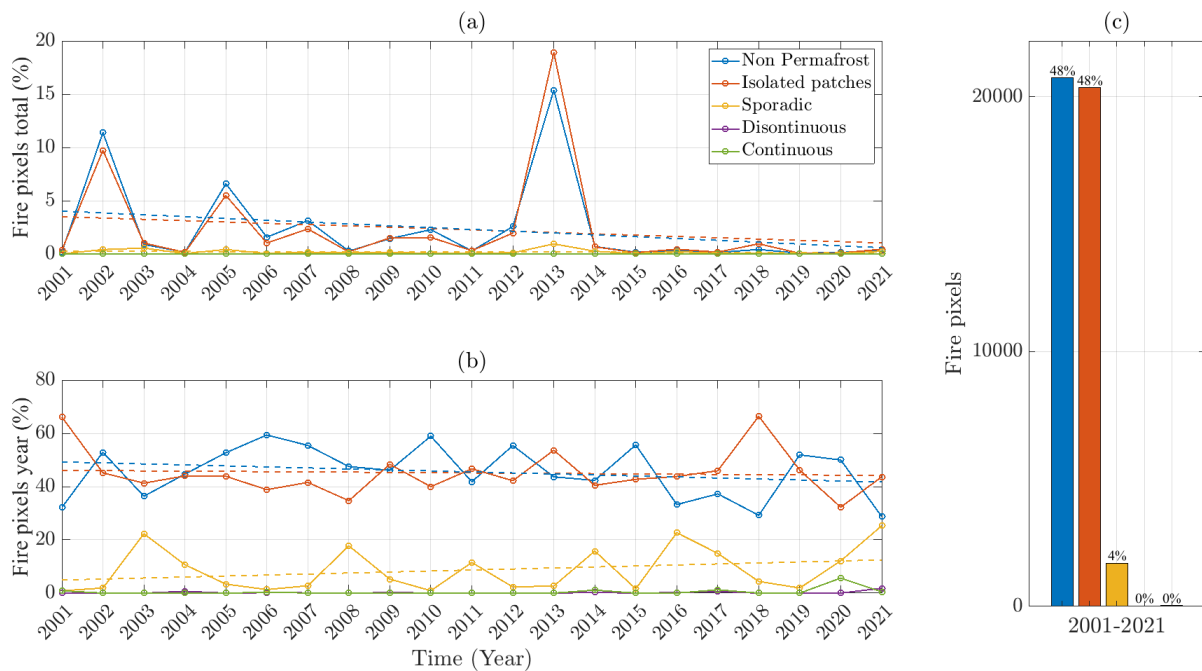*Figure 20. (a) Percentage of all fires that occurred in the Central Canada (CC) in 2001-2021 for different permafrost zones and for a given year. (b) Percentage of all fires that occurred in CC in each year for the different permafrost zones. (c) Percentage of all fires that occurred in CC in 2001-2021 for the different permafrost zones.*

34

Finally, it is noteworthy that the total number of fire pixels registered in Central Canada exceeded 350,000 pixels or 39% of the total amount of all four study regions.

The heat map derived from the analysis of fire occurrences in the studied geographical zone indicates a considerably broader distribution of fires compared to the regions of QLP. Notably, there is a gradual increase in fire frequency from east to west along the latitudinal gradient, with Ontario exhibiting the lowest number of fires. East of Lake Winnipeg in Manitoba, fires become more frequent, extending towards the border with Ontario, while also occurring in the northern part of Manitoba. In Saskatchewan, which is located more central in Canada, fires are particularly prominent, including the south-eastern region near Yorkton, as well as throughout the northern part of the province, extending westward to Buffalo National Park in Alberta and northward to the Great Slave Lake (figure 21b).

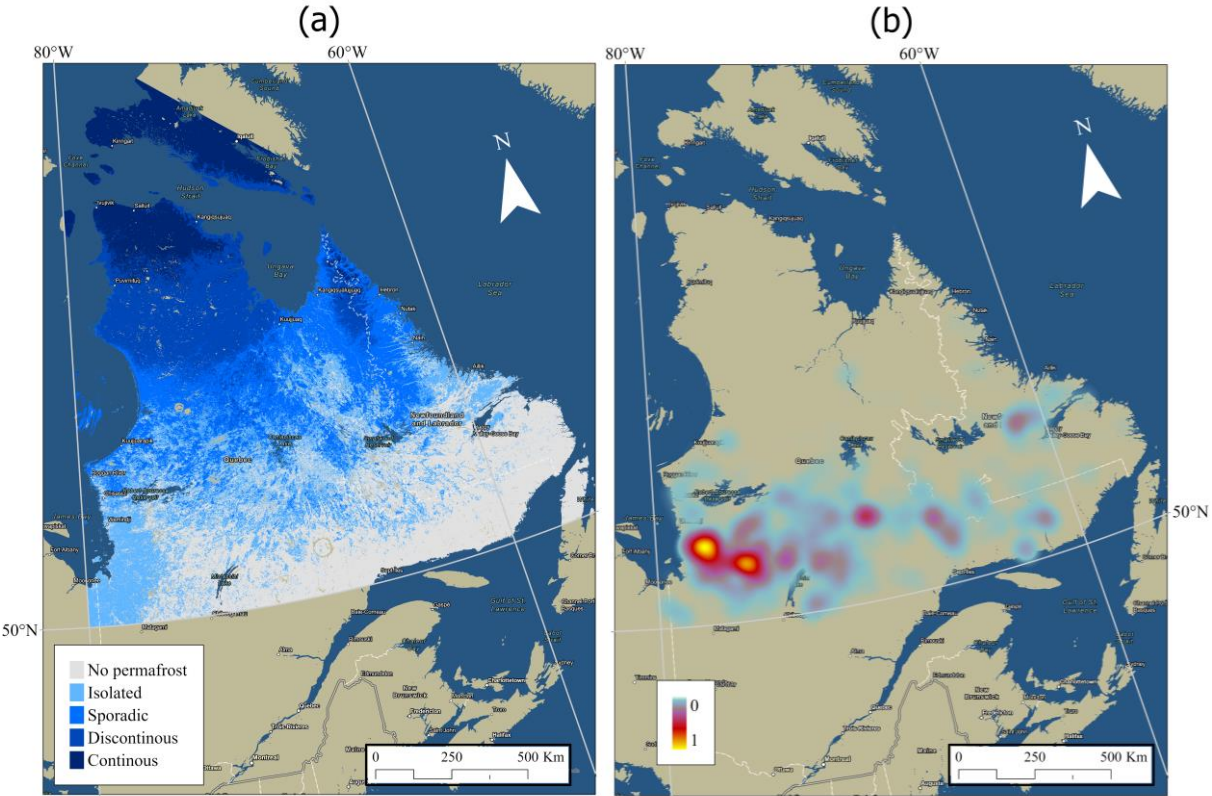*Figure 21. (a) TTOP map showing the different permafrost zones in the Central Canada (CC). (b) Heatmap generated with "Kernal Density estimation" where 0 shows no fires and 1 shows the most fires, for all fire pixels detected between 2001-2021 in CC.*

The analysis show that the mean latitude of fire pixels registered in CC has slightly shifted further south, with the highest mean latitude recorded in 2014 (figure 22a).

The mean month of fire pixels registered also exhibits significant variation across the years in this subregion. The latest mean month was observed in 2017, occurring in mid-July, while the earliest mean month occurred in 2016 in mid-May (figure 22b).

The data reveals that fires are more spread throughout the year in this subregion compared to fires in QLP, with the majority of fire pixels registered between 2001-2021 occurred in July and June, accounting for 34% and 24% of the total amount, respectively. Although, fire pixels were also recorded significantly in other months such as May and August with 14% and 13%, and late summer/early fall months such as September and October (figure 22c).

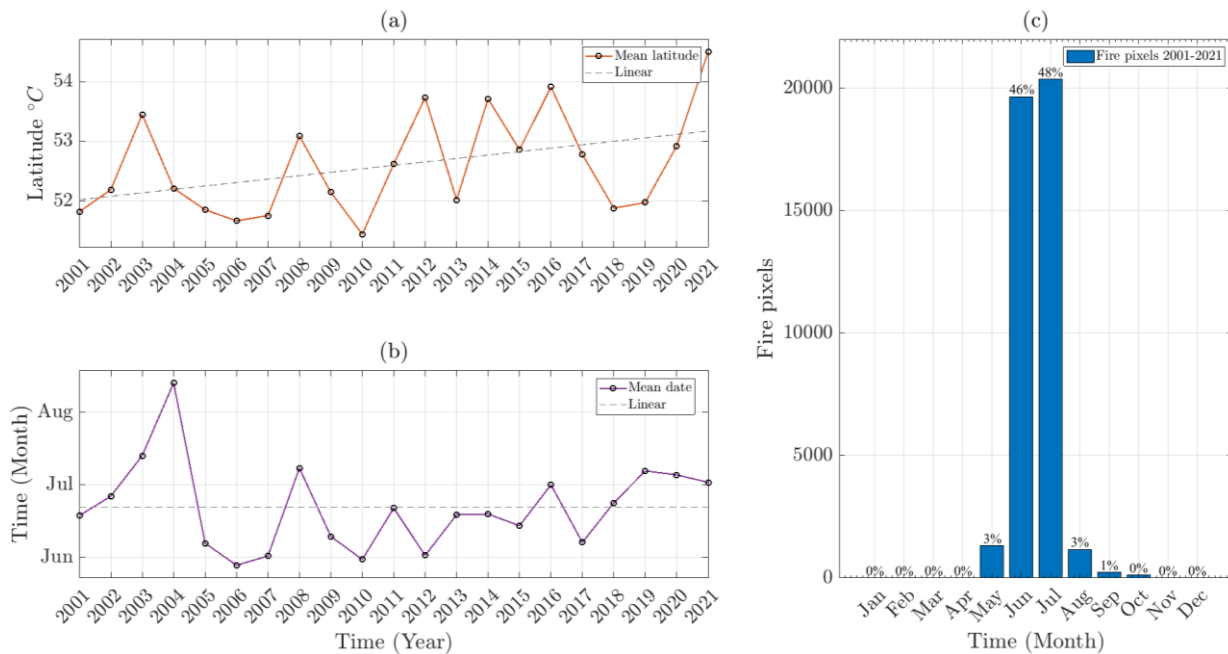*Figure 22. (a) The mean latitude of all detected fire pixels in the Central Canada (CC) for each year between 2001 and 2021. (b) Mean month of all detected fire pixels in CC for each year between 2001 and 2021. (c) Monthly distribution of all detected fire pixels in CC for the period of 2001-2021.*

4.3 Western Cordillera

The data analyses show that there has been a fluctuation in the occurrence of fire pixels in Western Cordillera (WC) over the years. Specifically, there were more fire events in 2017 and 2018 compared to other years. However, it is worth noting that the trend is not consistent across permafrost free areas and different types of permafrost zones. While there has been a significant increase in the number of fire pixels in non-permafrost areas, there has been a

slight increase in sporadic and continuous permafrost zones. Meanwhile, a bit more increase has been seen in fires in discontinuous and isolated patches of permafrost. Furthermore, it is notable that there are single years where fires in permafrost zones such as continuous and discontinuous permafrost outnumber fires in non-permafrost areas, such as in years 2004 and 2014 (figure 23b).

It's interesting to observe that fire pixels in WC have different distribution across different types of permafrost compared to CC and QLP study zones. Although non-permafrost areas still have the majority of fires of 55%, continuous and discontinuous zones registered 16% and 15% of the total amount, which is significantly more than in the other zones. Meanwhile isolated patches and sporadic permafrost have 7% each of the total fires registered (figure 23c).

Finally, it is noteworthy that the total number of fire pixels registered in Canadian Cordillera exceeded 300,000 pixels or 36% of the total amount.
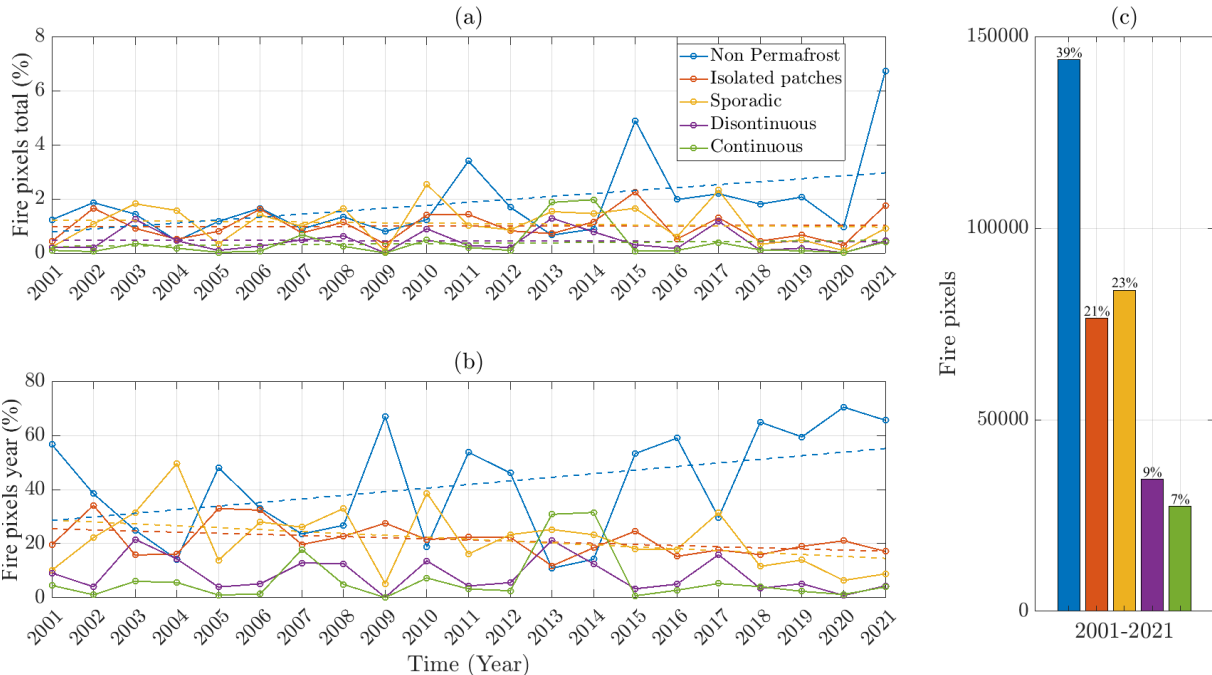

Figure 23. (a) Percentage of all fires that occurred in the Western Cordillera (WC) in 2001-2021 for different permafrost zones and for a given year. (b) Percentage of all fires that occurred in WC in each year for the different permafrost zones. (c) Percentage of all fires that occurred in WC in 2001-2021 for the different permafrost zones.

The heat map generated from the collective data of fires within the studied region indicates that areas with lower altitudes, specifically the North Central and South Central Interior regions of British Columbia, have experienced the highest levels of burning. However, it is noteworthy that fires are not uncommon in higher latitude regions, such as the Peace River Valley in northern Alberta and the western vicinity of the Great Slave Lake in South and North Slave. Additionally, a significant number of fires occur in the central western region of Yukon, near the border with Alaska (figure 24b).
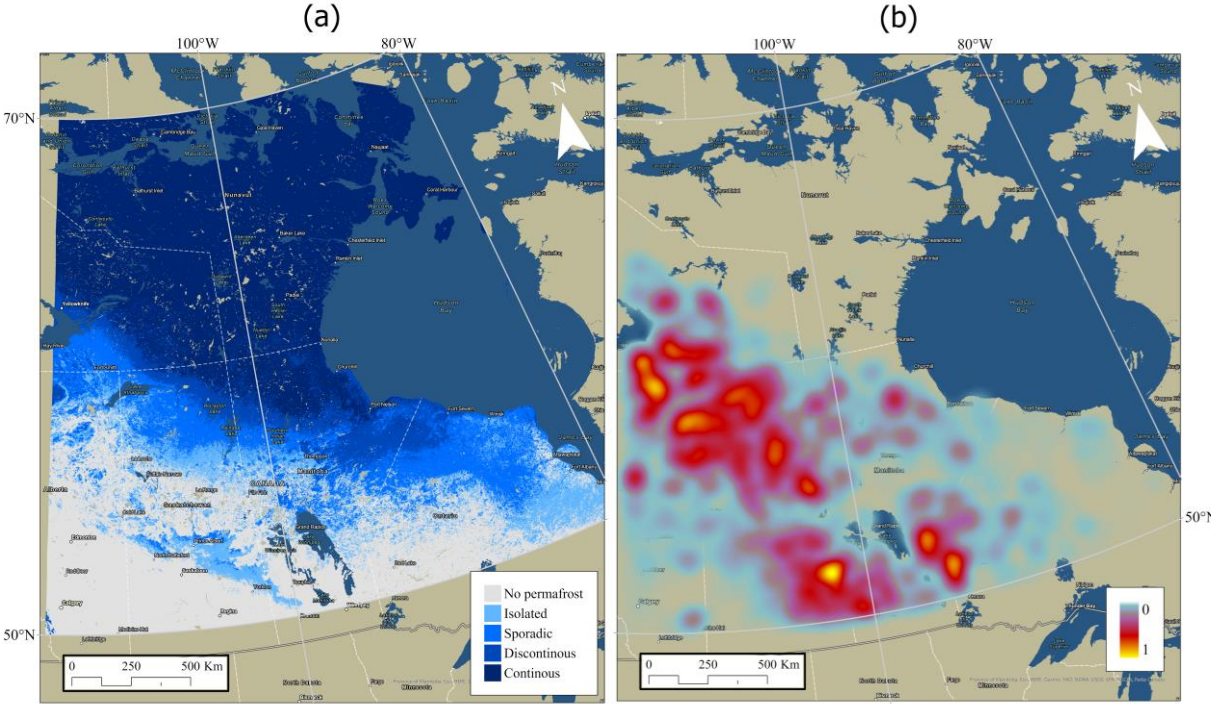

Figure 24. (a) TTOP map showing the different permafrost zones in the Western Cordillera (WC). (b) Heatmap generated with "Kernal Density estimation" where 0 shows no fires and 1 shows the most fires, for all fire pixels detected between 2001-2021 in WC.

The analysis from the fire pixels for this zone show that the mean latitude of fire pixels has pretty much stayed the same, with the highest mean latitude recorded in 2004 and 2014. These are the same years that recorded the highest number of fires in permafrost areas which lie furthest north (figure 25a).

The mean month of fire pixels registered also exhibits significant variation across the years. The latest mean month was observed in 2002, occurring in late-August, while the earliest mean month occurred in 2004, 2015 and 2019 in early-June and late-May respectively. Notable here that these years had the highest mean latitudes as well, thus indicating that early fires tend to be more in permafrost areas, which have a higher latitude (figure 25b).

The data reveals that fires in the Canadian Cordillera subregion are the most monthly spread throughout the year compared to fires in the other QLP and CC subregions, with the majority of fire pixels registered between 2001-2021 occurred in July and August, accounting for 30% and 23% of the total amount, respectively. Interesting to see that besides having the most fires in spring and autumn compared to the other zone, winter fires are as well notably higher. Winter months have a combined 5% of the total fire pixels, with December having the most, 2% of all fires (figure 25c).
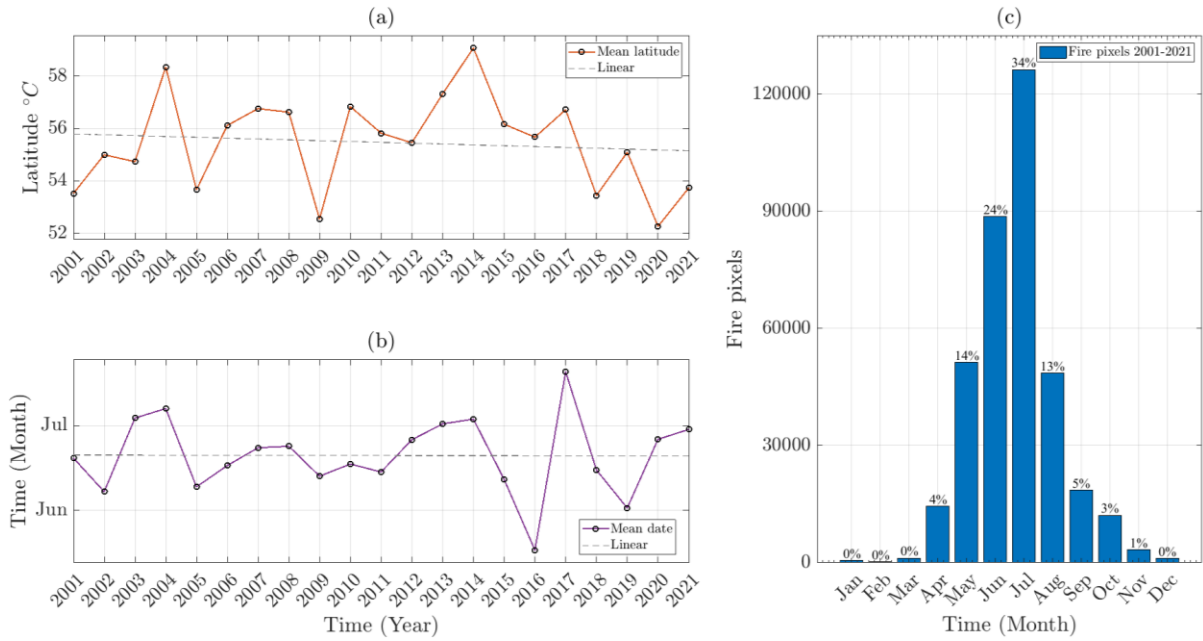

Figure 25. (a) The mean latitude of all detected fire pixels in the Western Cordillera (WC) for each year between 2001 and 2021. (b) Mean month of all detected fire pixels in WC for each year between 2001 and 2021. (c) Monthly distribution of all detected fire pixels in WC for the period of 2001-2021.

Additional analysis on winter fires in this region indicates that the majority of such events transpire within the boreal forest located in the Interior Plateau of the Western Cordillera. These fires are commonly observed to occur in the geographical region stretching between the

Coast Mountains and Rocky Mountains of British Columbia, as well as the eastern regions of the Canadian Rockies situated in British Columbia and Alberta (figure 26).
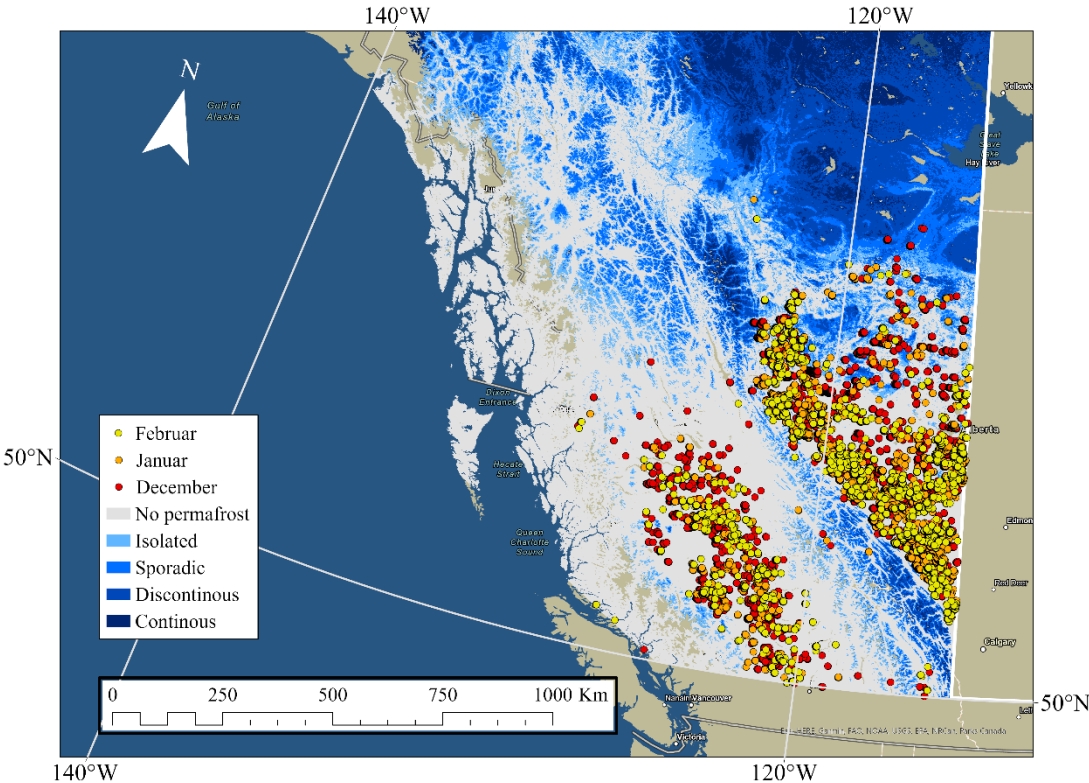
Figure 26. Map shows the spatial distribution of detected fires in December, January and February for all the years between 2001-2021 in Western Cordillera (WC).

4.4 Alaska

Besides the variation of fire events between the years, analyses from the data of the Alaska (AL) subregion show a rather different distributions of fire in non-permafrost and permafrost areas. Contrary to other zones, permafrost areas dominate almost all fires with 96% of the total fires, where discontinuous permafrost has the majority of 40% of the total fires. Sporadic and continuous permafrost follow with 28% and 17% respectively (figure 27c).

The AL subregion has by far the most diverse percentage of fires in different permafrost zones, that occur within the year, compared to other three subregions (QLP, CC and WC) (figure 27b).

The year 2004 is the year with the most fires of 23 % of the total amount, where 15% has occurred in discontinuous permafrost (figure 27a).

40

Finally, Alaska had a total of 200,000 fire pixels registered or 20% of the total amount of all four zones.
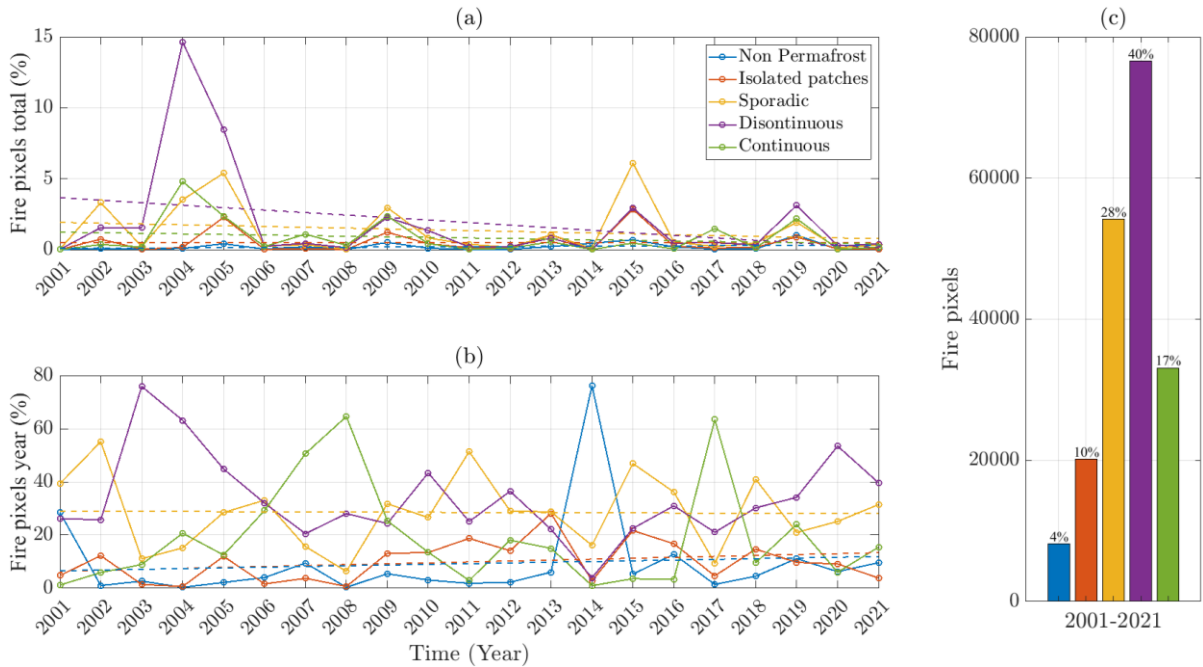
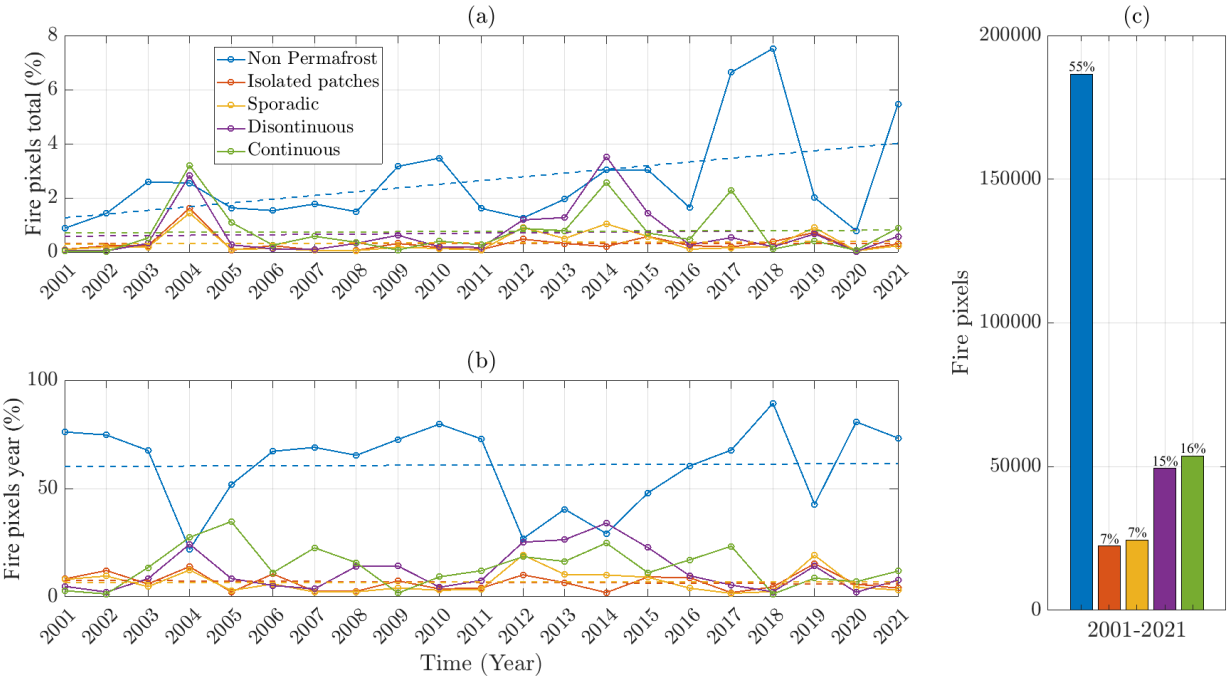*Figure 27. (a) Percentage of all fires that occurred in the Alaska (AL) in 2001-2021 for different permafrost zones and for a given year. (b) Percentage of all fires that occurred in AL in each year for the different permafrost zones. (c) Percentage of all fires that occurred in AL in 2001-2021 for the different permafrost zones.*

The analysis of the spatial distribution of fires in regions characterized by permafrost reveals that fires in areas with continuous permafrost are predominantly found in the eastern portion of Interior Alaska, with some occurrences in the northern Arctic region. In contrast, fires in areas with discontinuous permafrost are primarily concentrated in central Interior Alaska and Western Alaska. Sporadic and isolated permafrost fires, on the other hand, are primarily located in the western part of Interior Alaska and extend towards the southern region (figure 28).

The analysis of the spatial distribution of wildfires indicates that the majority of these events are concentrated in the Interior Alaska region, particularly in the eastern part of Interior Alaska. A heat map generated from the fire pixel data further highlights areas with the highest frequency of wildfire events, such as Southeast Fairbanks, the eastern and western regions of Yukon Flats, and the eastern part of Fort Yukon (figure 29b).
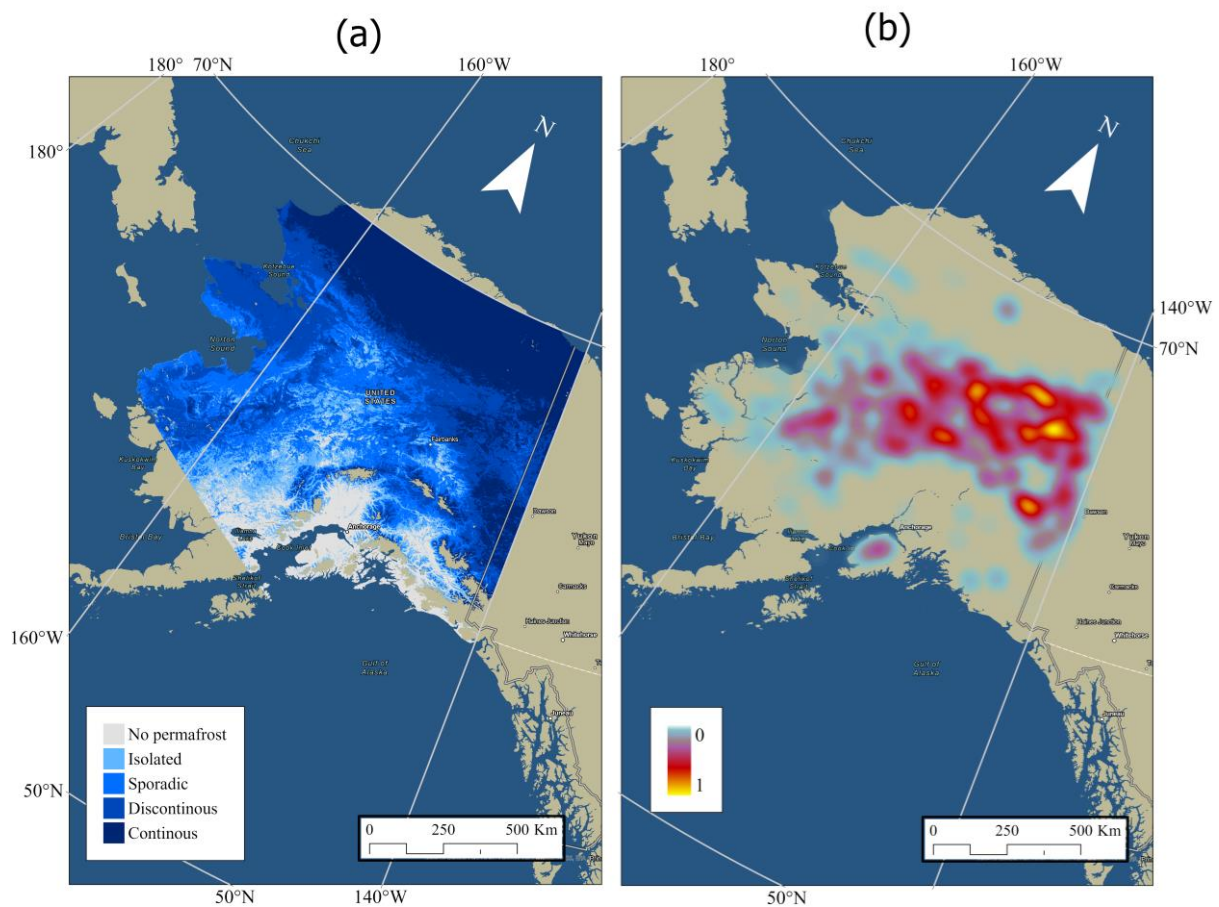
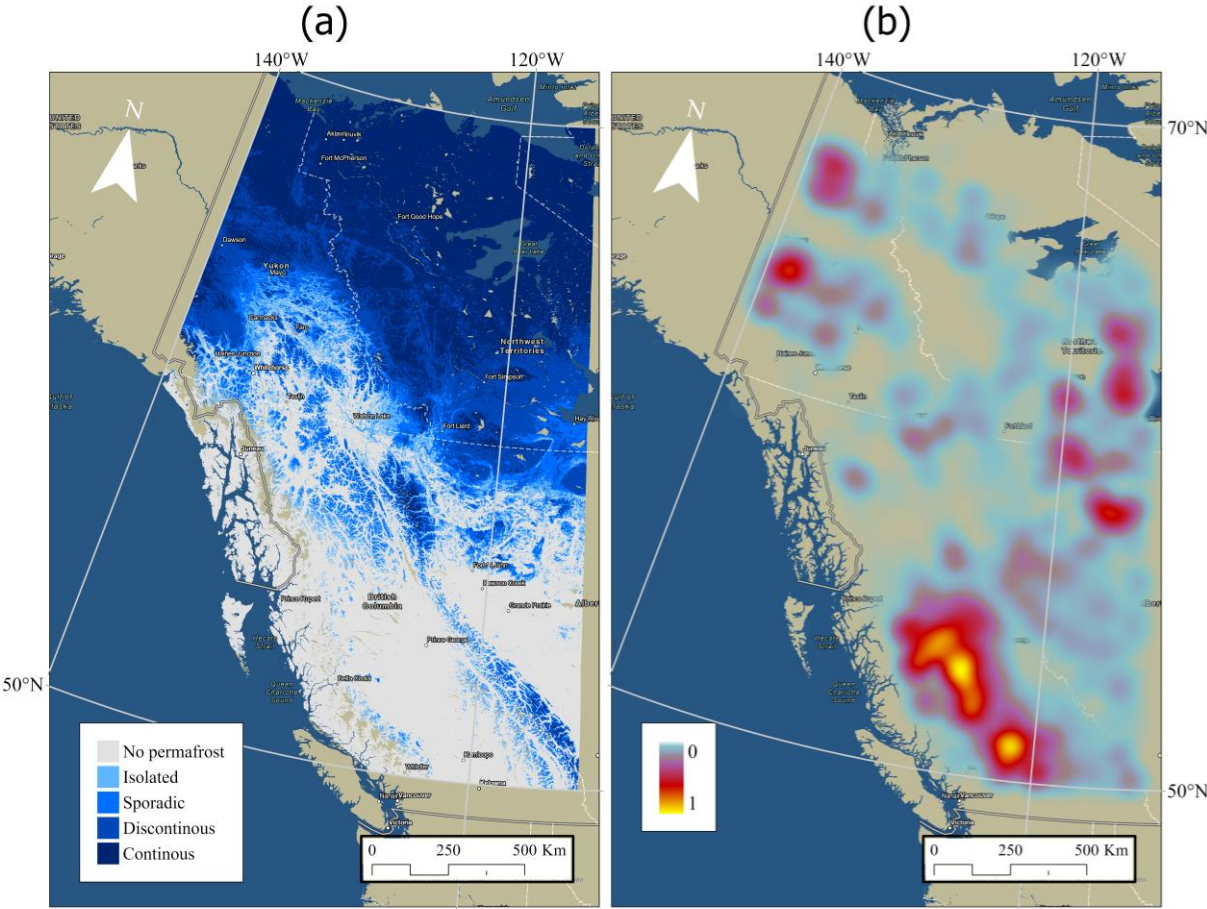*Figure 28. (a) TTOP map showing the different permafrost zones in Alaska (AL). (b) Heatmap generated with "Kernal Density estimation" where 0 shows no fires and 1 shows the most fires, for all fire pixels detected between 2001-2021 in AL.*

The mean latitude of fire pixels registered has shifted towards south, with the years 2008, 2012 and 2017 having the highest mean latitude compared to other years at approximately over 66 degrees north, while the lowest mean latitude with 61 degrees north was registered in 2014 (figure 30a).

The mean month of fire pixels registered varies between the years, with the year 2001 having the latest mean calendar month in mid-July, meanwhile 2014 having the earliest mean month in early- June (figure 30b). Linear regression shows the average month of fire pixels has changed towards earlier in the year by almost a month.

Similar to Quebec and Labrador Peninsula, in Alaska, fires mostly concentrated in the summer months, with the majority of fires occurring in June, July and August with 29%, 41%

and 25% respectively. Fires occurred in spring as well with May having 4% and September 1% (figure 30c).

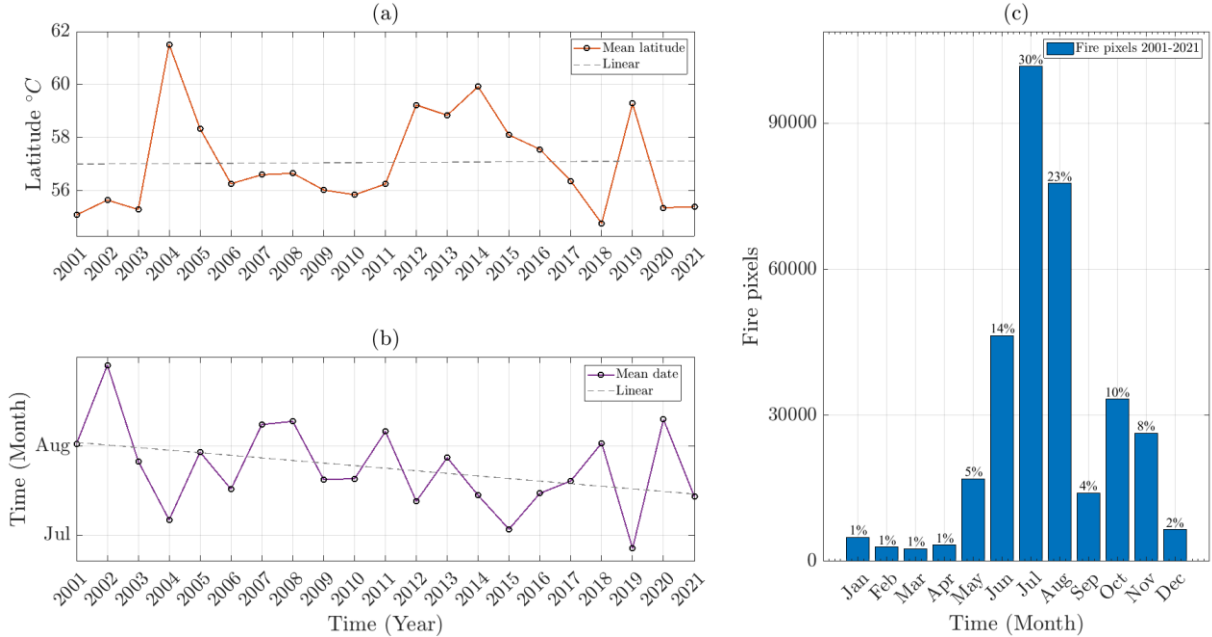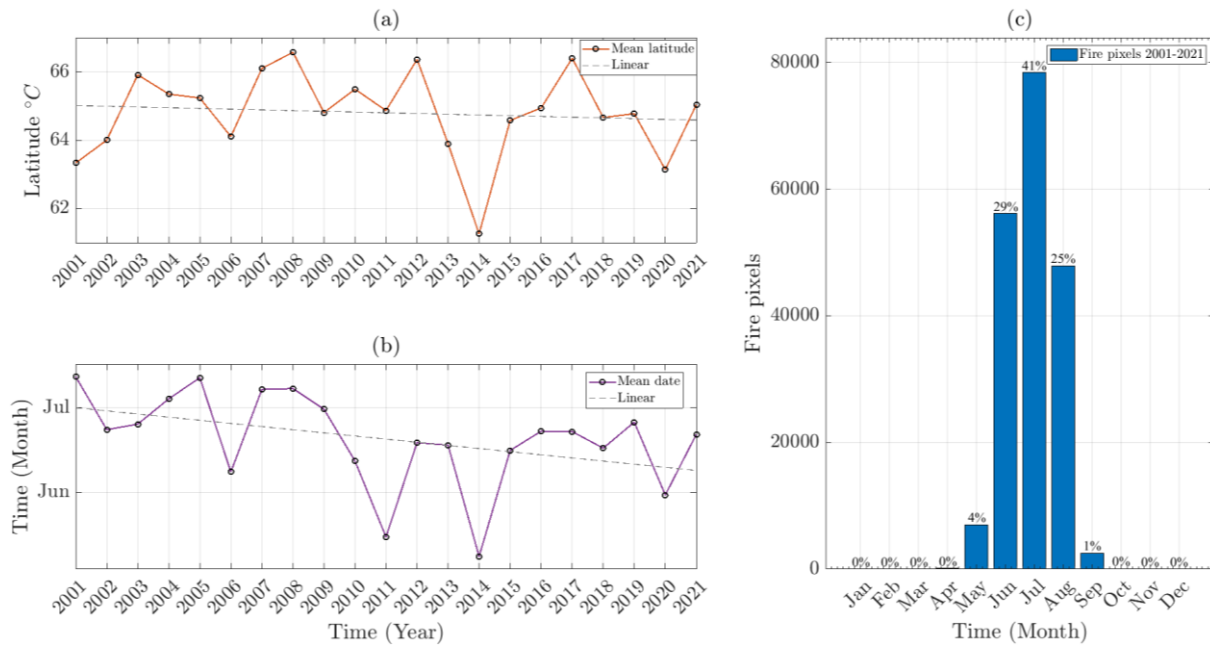*Figure 29. (a) The mean latitude of all detected fire pixels in the Alaska (AL) for each year between 2001 and 2021. (b) Mean month of all detected fire pixels in AL for each year between 2001 and 2021. (c) Monthly distribution of all detected fire pixels in AL for the period of 2001-2021.*

5   Discussion

5.1   Uncertainties of the MODIS Fire product

The present report employs MODIS Fire products, such as MOD14A2. Nonetheless, it is crucial to acknowledge the limitations of these products. For instance, validation against other satellite data shows that the detectable size of fires ranges from 2-7 ha (Giglio et al., 2016), which falls short when compared to real fire data, where fires had to reach the size of 10 ha in the east and 78 ha in the west of USA, in order to be detected (Fusco et al., 2019).

Hardware issues on board Terra satellites were identified post-launch prior to November 2000. These issues caused an entire scan line to be identified as fires (Giglio et al., 2020b). Moreover, during the analysis of fire products, a similar problem was detected in August 2001, where several scan lines were erroneously identified as fire pixels instead of water pixels in the ocean (figure 30).
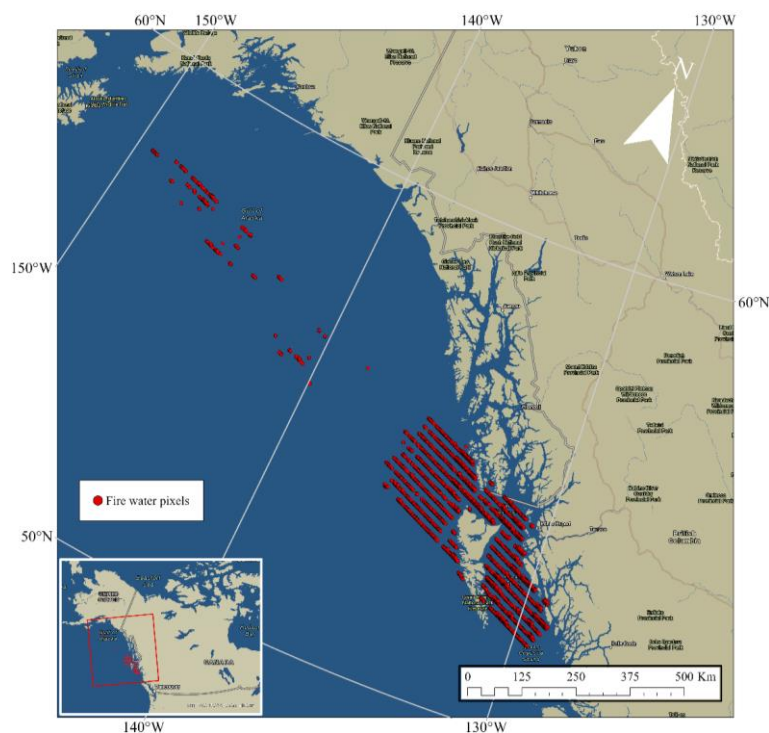
Figure 30. Map showing fire pixels erroneously classified as fire pixels from the British Columbia coast to the Gulf of Alaska in the northwest. All these fire pixels were registered in the same file with the same date, meaning that entire scans were identified as fires. Overview map shows the location of the main map in a red rectangle.

44

Such errors, which can contain over 8000 pixels, have the potential to significantly alter the fire regime in the affected area. Identifying these errors in land cover can be particularly challenging, especially when dealing with almost a million fire pixels such as in this study, particularly in zones where fires are frequent.

Another issue with active fire products, is that it may classify pixels as fires when the brightness temperature of a particular pixel exceeds that of its neighbouring pixels. Such a phenomenon may occur in industrial or construction sites, where a pixel may emit more brightness temperature than its surroundings and may thus be erroneously classified as a fire pixel (figure 32).
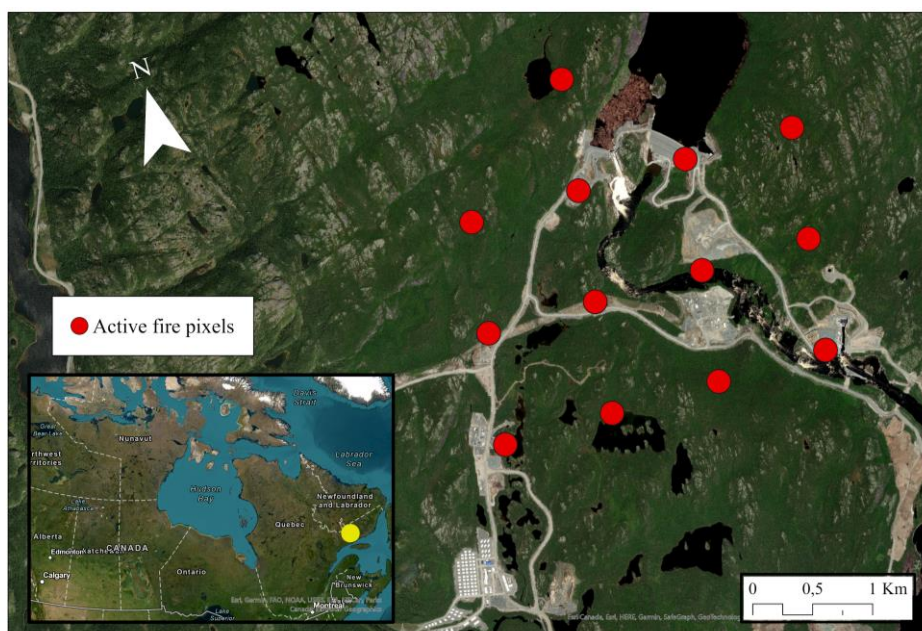
Figure 31. Example of a construction site in south-eastern part of Quebec province, where the area was identified as fire pixels due the brightness temperature release from these pixels being higher than the neighbouring pixels, at the time scanned by MODIS. Overview map shows the location of the main map in yellow.

Furthermore, this study found an example of fire pixels being erroneously classified as such, in the Copper River in southern Alaska. This error could be attributed to factors such as the sun glint over small bodies of water, wet soil, cirrus cloud and bare soil which can cause false alarms (Giglio et al., 2003). Since the Copper River is a large water body and the area where these fire pixels are located in the middle part of the river where the water seems shallower,

45

and the fires can be classified due to the wet soils. Furthermore, the sun glint rejection test (section 3.1.4) for the updated fire detection algorithm in Collection 6.0 (used in this study), increased two angular thresholds to make the test slightly more aggressive in order to identify somewhat smaller and/or cooler fires than possible for the previous fire detection algorithm in Collection 5.0 (Giglio et al., 2016). In this example an area of 61 pixels were registered as fire pixels 487 times, during the course of the 20-year period from 2001-2021.
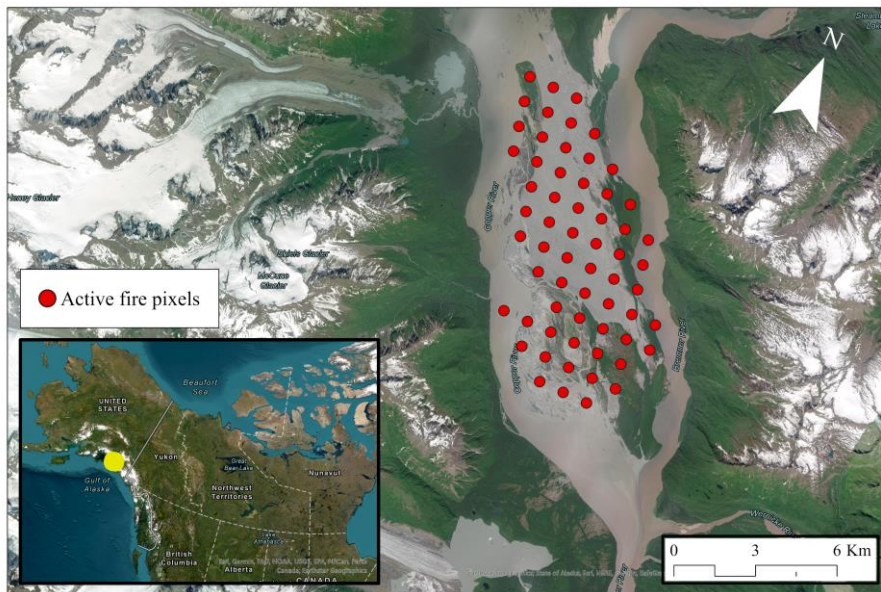
Figure 32. Map shows the river called Copper River in south central part of Alaska, where the area was identified as fire pixels due the high contrast change from the water in these pixels and the green vegetation in the neighbouring pixels, at the time scanned by MODIS. Overview map shows the location of the main map as a yellow point.

It is interesting to note that further analyses show that all the fire pixels in the figure 32 have a value of 7, indicating they were classified as low confidence fires. It is worth noting that this study did not analyse the percentage distribution of fire pixels between values 7, 8, and 9, and instead used all three values together in the analysis. This suggests that using only values 8 and 9 for fire pixels would increase the likelihood of excluding erroneously classified fires.

Moreover, in this study, only MODIS data from the Terra satellite (MOD14A2) was used, while data from the Aqua satellite (MYD14A2) was excluded due to its extensive size. Previous research conducted by Hawbaker et al. (2008) on active fire product detection rates in United States, found that Aqua detected more fires (73%) compared to Terra (66%). This is likely due to Aqua's overpass occurring at 13:30, which is closer to the peak of fire activity in

the afternoon when weather conditions are most conducive to burning, compared to Terra's overpass at 10:30. Additionally, the highest detection of fires (82%) was found when both satellites were used simultaneously (Hawbaker et al., 2008).

5.2 Spatial and temporal fire patterns in North America

The results show that most fires occur in the central (CC) and western Canada (WC) and only 5% occur in the eastern part (QLP) and 20% in Alaska (AL). Similar, fires in permafrost areas are very scarce in the eastern sector but become much more frequent further towards the west with the highest number reaching in Alaska. Additionally, the timing of the fires differs remarkably among the four sectors, with central and western Canada having fires all year around even though the majority still occurring in the summer months. Meanwhile the eastern sector and Alaska experience fires only in the summer months. Therefore, the following sections provide a thorough analysis of the findings for each subregion.

5.2.1 Quebec and Labrador Peninsula

The majority of the fires occur south of 55° latitude. This is due to vegetation not being present at higher latitudes. The tree line is considered to coincide with the 10 °C July isotherm of air temperature in the latitude range 40 to 70° (Grace et al., 2002). Furthermore, this is an area which is predominated by isolated and sporadic permafrost, and no permafrost (Obu et al., 2019), meaning that mean annual temperatures in this area are lower than -6 °C and can be as warm as 2 °C and still support permafrost. This is due to the vegetation on the surface which can act as an insulator (Shur & Jorgenson, 2007). Therefore, only isolated and sporadic permafrost zones are affected with 48% and 4%, respectively, and no fires occur in other permafrost zones (figure 17c).

Fires in 2013 occurred due to one of the driest years in the last 40 years according to the article by NASA (2013). 2013 registered the largest forest fire ever recorded in Quebec province and second largest in Canada that occurred in Eastmain, east of James Bay (Masters, 2013). According to models in Boulanger et al. (2013), this region is going to have both the most annual areas burned (AAB) and annual number of fire occurrence (OCC) per 100 kha for the years 2011-2040, 2041-2070 and 2071-2100. Dry spells are predicted most in north

and north-east of Quebec and Labrador Peninsula as well by Sushama et al. (2010), which favour more the occurrence of fires.

The mean fire latitudes have changed a degree further north from 52 to 53 degrees, and the reason might be the tree regeneration above the tree line during periods when summers are warm, such as the present time (Grace et al., 2002). Although linear regression generated from the 20-year period is heavily influenced by single year events, which vary significantly between this time period.

The results in this study show that more than 90 % of the fires occur in June and July and very little of less than 3 % occur in August (figure 19c), despite very little difference in mean temperature and mean precipitation between these months. Weather data obtained from "Weather Spark" ("Weather Spark" 2023) for La Grande Riviere Airport, located 100 km north from Eastmain where most of the fires occurred according to the heatmap, reveal that mean temperature for August (18 °C and 86 mm) is only 1 °C colder and has 8 mm more rain than July (19 °C and 78 mm). This could be due to the precipitation in August being more spread throughout the month, keeping the ground moist for longer periods of the time, making it less favourable for fires to start.

5.2.2 Central Canada

The study region of CC is extensive, and its continental climate features low annual temperatures that allow for the existence of permafrost. Additionally, the region has relatively warm and dry summers that extend the tree line further north than the QLP subregion. As a result, fires have been registered in all types of permafrost zones. However, only 7% of the fires are registered in the 39% of land cover that is continuous permafrost. This is because most of the areas with continuous permafrost in northern latitude areas are dominated by taiga or treeless tundra (Matasci et al., 2018). Discontinuous permafrost covers only 8%, sporadic 13%, and isolated 12% (figure 5b) of this study area. However, fires occurred in 9%, 23%, and 21% of these land covers, respectively (figure 20c).

The observed heatmap exhibits a strong agreement with notable large-scale wildfire events, such as the 2017 wildfire in the southeastern region of Great Slave Lake (NASA, 2017), contributing to 20% of the total fire occurrences in that specific area. Similarly, the Fort MacMurray fires in 2016 north of the Alberta city (Landis et al., 2018) represented

48

approximately 60% of all fire pixels recorded in that specific region. Additionally, the eastern region of Lake Winnipeg in 2021 (as documented in the "2021 Bloodvein River Wildfires," 2022) accounted for more than 50% of all fire events in that specific location.

The majority of fires in the CC study region are observed in areas with minimal precipitation, such as the northern regions of Saskatchewan and Alberta, as evidenced by Wang et al., (2013) and areas with the highest occurrence of dry days and dry spells, as reported by Sushama et al., (2010). The climate in Yorkton, located in the southeastern part of Saskatchewan, is akin to that of the previously mentioned zones, leading to the occurrence of fires in that region as well. Although the southwest zone, predominantly composed of grassland, also falls under this climate category, the frequency of fires observed in this area is comparatively lower. This difference may be attributed to variations in land cover, as the regions where fires occur are classified as boreal plain and taiga shield ecozones (Statistics Canada, 2021; Langor, 2019), distinct from the prairie landscape of the southwestern zone.

The mean latitudes of the fire pixels in our study exhibit a high degree of variability, ranging from 52 to nearly 60 degrees north. This range highlights the expansive nature of our study area, which is also influenced by individual major fire events occurring at varying latitudes from one year to the next. Given the considerable diversity of fire events, a 20-year period may be insufficient to observe significant shifts in fire latitude trends.

The warmer summers associated with a continental climate (section 2.2.2) lead to a wider window of fire occurrence throughout the year, as compared to the QLP study region. Although the mean month of the fire occurrences for each year shows that fires are mostly registered in June and July, emphasising that for each year fires occur mostly during these summer months (figure 22c).

5.2.3 Western Cordillera

In the WC study zone, 30% of the landcover is characterized by continuous permafrost (figure 7b), and 16% of all fires in this study region have occurred in these areas (figure 23c). This is a higher proportion compared to the CC study region, which can be attributed to the higher tree line in western Canada, reaching as high as 69 degrees north in Mackenzie Bay, Northwest Territories (Mirabel et al., 2022). Additionally, 15% of all fires in the WC study region occur in areas with discontinuous permafrost, which covers 14% of the study region, a

proportion similar to that in the CC study zone. The remaining landcover in WC is sporadic and isolated permafrost, which covers 9% and 9% of the study zone, respectively. Fires occur in these areas as well, with 7% of all fires occurring in each of these permafrost zones.

The years 2017 and 2018 marked the occurrence of the most severe wildfires in the recorded history of British Columbia (BC Wildfire Service, 2017, 2018) resulting in the burning of a vast expanse of land measuring 12,000 km^2 and 13,500 km^2, respectively (Brookes et al., 2021). Our study findings concur with this data, showing that the previously mentioned years had the highest number of wildfires. Furthermore, our results indicate that the fires in the permafrost regions during the year 2004 were consistent with the wildfires that occurred in Yukon (Government of Yukon, 2005), which resulted in a burned area of approximately 17,000 km^2. Similarly, significant fire events were observed in 2014 in the northwest of Great Slave Lake in the permafrost areas (Kochtubajda et al., 2019).

The 2004 fire season in the Yukon, Canada was severe despite above-normal snowpack during the winter. Early spring snowmelt did not benefit forest fuel moisture content due to sublimation and runoff. The drought code carry-over from the previous year was significant in some areas. The fire season became very active in June, with lightning fires and a long-range forecast of hot and dry weather. July saw high wind, record temperatures, and extreme fire behaviour, leading to a fire ban across the Yukon. August brought another wave of lightning storms, and September finally brought the fire season to a close after a summer of record-breaking events. The final area burned for the season was 5.6% of the forested region of the Yukon, 14 times the average area burned from 1950-2003 (Government of Yukon, 2005).

In a manner comparable to the wildfires that occurred in 2004, those that took place in 2017 were marked by a notably hot and dry summer, ranking highest in both regards within a time series that spans back to 1961. As a result, there was a highly extraordinary fire season that transpired in the southern Cordillera region, as highlighted by Kirchmeier-Young et al., (2019). This research indicates that the underlying cause of such anomalies is anthropogenic factors.

The mean latitudes of the fire pixels in the WC region also demonstrate a high degree of variability (figure 25a), ranging from 54 to almost 62 degrees north, similar to the CC region. This vast range emphasizes the extensive coverage of our study area and how it is influenced by major fire events that occur at different latitudes every year. With such a significant

variation in fire events, it is possible that a 20-year period may not be adequate to observe any significant changes in the trends of fire latitudes.

It appears that the mean month for annual fires has shifted earlier by half a month. However, this statistic appears more drastic since it is heavily influenced by 2002, which had less than 2% of all fires recorded during the 20-year period but had a mean month of late August.

The majority of fires were concentrated within the Interior Plateau region of British Columbia (figure 24b) which has a longer fire season today as compared with 1959-2000 (Hanes et al., 2019). This region has the lowest level of precipitation across the area, amounting to approximately 300-600 mm annually. Notably, the months spanning from May to September constitute the driest period, with an average precipitation level of less than 100 mm (Moore et al., 2008). The conditions in question create a favourable environment for fires to occur, even in the winter months of December, January, and February although as reported from Coogan et al. (2021), most of the fires occurring outside the fire season are caused by human ignition. However, there is a lack of literature reporting fire events that support these observations, implying that while certain pixels may burn during this period, they may not necessarily escalate into significant fire events.

5.2.4 Alaska

The Alaska study region has by far the most fires occurring in permafrost compared to the other regions, or 96% of the total amount that occur in this region (figure 27c). This is mainly due to the region's northern location which supports a high percentage (89%) of permafrost (figure 8b), while its continental climate categorized with warm summers, enables the vegetation growth (Mirabel et al., 2022).

The majority of fires took place in the Interior region of Alaska, which is characterized by a continental climate. This region experiences high average temperatures during the summer months, exceeding 21 °C (Shulski & Wendler, 2007). As the summer season brings about the highest temperatures in this area, it is recognized for being associated with a disproportionately large occurrence of lightning strikes that amount to over 80% of Alaska's overall lightning activity. This is likely due to the positive correlation between the incidence of lightning and temperatures that exceed 15 °C (Wendler et al., 2011). Despite the occurrence of precipitation being most common during summer season, it is limited, with an

average of only 123 mm in the summer months within the Interior of Alaska (Wendler et al., 2011).

The year with most wildfires was 2004 that was categorized with a combination of the highest mean summer temperatures recorded for the last 50 years in Fairbanks by almost 3 °C, led by a record number of almost 5 times average more lightning strikes recorded since 1986 and the third lowest precipitation recorded of only 38% for normal summer precipitation (Shulski et al., 2005). Similar to 2004, 2015 registered the second highest number of wildfires caused by warm and dry spring leading to early fire starts which continued through some of the highest temperatures recorded in June for most of the state except in the very central and eastern Interior (Strader & Alden, 2015). The Bureau of Land Management (BLM) report by Strader and Alden (2015) indicates that in 2015, wildfires burned an area of approximately 20,000 km^2, which is smaller compared to the approximately 25,000 km^2 that burned in 2004 as reported by Wendler et al. (2011). However, the result from this report reveals that the number of fire pixels registered in 2015 accounted for only 13% of all fire pixels, while in 2004, this figure was 23% (figure 27a). This disparity may be attributed to the bow tie effect, wherein the fire appears as more than one pixel when it is situated close or overlaps with other pixels (Fearns et al., 2017). Another reason could be the difference between fires registered from MODIS contra fire data from databases.

The permafrost in Alaska is especially vulnerable to wildfires, as a significant proportion of its expanse is comprised of permafrost (Jorgenson et al., 2008; Obu et al., 2019). Furthermore, the majority of fires occur in the Interior Alaska, where approximately 40% of the land area is situated on permafrost (Douglas et al., 2021). This region is mostly discontinuous permafrost which is typically within few degrees of thawing and ecosystem protected by an insulating organic soil or vegetation (Grosse et al., 2011). This protection cover is particularly vulnerable to wildfires (Nossov et al., 2013). Although, the TTOP map indicates that a portion of Interior Alaska is situated on continuous permafrost as well, where fires occur in about 14% of cases. North Alaska, which has an arctic climate and also features continuous permafrost, is another area where fires occur.

The fires that occurred in early May 2014 in the Funny River area of the Kenai National Wildlife Refuge had a significant impact on the year's overall statistics. These fires accounted for about 90% of all fires that occurred during the year, resulting in the lowest mean latitude and earliest mean fire month (figure 29b).

Since most of the fires occur during summer months in Interior Alaska and summer Tmax have shown a rise in Fairbanks since 1950 (Sulikowska et al., 2019) and the mean annual temperature are expect to increase with 4-6 °C by 2100 (Walsh et al., 2018), wildfires are expected to increase as a feedback.

5.3 Future research

The impact of fires in permafrost zones is determined by the severity and the intensity of the fire, affecting the active layer thickness (ALT) and the vegetation restauration. Furthermore, fires impact the boreal forest and the permafrost ground depending on the type of vegetation where it occurs, since different types of vegetation have different periods of post-fire regeneration. Since this study did not conduct any analysis on these fronts such as severity, intensity and the vegetation type, the importance of these is shown in the sections below with examples of how such information could have been obtained.

5.3.1 Fire severity

Apart from The Active Fire product, such as the one used in our study (MOD14A2), MODIS also provides the Burned Area product. The Burned Area product such as the latest one (MCD64A1), contains information on burning and quality at a spatial resolution of 500 meters per pixel (Giglio et al., 2020a). The product is generated by analysing daily surface reflectance data from MODIS instruments and identifying rapid changes that are indicative of recent fires. It maps the spatial extent of these fires and provides diverse quality metrics, along with a summary score for each pixel (Giglio et al., 2018). Although our study did not use the Burned Area product, it could have facilitated a more comprehensive analysis of the fires severity and provided validation for the active fire pixels that actually burned.

For example, the Burned Area product can provide valuable information on the recovery of post-fire vegetation restoration, which exhibits a strong dependence on the severity of the burn, as documented by Li et al. (2019). Light burns are generally associated with a fast recovery of the pre-fire conditions. However, severe burns the natural recovery process is very long, spanning several centuries. In such cases, the re-establishment of the original coniferous forest ecological community is possible, but not guaranteed, given the dominance of broadleaf trees (Li et al., 2019).

The active layer thickness (ALT) is highly depended on the severity of the fire as well. In permafrost regions, burned sites will have warmer soil than unburned sites for many decades, causing a long-term decrease in soil moisture content. However, light burns, which leave some dead moss and fibric layer behind, do not significantly impact permafrost (Yoshikawa et al., 2002).

Furthermore, the degree of influence on frozen grounds after a fire is determined by the threshold of organic material remaining. The thickness of moss, thermal conductivity of moss, and thawing index at the ground surface all play a role in this threshold. Severe fires can cause talik formation, which is a layer of unfrozen ground that occurs when the permafrost thaws from the top down. Once a talik forms, it is unlikely that the permafrost will recover under current climate conditions (Yoshikawa et al., 2002). A study carried in Interior Alaska in Nossov et al. (2013) reported that talik formation after severe fires was only initiated in rocky uplands and sandy lowlands. Rocky uplands and sandy lowlands responded differently to fire-induced thawing due to soil texture, with deeper thawing leading to decreased soil moisture levels. Silty uplands were more resistant to fire because the active layer had high moisture content and the ground ice had high latent heat, which slowed the thawing process and allowed the deeper active layer to absorb more heat while vegetation recovered and changed surface characteristics.

Overall, the Burned Area product offers valuable information that can enhance the understanding of post-fire vegetation restoration and the impact of fire on permafrost regions. Therefore, it is recommended that future studies incorporate this product to facilitate a more comprehensive analysis of forest fires in the boreal region.

5.3.2 Fire intensity

The Active Fire product, such as the one used in this study (MOD14A2) provides fire intensity, or otherwise known as Fire Radiative Power (FRP), which calculates the amount of energy released during the burning process (Giglio et al., 2016). In this study, we did not employ FRP, nor did we gather data on the intensity of the fires that had the most significant effects on permafrost. Consequently, our analysis treated all fire pixels as having equal impact on permafrost, which could lead to inaccuracies when mapping the actual influence of fires.

For example, the restoration of post-fire vegetation is closely associated with the intensity of the fire, as demonstrated by Shi et al., (2019) conducted in Northeast China's Larch Forest. The study found that high-temperature fires can result in the destruction of most seeds and cones. Consequently, the regeneration of dominant species may rely on seed from external sources. Under normal circumstances, wetlands may develop in ravines and low-lying depressions after a fire, and the intensity of the fire is a significant factor in the expansion of such wetlands in valley sites with surface permafrost. In areas heavily affected by fire with a substantial loss of seed banks, the formation of new wetlands may impede seed movement, potentially contributing to the failure of tree regeneration in burned permafrost areas (Brown & Johnstone, 2012). A higher water table and increased distance between tree seed sources and burned areas, caused reduced tree recruitment following permafrost thaw. Therefore, the use of fire intensity, such as FRP, is crucial in accurately assessing the impact of fires on permafrost and associated ecosystems.

5.3.3 Fire impacts on vegetation

Our study excludes fires that occur within particular ecozones or types of vegetation, which may offer a more thorough comprehension of the ecozones and vegetation types that are most impacted and prone to intense and severe burning.

Viereck et al. (2008) (Li et al., 2021) conducted a study on a black spruce forest in Alaska to assess post-fire recovery from 1971 to 2006. They found that after 36 years, vegetation had been essentially restored to its original state, with an increase in plant species, particularly mosses. Gibson et al. (2016) examined a black spruce ecosystem in interior Alaska and found that ten years after a fire, areas with more severe combustion had a higher abundance of deciduous tree species, resulting in thinner organic layer soils. However, the post-fire abundance of evergreen shrubs and Sphagnum mosses was lower. Deciduous trees dominated the seedling community in severely-burned areas, likely due to changes in seedbed quality (Johnstone et al., 2010). This pattern was observed in Alaska, Northeast China, and northern Mongolia, where the vegetation changed to deciduous forest over time, with a shift in species composition and incomplete recovery to pre-fire levels (Barrett et al., 2011; Li et al., 2019). Therefore, excluding fires in certain ecozones or vegetation types may limit our understanding of the impact of fires on these areas and their recovery over time.

6   Conclusion

The main objective of this thesis was to examine the fire patterns in permafrost regions in North America using the Active Fire product generated by MODIS. The study investigated (1) the percentage of all fires in 2001-2021 for different permafrost zones and for a given year, (2) percentage of all fires that occurred within each year for the different permafrost zones, (3) percentage of fire distribution across different permafrost zones for 2001-2021 time period, (4) the spatial distribution of fires, (5) the mean yearly latitudinal distribution for each year between 2001-2021, (6) the mean monthly distribution of fires for each year between 2001-2021 and (7) the month distribution of all fires that occurred in the 2001-2021 time period, in the four subregions of North America.

(1) The study discovered that fire is present in all permafrost areas, with vegetation being the decisive factor in AL, CC, and WC regardless of the permafrost type. The July 10°C isotherm determines the tree line, and areas with a maritime climate influence and cold summers do not support forest growth in high latitudes where permafrost covers exist, unlike other study areas with a more continental climate. Fires in QLP occurred mainly in isolated and, as little as 4%, sporadic permafrost.

(2) The percentage distribution of fires with respect to permafrost zones within the year they occurred varies most in AL, where every year had a different combination of fires in different permafrost zones, while the most homogenous was QLP with every year having almost 50-50% between no permafrost and isolated permafrost. Meanwhile, the highest percentage almost every year had non-permafrost areas in both CC and WC.

(3) The majority of fires occurred in CC with 39%, followed by WC with 36%, AL with 20%, and only 5% in QLP of the total fires detected in these four subregions. In comparison with the permafrost percentage zone, fires in permafrost occurred most in AL with 96% of total fires in this region, followed by CC with 59%. In QLP, permafrost fires occurred 52% in permafrost, and the least permafrost fires occurred in WC with 45%.

(4) The heatmap density for the four subregions shows that fires occurred most in the east of James Bay in QLP, south of the Great Slave Lake, and continuing to the border with Alberta in CC, Interior plains in British Columbia in WC, and east of Interior Alaska in AL. All these regions correspond well with a climate favourable for fires.

(5) (6) The study results indicate that the trends in permafrost and non-permafrost grounds are significantly impacted by specific events occurring in a single year, and no conclusive

trends can be inferred from the 20-year period examined in this study. Due to the 20-year period, it is not possible to discern any patterns in either the mean latitudinal trend or the mean temporal trend changes during this period.

(7) Fires occur all year round in WC and CC, with as much as 33% and 29%, respectively, outside the summer months (June, July, August). Meanwhile QLP and AL register only 4% and 5% of fires, respectively, outside the summer months.

Although MODIS has its limitations, it can still easily identify major fire events every year, which is evident when compared to normal years. However, the intensity and severity of the fire cannot be accurately determined without additional fire products such as Burned Area product and FRP. Additionally, fire trends cannot be fully analysed without incorporating other fire records databases such as CNFDB and NIFC, which date back to before the use of MODIS.

Bibliography

Abraham, K. F., & Keddy, C. J. (2005). The Hudson Bay Lowland. In L. H. Fraser & P. A. Keddy (Eds.), *The World's Largest Wetlands: Ecology and Conservation* (pp. 118–148). Cambridge University Press. https://doi.org/10.1017/CBO9780511542091.005

Albert-Green, A., Dean, C. B., Martell, D. L., & Woolford, D. G. (2013). A methodology for investigating trends in changes in the timing of the fire season with applications to lightning-caused forest fires in Alberta and Ontario, Canada. *Canadian Journal of Forest Research*, *43*(1), 39–45. https://doi.org/10.1139/cjfr-2011-0432

ArcGIS Pro. (n.d.). Pro.Arcgis.Com. Retrieved 4 May 2023, from https://pro.arcgis.com/en/pro-app/latest/help/mapping/layer-properties/heat-map.htm

Barrett, K., McGuire, A. D., Hoy, E. E., & Kasischke, E. S. (2011). Potential shifts in dominant forest cover in interior Alaska driven by variations in fire severity. *Ecological Applications*, *21*(7), 2380–2396. https://doi.org/10.1890/10-0896.1

Batenipour, H., Kurz, D., Alfaro, M., Graham, J., & Ng, T. (2009). Highway Embankment on Degrading Permafrost. In *Proceedings of the International Conference on Cold Regions Engineering* (p. 521). https://doi.org/10.1061/41072(359)50

BC Wildfire Service, B. W. (2017). *Wildfire Season Summary—Province of British Columbia*. Province of British Columbia. https://www2.gov.bc.ca/gov/content/safety/wildfire-status/about-bcws/wildfire-history/wildfire-season-summary

BC Wildfire Service, B. W. (2018). *Wildfire Season Summary—Province of British Columbia*. Province of British Columbia. https://www2.gov.bc.ca/gov/content/safety/wildfire-status/about-bcws/wildfire-history/wildfire-season-summary

Beck, H. E., Zimmermann, N. E., McVicar, T. R., Vergopolan, N., Berg, A., & Wood, E. F. (2018). Present and future Köppen-Geiger climate classification maps at 1-km resolution. *Scientific Data*, *5*(1), Article 1. https://doi.org/10.1038/sdata.2018.214

Bevington, A., & Lewkowicz, A. (2015). *Assessment of a land cover driven TTOP model for mountain and lowland permafrost using field data, southern Yukon and northern British Columbia, Canada.*

Boulanger, Y., Gauthier, S., Gray, D. R., Le Goff, H., Lefort, P., & Morissette, J. (2013). Fire regime zonation under current and future climate over eastern Canada. *Ecological Applications*, *23*(4), 904–923. https://doi.org/10.1890/12-0698.1

Brookes, W., Daniels, L. D., Copes-Gerbitz, K., Baron, J. N., & Carroll, A. L. (2021). A Disrupted Historical Fire Regime in Central British Columbia. *Frontiers in Ecology and Evolution*, *9*. https://www.frontiersin.org/articles/10.3389/fevo.2021.676961

Brown, C. D., & Johnstone, J. F. (2012). Once burned, twice shy: Repeat fires reduce seed availability and alter substrate constraints on Picea mariana regeneration. *Forest Ecology and Management*, *266*, 34–41. https://doi.org/10.1016/j.foreco.2011.11.006

Brown, D. R. N., Jorgenson, M. T., Douglas, T. A., Romanovsky, V. E., Kielland, K., Hiemstra, C., Euskirchen, E. S., & Ruess, R. W. (2015). Interactive effects of wildfire and climate on permafrost degradation in Alaskan lowland forests. *Journal of Geophysical Research: Biogeosciences*, *120*(8), 1619–1637. https://doi.org/10.1002/2015JG003033

Brown, R. (2010). *Permafrost Investigations in Saskatchewan and Manitoba*. https://www.researchgate.net/publication/44060072_Permafrost_Investigations_in_Sa skatchewan_and_Manitoba

Brown, R. J. E. (1979). Permafrost distribution in the southern part of the discontinuous zone in Quebec and Labrador. *Géographie Physique et Quaternaire*, *33*(3–4), 279–289.

Chen, D., Pereira, J., Pirotti, F., & Masiero, A. (2017). Mapping fire regimes in China using MODIS active fire and burned area data. *Applied Geography*, *85*. https://doi.org/10.1016/j.apgeog.2017.05.013

Chen, Y., Velicogna, I., Famiglietti, J. S., & Randerson, J. T. (2013). Satellite observations of terrestrial water storage provide early warning information about drought and fire season severity in the Amazon. *Journal of Geophysical Research: Biogeosciences*, *118*(2), 495–504. https://doi.org/10.1002/jgrg.20046

Colpron, M., & Nelson, J. L. (2021). Northern Cordillera: Canada and Alaska☆. In D. Alderton & S. A. Elias (Eds.), *Encyclopedia of Geology (Second Edition)* (pp. 93–106). Academic Press. https://doi.org/10.1016/B978-0-12-409548-9.12502-3

Coogan, S. C. P., Daniels, L. D., Boychuk, D., Burton, P. J., Flannigan, M. D., Gauthier, S., Kafka, V., Park, J. S., & Wotton, B. M. (2021). Fifty years of wildland fire science in Canada. *Canadian Journal of Forest Research*, *51*(2), 283–302. https://doi.org/10.1139/cjfr-2020-0314

Douglas, T. A., Hiemstra, C. A., Anderson, J. E., Barbato, R. A., Bjella, K. L., Deeb, E. J., Gelvin, A. B., Nelsen, P. E., Newman, S. D., Saari, S. P., & Wagner, A. M. (2021). Recent degradation of interior Alaska permafrost mapped with ground surveys, geophysics, deep drilling, and repeat airborne lidar. *The Cryosphere*, *15*(8), 3555–3575. https://doi.org/10.5194/tc-15-3555-2021

Erives, H., Xiong, X., Sun, J., Esposito, J., Xiong, S., & Barnes, W. (2004). Terra MODIS RSB on-orbit calibration and performance: Four years of data. *Proceedings of SPIE - The International Society for Optical Engineering*, *5570*. https://doi.org/10.1117/12.565060

Fearns, P., Greenwood, J., Chedzey, H., Dorji, P., Broomhall, M., King, E., Cherukuru, N., Hardman-Mountford, N., & Antoine, D. (2017). *Remote Sensing for Environmental Monitoring and Management in the Kimberley WAMSI Kimberley Marine Research Program Final Report Project 1.4*. https://doi.org/10.13140/RG.2.2.21163.13603

Fusco, E. J., Finn, J. T., Abatzoglou, J. T., Balch, J. K., Dadashi, S., & Bradley, B. A. (2019). Detection rates and biases of fire observations from MODIS and agency reports in the conterminous United States. *Remote Sensing of Environment*, *220*, 30–40. https://doi.org/10.1016/j.rse.2018.10.028

Gibson, C. M., Turetsky, M. R., Cottenie, K., Kane, E. S., Houle, G., & Kasischke, E. S. (2016). Variation in plant community composition and vegetation carbon pools a decade following a severe fire season in interior Alaska. *Journal of Vegetation Science*, *27*(6), 1187–1197. https://doi.org/10.1111/jvs.12443

Giglio, L., Boschetti, L., Roy, D., Hoffmann, A. A., Humber, M., & Hall, J. V. (2020). *Collection 6 MODIS Burned Area Product User's Guide Version 1.3*. https://lpdaac.usgs.gov/documents/875/MCD64_User_Guide_V6.pdf

Giglio, L., Boschetti, L., Roy, D. P., Humber, M. L., & Justice, C. O. (2018). The Collection 6 MODIS burned area mapping algorithm and product. *Remote Sensing of Environment*, *217*, 72–85. https://doi.org/10.1016/j.rse.2018.08.005

Giglio, L., Descloitres, J., Justice, C. O., & Kaufman, Y. J. (2003). An Enhanced Contextual Fire Detection Algorithm for MODIS. *Remote Sensing of Environment*, *87*(2), 273–282. https://doi.org/10.1016/S0034-4257(03)00184-6

Giglio, L., Schroeder, W., & Hall, J. V. (2020). *MODIS Collection 6 Active Fire Product User's Guide Revision C*. 63.

Giglio, L., Schroeder, W., & Justice, C. O. (2016). The collection 6 MODIS active fire detection algorithm and fire products. *Remote Sensing of Environment*, *178*, 31–41. https://doi.org/10.1016/j.rse.2016.02.054

Gillett, N. P., Weaver, A. J., Zwiers, F. W., & Flannigan, M. D. (2004). Detecting the effect of climate change on Canadian forest fires. *Geophysical Research Letters*, *31*(18). https://doi.org/10.1029/2004GL020876

Government of Yukon. (2005). *2004 Wildland Fire Review- Final Report*. https://emrlibrary.gov.yk.ca/cs/2004_wildland_fire_review.pdf

Grace, J., Beringer, F., & Nagy, L. (2002). Impacts of Climate Change on the Tree Line. *Annals of Botany*, *90*(4), 537–544. https://doi.org/10.1093/aob/mcf222

Grosse, G., Romanovsky, V., Jorgenson, T., Walter Anthony, K., Brown, J., & Overduin, P. (2011). Vulnerability and Feedbacks of Permafrost to Climate Change. *EOS Transactions*, *92*. https://doi.org/10.1029/2011EO090001

Hanes, C. C., Wang, X., Jain, P., Parisien, M.-A., Little, J. M., & Flannigan, M. D. (2019). Fire-regime changes in Canada over the last half century. *Canadian Journal of Forest Research*, *49*(3), 256–269. https://doi.org/10.1139/cjfr-2018-0293

Harden, J. W., Manies, K. L., Turetsky, M. R., & Neff, J. C. (2006). Effects of wildfire and permafrost on soil organic matter and soil climate in interior Alaska. *Global Change Biology*, *12*(12), 2391–2403. https://doi.org/10.1111/j.1365-2486.2006.01255.x

Hasler, A., Geertsema, M., Foord, V., Gruber, S., & Noetzli, J. (2015). The influence of surface characteristics, topography and continentality on mountain permafrost in British Columbia. *The Cryosphere*, *9*, 1025–1038. https://doi.org/10.5194/tc-9-1025-2015

Hawbaker, T. J., Radeloff, V. C., Syphard, A. D., Zhu, Z., & Stewart, S. I. (2008). Detection rates of the MODIS active fire product in the United States. In *Remote Sensing of Environment* (Vol. 112, Issue 5, p. 9). https://doi.org/10.1016/j.rse.2007.12.008

Johnstone, J. F., Hollingsworth, T. N., Chapin Iii, F. S., & Mack, M. C. (2010). Changes in fire regime break the legacy lock on successional trajectories in Alaskan boreal forest. *Global Change Biology*, *16*(4), 1281–1295. https://doi.org/10.1111/j.1365-2486.2009.02051.x

Jorgenson, M., Yoshikawa, K., Kanevskiy, M., Shur, Y., Romanovsky, V., Marchenko, S., Grosse, G., Brown, J., & Jones, B. (2008). Permafrost characteristics of Alaska. In *Proceedings of the Ninth International Conference on Permafrost*.

Justice, C. O., Giglio, L., Korontzi, S., Owens, J., Morisette, J. T., Roy, D., Descloitres, J., Alleaume, S., Petitcolin, F., & Kaufman, Y. (2002). The MODIS fire products. *Remote Sensing of Environment*, *83*(1), 244–262. https://doi.org/10.1016/S0034-4257(02)00076-7

Justice, C. O., Townshend, J., Vermote, E., Ed, M., Wolfe, R., Saleous, N., Roy, D., & Morisette, J. (2002). An overview of MODIS Land data processing and product status. *Remote Sensing of Environment*, *83*, 3–15. https://doi.org/10.1016/S0034-4257(02)00084-6

Kasischke, E. S., & Turetsky, M. R. (2006). Recent changes in the fire regime across the North American boreal region—Spatial and temporal patterns of burning across Canada and Alaska. *Geophysical Research Letters*, *33*(9). https://doi.org/10.1029/2006GL025677

Kasischke, E. S., Verbyla, D. L., Rupp, T. S., McGuire, A. D., Murphy, K. A., Jandt, R., Barnes, J. L., Hoy, E. E., Duffy, P. A., Calef, M., & Turetsky, M. R. (2010). Alaska's changing fire regime — implications for the vulnerability of its boreal forestsThis article is one of a selection of papers from The Dynamics of Change in Alaska's Boreal Forests: Resilience and Vulnerability in Response to Climate Warming. *Canadian Journal of Forest Research*, *40*(7), 1313–1324. https://doi.org/10.1139/X10-098

Kaufman, Y. J., Justice, C. O., Flynn, L. P., Kendall, J. D., Prins, E. M., Giglio, L., Ward, D. E., Menzel, W. P., & Setzer, A. W. (1998). Potential global fire monitoring from EOS-MODIS. *Journal of Geophysical Research: Atmospheres*, *103*(D24), 32215–32238. https://doi.org/10.1029/98JD01644

Kirchmeier-Young, M. C., Gillett, N. P., Zwiers, F. W., Cannon, A. J., & Anslow, F. S. (2019). Attribution of the Influence of Human-Induced Climate Change on an Extreme Fire Season. *Earth's Future*, *7*(1), 2–10. https://doi.org/10.1029/2018EF001050

Kirchmeier-Young, M. C., Zwiers, F. W., Gillett, N. P., & Cannon, A. J. (2017). Attributing extreme fire risk in Western Canada to human emissions. *Climatic Change*, *144*(2), 365–379. https://doi.org/10.1007/s10584-017-2030-0

Kochtubajda, B., Stewart, R. E., Flannigan, M. D., Bonsal, B. R., Cuell, C., & Mooney, C. J. (2019). An Assessment of Surface and Atmospheric Conditions Associated with the

Extreme 2014 Wildfire Season in Canada's Northwest Territories. *Atmosphere-Ocean*, *57*(1), 73–90. https://doi.org/10.1080/07055900.2019.1576023

La Grande-4 Airport Climate, Weather By Month, Average Temperature (Canada)—Weather Spark. (n.d.). Retrieved 1 May 2023, from https://weatherspark.com/y/149583/Average-Weather-at-La-Grande-4-Airport-Canada-Year-Round

Langor, D. (2019). The diversity of terrestrial arthropods in Canada. *ZooKeys*, *819*, 9–40. https://doi.org/10.3897/zookeys.819.31947

Li, X., Jin, H., He, R., Huang, Y., Wang, H., Luo, D., Jin, X., Lü, L., Wang, L., Li, W., Wei, C., Chang, X., Yang, S., & Yu, S. (2019). Effects of forest fires on the permafrost environment in the northern Da Xing'anling (Hinggan) mountains, Northeast China. *Permafrost and Periglacial Processes*, *30*(3), 163–177. https://doi.org/10.1002/ppp.2001

Li, X.-Y., Jin, H.-J., Wang, H.-W., Marchenko, S. S., Shan, W., Luo, D.-L., He, R.-X., Spektor, V., Huang, Y.-D., Li, X.-Y., & Jia, N. (2021). Influences of forest fires on the permafrost environment: A review. *Advances in Climate Change Research*, *12*(1), 48–65. https://doi.org/10.1016/j.accre.2021.01.001

Lindgren, P. R., Farquharson, L. M., Romanovsky, V. E., & Grosse, G. (2021). Landsat-based lake distribution and changes in western Alaska permafrost regions between the 1970s and 2010s. *Environmental Research Letters*, *16*(2), 025006. https://doi.org/10.1088/1748-9326/abd270

Mahdianpari, M., Brisco, B., Granger, J., Mohammadimanesh, F., Salehi, B., Banks, S. N., Homayouni, S., & Bourgeau-Chavez, L. (2020). The Second Generation Canadian Wetland Inventory Map at 10 Meters Resolution Using Google Earth Engine. *Canadian Journal of Remote Sensing*, *46*. https://doi.org/10.1080/07038992.2020.1802584

Masters, J. (2013). *Canada's 2nd Largest Fire on Record Spreading Smoke to Europe | Category 6^{TM}*. Weather Underground. https://www.wunderground.com/blog/JeffMasters/canadas-2nd-largest-fire-on-record-spreading-smoke-to-europe.html

Matasci, G., Hermosilla, T., Wulder, M. A., White, J. C., Coops, N. C., Hobart, G. W., & Zald, H. S. J. (2018). Large-area mapping of Canadian boreal forest cover, height, biomass and other structural attributes using Landsat composites and lidar plots.

Remote Sensing of Environment, 209, 90–106. https://doi.org/10.1016/j.rse.2017.12.020

MATLAB. (n.d.). Mathworks.Com. Retrieved 4 May 2023, from https://se.mathworks.com/discovery/what-is-matlab.html

Mirabel, A., Girardin, M. P., Metsaranta, J., Campbell, E. M., Arsenault, A., Reich, P. B., & Way, D. (2022). New tree-ring data from Canadian boreal and hemi-boreal forests provide insight for improving the climate sensitivity of terrestrial biosphere models. Science of The Total Environment, 851, 158062. https://doi.org/10.1016/j.scitotenv.2022.158062

Moore, R. D., Spittlehouse, D., Whitfield, P., & Stahl, K. (2008). Weather and Climate. In Draft (pp. 3–55). https://www.researchgate.net/publication/255712273_Weather_and_Climate

Muller, S. W. (1947). Permafrost; or, Permanently frozen ground and related engineering problems. J.W. Edwards. https://nrc-publications.canada.ca/eng/view/ft/?id=f69708cf-4c0f-4d8b-9126-c43cb7b89a6e

NASA. (2009, September 20). NASA Scientific Visualization Studio—Aqua Satellite and MODIS Swath. SVS. https://svs.gsfc.nasa.gov/3348

NASA. (2013). Quebec fires continue raging. https://phys.org/news/2013-07-quebec-raging.html

NASA MODIS. (n.d.). MODIS Land Team Home Page. Retrieved 25 April 2023, from https://modis-land.gsfc.nasa.gov/MODLAND_grid.html

NASA MODIS Web. (n.d.). Retrieved 4 May 2023, from https://modis.gsfc.nasa.gov/data/dataprod/

Nossov, D., Jorgenson, M., Kielland, K., & Kanevskiy, M. (2013). Edaphic and microclimatic controls over permafrost response to fire in interior Alaska. Environmental Research Letters, 8, 035013. https://doi.org/10.1088/1748-9326/8/3/035013

Obu, J., Westermann, S., Bartsch, A., Berdnikov, N., Christiansen, H. H., Dashtseren, A., Delaloye, R., Elberling, B., Etzelmüller, B., Kholodov, A., Khomutov, A., Kääb, A., Leibman, M. O., Lewkowicz, A. G., Panda, S. K., Romanovsky, V., Way, R. G., Westergaard-Nielsen, A., Wu, T., … Zou, D. (2019). Northern Hemisphere permafrost map based on TTOP modelling for 2000–2016 at 1 km2 scale. Earth-Science Reviews, 193, 299–316. https://doi.org/10.1016/j.earscirev.2019.04.023

Overland, J. E., Wang, M., Walsh, J. E., & Stroeve, J. C. (2014). Future Arctic climate changes: Adaptation and mitigation time scales. *Earth's Future*, *2*(2), 68–74. https://doi.org/10.1002/2013EF000162

Pastick, N. J., Jorgenson, M. T., Wylie, B. K., Nield, S. J., Johnson, K. D., & Finley, A. O. (2015). Distribution of near-surface permafrost in Alaska: Estimates of present and future conditions. *Remote Sensing of Environment*, *168*, 301–315. https://doi.org/10.1016/j.rse.2015.07.019

Peterson, D., Hyer, E., & Wang, J. (2014). Quantifying the potential for high-altitude smoke injection in the North American boreal forest using the standard MODIS fire products and subpixel-based methods. *Journal of Geophysical Research: Atmospheres*, *119*(6), 3401–3419. https://doi.org/10.1002/2013JD021067

Rowe, J. S., & Scotter, G. W. (1973). Fire in the boreal forest. *Quaternary Research*, *3*(3), 444–464. https://doi.org/10.1016/0033-5894(73)90008-2

Salomonson, V. V., Barnes, W., & Masuoka, E. J. (2006). Introduction to MODIS and an Overview of Associated Activities. In J. J. Qu, W. Gao, M. Kafatos, R. E. Murphy, & V. V. Salomonson (Eds.), *Earth Science Satellite Remote Sensing: Vol. 1: Science and Instruments* (pp. 12–32). Springer. https://doi.org/10.1007/978-3-540-37293-6_2

Saucier, J.-P. (2007). *Defining the Boreal in the Ecological Land Classification for Québec*. https://www.researchgate.net/publication/269095315_Defining_the_Boreal_in_the_Ec ological_Land_Classification_for_Quebec

Schroeder, W., Prins, E., Giglio, L., Csiszar, I., Schmidt, C., Morisette, J., & Morton, D. (2008). Validation of GOES and MODIS active fire detection products using ASTER and ETM+ data. *Remote Sensing of Environment*, *112*(5), 2711–2726. https://doi.org/10.1016/j.rse.2008.01.005

Shi, L., Dech, J. P., Liu, H., Zhao, P., Bayin, D., & Zhou, M. (2019). Post-fire vegetation recovery at forest sites is affected by permafrost degradation in the Da Xing'an Mountains of northern China. *Journal of Vegetation Science*, *30*(5), 940–949. https://doi.org/10.1111/jvs.12780

Shulski, M., & Wendler, G. (2007). *The Climate of Alaska*. University of Alaska Press.

Shulski, M., Wendler, G., Alden, S., & Larkin, N. (2005). Alaska's exceptional 2004 fire season. *Joint Meeting of the Sixth Symposium on FIre and Forest Meteorology and the 19th Interior West Fire Council Meeting*.

https://www.researchgate.net/publication/237726895_Alaska%27s_exceptional_2004
_fire_season

Shur, Y. L., & Jorgenson, M. T. (2007). Patterns of permafrost formation and degradation in relation to climate and ecosystems. *Permafrost and Periglacial Processes*, *18*(1), 7–19. https://doi.org/10.1002/ppp.582

Slaymaker, O., Acton, D. F., Brookes, I. a, French, H., & Ryder, J. m. (2023). *Physiographic Regions*. The Canadian Encyclopedia. https://www.thecanadianencyclopedia.ca/en/article/physiographic-regions

Smith, S. l., Romanovsky, V. e., Lewkowicz, A. g., Burn, C. r., Allard, M., Clow, G. d., Yoshikawa, K., & Throop, J. (2010). Thermal state of permafrost in North America: A contribution to the international polar year. *Permafrost and Periglacial Processes*, *21*(2), 117–135. https://doi.org/10.1002/ppp.690

Stafford, J. M., Wendler, G., & Curtis, J. (2000). Temperature and precipitation of Alaska: 50 year trend analysis. *Theoretical and Applied Climatology*, *67*(1), 33–44. https://doi.org/10.1007/s007040070014

Statistics Canada. (2021). *Terrestrial ecozones and ecoprovinces of Canada*. https://www.statcan.gc.ca/en/subjects/standard/environment/elc/2017-map

Strader, H., & Alden, S. (2015). *2015 Fire Season Weather Summary*. https://fire.ak.blm.gov/content/Weather%20Folder/Fire%20Season%20Summaries/2015%20Fire%20Season.pdf

Sulikowska, A., Walawender, J. P., & Walawender, E. (2019). Temperature extremes in Alaska: Temporal variability and circulation background. *Theoretical and Applied Climatology*, *136*(3), 955–970. https://doi.org/10.1007/s00704-018-2528-z

Sushama, L., Khaliq, N., & Laprise, R. (2010). Dry spell characteristics over Canada in a changing climate as simulated by the Canadian RCM. *Global and Planetary Change*, *74*(1), 1–14. https://doi.org/10.1016/j.gloplacha.2010.07.004

Tarnocai, C., Canadell, J. G., Schuur, E. a. G., Kuhry, P., Mazhitova, G., & Zimov, S. (2009). Soil organic carbon pools in the northern circumpolar permafrost region. *Global Biogeochemical Cycles*, *23*(2). https://doi.org/10.1029/2008GB003327

Taylor, A., & Judge, A. (1979). Permafrost studies in northern Québec. *Géographie Physique et Quaternaire*, *33*(3–4), 245–251. https://doi.org/10.7202/1000361ar

Turetsky, M. R., Kane, E. S., Harden, J. W., Ottmar, R. D., Manies, K. L., Hoy, E., & Kasischke, E. S. (2011). Recent acceleration of biomass burning and carbon losses in

Alaskan forests and peatlands. *Nature Geoscience*, *4*(1), Article 1. https://doi.org/10.1038/ngeo1027

Vadrevu, K. P., Ellicott, E., Giglio, L., Badarinath, K. V. S., Vermote, E., Justice, C., & Lau, W. K. M. (2012). Vegetation fires in the himalayan region – Aerosol load, black carbon emissions and smoke plume heights. *Atmospheric Environment*, *47*, 241–251. https://doi.org/10.1016/j.atmosenv.2011.11.009

Veraverbeke, S., Rogers, B. M., Goulden, M. L., Jandt, R. R., Miller, C. E., Wiggins, E. B., & Randerson, J. T. (2017). Lightning as a major driver of recent large fire years in North American boreal forests. *Nature Climate Change*, *7*(7), Article 7. https://doi.org/10.1038/nclimate3329

Vincent, W. F., Lemay, M., & Allard, M. (2017). Arctic permafrost landscapes in transition: Towards an integrated Earth system approach. *Arctic Science*, *3*(2), 39–64. https://doi.org/10.1139/as-2016-0027

Walsh, J. E., Bhatt, U. S., Littell, J. S., Leonawicz, M., Lindgren, M., Kurkowski, T. A., Bieniek, P. A., Thoman, R., Gray, S., & Rupp, T. S. (2018). Downscaling of climate model output for Alaskan stakeholders. *Environmental Modelling & Software*, *110*, 38–51. https://doi.org/10.1016/j.envsoft.2018.03.021

Wang, S., Yang, Y., Luo, Y., & Rivera, A. (2013). Spatial and seasonal variations in evapotranspiration over Canada's landmass. *Hydrology and Earth System Sciences*, *17*(9), 3561–3575. https://doi.org/10.5194/hess-17-3561-2013

Wendler, G., Conner, J., Moore, B., Shulski, M., & Stuefer, M. (2011). Climatology of Alaskan wildfires with special emphasis on the extreme year of 2004. *Theoretical and Applied Climatology*, *104*(3), 459–472. https://doi.org/10.1007/s00704-010-0357-9

Yoshikawa, K., Bolton, W. R., Romanovsky, V. E., Fukuda, M., & Hinzman, L. D. (2002). Impacts of wildfire on the permafrost in the boreal forests of Interior Alaska. *Journal of Geophysical Research: Atmospheres*, *107*(D1), FFR 4-1-FFR 4-14. https://doi.org/10.1029/2001JD000438

Zhang, T., Heginbottom, J. A., Barry, R. G., & Brown, J. (2000). Further statistics on the distribution of permafrost and ground ice in the Northern Hemisphere. *Polar Geography*, *24*(2), 126–131. https://doi.org/10.1080/10889370009377692

Zhang, Y., Wolfe, S. A., Morse, P. D., Olthof, I., & Fraser, R. H. (2015). Spatiotemporal impacts of wildfire and climate warming on permafrost across a subarctic region,

Canada. *Journal of Geophysical Research: Earth Surface*, *120*(11), 2338–2356. https://doi.org/10.1002/2015JF003679

Appendix A

The following script is used to download the MODIS Active Fire product MOD14A2 used in the study. The code furthermore shows the 20-year period of downloaded data with additional information such as the MODIS tiles and the website where it downloaded from.

```
startdate=datenum(2001,01,01);
enddate=datenum(2021,12,31);


%path= '/var/sshfs/jaroslav-nird/MODIS_006/'
path= 'M:\pc\Dokumenter\MATLAB\MODIS_LST/';

%, 'CertificateFilename','/etc/pki/ca-trust/extracted/pem/tls-ca-bundle.pem'
options = weboptions('Username','XXXXX','Password','XXXXXXXX', 'Timeout', 200);


%Northern America
all_tiles =
['h10v02';'h10v03';'h11v02';'h12v02';'h13v02';'h11v03';'h12v03';'h13v03';'h14v02';
'h14v03'];



for tile_count=1:size(all_tiles,1)

    tile=all_tiles(tile_count,:);
    mkdir([path tile])



    for i=startdate:1:enddate
        DOY=num2str(i-datenum(datestr(i,'yyyy'),'yyyy')+1001);

        try
            str=webread(['https://e4ftl01.cr.usgs.gov/MOLT/MOD14A2.006/'
datestr(i, 'yyyy.mm.dd') '/'], options);
            test=strfind(str, ['MOD14A2.A' datestr(i, 'yyyy') DOY(2:4) '.' tile]
);
            if length(test)>=6
                fname=str(test(6):test(6)+44);
                filestr= websave([path tile '/' fname],
['https://e4ftl01.cr.usgs.gov/MOLT/MOD14A2.006/' datestr(i, 'yyyy.mm.dd') '/'
fname], options);
                disp([fname ' downloaded'])
            end
        catch
            disp(['folder ' datestr(i, 'yyyy.mm.dd') ' not available'])
        end

    end

end
```

70

Appendix B

The main script that is used to retreat relevant information from the MODSI Active Fire product. The catalogue called "fire_list" has information such as the values of the fire pixels 7,8 or 9, followed up with latitude and longitude of the pixels, as well as other temporal information such as a day of the year, month and year. The catalogue was further extended with permafrost information for every pixel such as the permafrost fraction, and the mean annual temperature.

After the catalogue was complete, different variables were obtained from it, and analyses were run.

```matlab
clear; close all; clc

% Create filename using generateFileName.m and load

date_start = datenum(2001,1,01);
date_end = datenum(2021,12,31);
satellite = 0;
tile_list =
{'h10v02';'h10v03';'h11v02';'h12v02';'h13v02';'h11v03';'h12v03';'h13v03';'h14v02';
'h14v03'};
version = 6;

fire_list = [];
for ii = 1:size(tile_list,1)
    tile = tile_list{ii,1};
    [lon,lat] = sin2ll_MOD(1200,str2num(tile(2:3)),str2num(tile(5:6)));
    path = ['m:\pc\dokumenter\MATLAB\MODIS_LST/' tile '/']; %windows

    permafrost_percentage =
hdfread(['m:\pc\dokumenter\MATLAB\MODIS_LST\TTOP/TTOP_' tile '_2000_2016.hdf'] ,
'PF_percentage');
    TTOP = hdfread(['m:\pc\dokumenter\MATLAB\MODIS_LST\TTOP/TTOP_' tile
'_2000_2016.hdf'], 'TTOP_mean');

    for yr=2001:2021\\hume.uio.no\student-
u78\milotm\pc\Dokumenter\MATLAB\MODIS_LST\h11v03
        date_start = datenum([yr,01,01]);
        date_end = datenum([yr,12,31]);
        Fire_max = zeros(1200,1200);

        for date = date_start:1:date_end
            fname = generateFileName(date, satellite, path, tile,version);

            if fname ~= 0
                FireMask = double(hdfread(fname,'FireMask'));

                index_fire = find(FireMask >=7 & FireMask <=9); % Pixel values 7,8
& 9 of FireMask
```

```matlab
                vector_fire = [FireMask(index_fire) lat(index_fire)
lon(index_fire)]; % lat & lon of the fire pixels
                vector_fire = [vector_fire index_fire];
                vector_fire = [vector_fire
zeros(size(index_fire,1),1)+str2num(tile(2:3))]; % horisontal tile
                vector_fire = [vector_fire
zeros(size(index_fire,1),1)+str2num(tile(5:6))];  % vertical tile
                vector_fire = [vector_fire zeros(size(index_fire,1),1)+yr]; % year
                vector_fire = [vector_fire zeros(size(index_fire,1),1)+date]; %
matlab date
                vector_fire = [vector_fire
month(zeros(size(index_fire,1),1)+date)];  % month of fire
                vector_fire = [vector_fire permafrost_percentage(index_fire)]; %
Permafrost procentage of the index fire
                vector_fire = [vector_fire TTOP(index_fire)]; % TTOP mean of the
index fire

                fire_list = [fire_list; vector_fire];
            end
        end

    end
end


%%

fires_discontinuous_zone1 = [];
for year=2001:2021
    index = fire_list(:,3)<=-46 & fire_list(:,3)>=-80 & fire_list(:,10)>=0.5 &
fire_list(:,10) <0.9 & fire_list(:,7)==year;
    fires_discontinuous_zone1 = [fires_discontinuous_zone1;
numel(fire_list(index,1))];
end

fires_discontinuous_zone2 = [];
for year=2001:2021
    index = fire_list(:,3)<=-80 & fire_list(:,3)>=-115 & fire_list(:,10)>=0.5 &
fire_list(:,10) <0.9 & fire_list(:,7)==year;
    fires_discontinuous_zone2 = [fires_discontinuous_zone2;
numel(fire_list(index,1))];
end

fires_discontinuous_zone3 = [];
for year=2001:2021
    index = fire_list(:,3)<=-115 & fire_list(:,3)>=-140 & fire_list(:,10)>=0.5 &
fire_list(:,10) <0.9 & fire_list(:,7)==year;
    fires_discontinuous_zone3 = [fires_discontinuous_zone3;
numel(fire_list(index,1))];
end

fires_discontinuous_zone4 = [];
for year=2001:2021
    index = fire_list(:,3)<=-140 & fire_list(:,3)>=-170 & fire_list(:,10)>=0.5 &
fire_list(:,10) <0.9 & fire_list(:,7)==year;
    fires_discontinuous_zone4 = [fires_discontinuous_zone4;
numel(fire_list(index,1))];
end
%%
```

```matlab
fires_continuous_zone1 = [];
for year=2001:2021
    index = fire_list(:,3)<=-46 & fire_list(:,3)>=-80 & fire_list(:,10)>=0.9 &
fire_list(:,7)==year;
    fires_continuous_zone1 = [fires_continuous_zone1; numel(fire_list(index,1))];
end

fires_continuous_zone2 = [];
for year=2001:2021
    index = fire_list(:,3)<=-80 & fire_list(:,3)>=-115 & fire_list(:,10)>=0.9 &
fire_list(:,7)==year;
    fires_continuous_zone2 = [fires_continuous_zone2; numel(fire_list(index,1))];
end

fires_continuous_zone3 = [];
for year=2001:2021
    index = fire_list(:,3)<=-115 & fire_list(:,3)>=-140 & fire_list(:,10)>=0.9 &
fire_list(:,7)==year;
    fires_continuous_zone3 = [fires_continuous_zone3; numel(fire_list(index,1))];
    endires_continuous_autumn_zone3 = [fires_continuous_autumn_zone3;
numel(fire_list(index,1))];
end

fires_continuous_zone4 = [];
for year=2001:2021
    index = fire_list(:,3)<=-140 & fire_list(:,3)>=-170 & fire_list(:,10)>=0.9 &
fire_list(:,7)==year;
    fires_continuous_zone4 = [fires_continuous_zone4; numel(fire_list(index,1))];
end
%%

fires_sporadic_zone1 = [];
for year=2001:2021
    index = fire_list(:,3)<=-46 & fire_list(:,3)>=-80 & fire_list(:,10)>=0.1 &
fire_list(:,10) <0.5 & fire_list(:,7)==year;
    fires_sporadic_zone1 = [fires_sporadic_zone1; numel(fire_list(index,1))];
end

fires_sporadic_zone2 = [];
for year=2001:2021
    index = fire_list(:,3)<=-80 & fire_list(:,3)>=-115 & fire_list(:,10)>=0.1 &
fire_list(:,10) <0.5 & fire_list(:,7)==year;
    fires_sporadic_zone2 = [fires_sporadic_zone2; numel(fire_list(index,1))];
end

fires_sporadic_zone3 = [];
for year=2001:2021
    index = fire_list(:,3)<=-115 & fire_list(:,3)>=-140 & fire_list(:,10)>=0.1 &
fire_list(:,10) <0.5 & fire_list(:,7)==year;
    fires_sporadic_zone3 = [fires_sporadic_zone3; numel(fire_list(index,1))];
end

fires_sporadic_zone4 = [];
for year=2001:2021
    index = fire_list(:,3)<=-140 & fire_list(:,3)>=-170 & fire_list(:,10)>=0.1 &
fire_list(:,10) <0.5 & fire_list(:,7)==year;
    fires_sporadic_zone4 = [fires_sporadic_zone4; numel(fire_list(index,1))];
end
```

```matlab
%%
fires_isolated_zone1 = [];
for year=2001:2021
    index = fire_list(:,3)<=-46 & fire_list(:,3)>=-80 & fire_list(:,10)>0 &
fire_list(:,10)<0.1 & fire_list(:,7)==year;
    fires_isolated_zone1 = [fires_isolated_zone1; numel(fire_list(index,1))];
end

fires_isolated_zone1 = [];
for year=2001:2021
    index = fire_list(:,3)<=-46 & fire_list(:,3)>=-80 & fire_list(:,10)>0 &
fire_list(:,10)<0.1 & fire_list(:,7)==year;
    fires_isolated_zone1 = [fires_isolated_zone1; numel(fire_list(index,1))];
end
fires_isolated_zone2 = [];
for year=2001:2021
    index = fire_list(:,3)<=-80 & fire_list(:,3)>=-115 & fire_list(:,10)>0 &
fire_list(:,10)<0.1 & fire_list(:,7)==year;
    fires_isolated_zone2 = [fires_isolated_zone2; numel(fire_list(index,1))];
end

fires_isolated_zone3 = [];
for year=2001:2021
    index = fire_list(:,3)<=-115 & fire_list(:,3)>=-140 & fire_list(:,10)>0 &
fire_list(:,10)<0.1 & fire_list(:,7)==year;
    fires_isolated_zone3 = [fires_isolated_zone3; numel(fire_list(index,1))];
end

fires_isolated_zone4 = [];
for year=2001:2021
    index = fire_list(:,3)<=-140 & fire_list(:,3)>=-170 & fire_list(:,10)>0 &
fire_list(:,10)<0.1 & fire_list(:,7)==year;
    fires_isolated_zone4 = [fires_isolated_zone4; numel(fire_list(index,1))];
end

%%
fires_non_permafrost_zone1 = [];
for year=2001:2021
    index = fire_list(:,3)<=-46 & fire_list(:,3)>=-80 & fire_list(:,10)<=0 &
fire_list(:,7)==year;
    fires_non_permafrost_zone1 = [fires_non_permafrost_zone1;
numel(fire_list(index,1))];
end

fires_non_permafrost_zone2 = [];
for year=2001:2021
    index = fire_list(:,3)<=-80 & fire_list(:,3)>=-115 & fire_list(:,10)<=0 &
fire_list(:,7)==year;
    fires_non_permafrost_zone2 = [fires_non_permafrost_zone2;
numel(fire_list(index,1))];
end

fires_non_permafrost_zone3 = [];
for year=2001:2021
    index = fire_list(:,3)<=-115 & fire_list(:,3)>=-140 & fire_list(:,10)<=0 &
fire_list(:,7)==year;
```

```matlab
    fires_non_permafrost_zone3 = [fires_non_permafrost_zone3;
numel(fire_list(index,1))];
end

fires_non_permafrost_zone4 = [];
for year=2001:2021
    index = fire_list(:,3)<=-140 & fire_list(:,3)>=-170 & fire_list(:,10)<=0 &
fire_list(:,7)==year;
    fires_non_permafrost_zone4 = [fires_non_permafrost_zone4;
numel(fire_list(index,1))];
end

%%
average_burn_latitude=[];
for year= 2001:2021
    index = fire_list(:,7)==year;
    average_burn_latitude =[average_burn_latitude; mean(fire_list(index,2))];
end

average_burn_latitude_zone1=[];
for year= 2001:2021
    index = fire_list(:,3)<=-46 & fire_list(:,3)>=-80 & fire_list(:,7)==year;
%index of fires between -46 and -80 longitudes for years 2001-2021
    average_burn_latitude_zone1 =[average_burn_latitude_zone1;
mean(fire_list(index,2))];
end

average_burn_latitude_zone2=[];
for year= 2001:2021
    index = fire_list(:,3)<=-80 & fire_list(:,3)>=-115 & fire_list(:,7)==year;
%index of fires between -46 and -80 longitudes for years 2001-2021
    average_burn_latitude_zone2 =[average_burn_latitude_zone2;
mean(fire_list(index,2))];
end

average_burn_latitude_zone3=[];
for year= 2001:2021
    index = fire_list(:,3)<=-115 & fire_list(:,3)>=-140 & fire_list(:,7)==year;
%index of fires between -46 and -80 longitudes for years 2001-2021
    average_burn_latitude_zone3 =[average_burn_latitude_zone3;
mean(fire_list(index,2))];
end

average_burn_latitude_zone4=[];
for year= 2001:2021
    index = fire_list(:,3)<=-140 & fire_list(:,3)>=-170 & fire_list(:,7)==year;
%index of fires between -46 and -80 longitudes for years 2001-2021
    average_burn_latitude_zone4 =[average_burn_latitude_zone4;
mean(fire_list(index,2))];
end

%%

average_burn_month_zone1=[];
for month = 1:12
    index =fire_list(:,3)<=-46 & fire_list(:,3)>=-80 & fire_list(:,9)==month;
    average_burn_month_zone1 = [average_burn_month_zone1;
numel(fire_list(index,9))];
end
```

```matlab
average_burn_month_zone2=[];
for month = 1:12
    index =fire_list(:,3)<=-80 & fire_list(:,3)>=-115 & fire_list(:,9)==month;
    average_burn_month_zone2 = [average_burn_month_zone2;
numel(fire_list(index,9))];
end

average_burn_month_zone3=[];
for month = 1:12
    index =fire_list(:,3)<=-115 & fire_list(:,3)>=-140 & fire_list(:,9)==month;
    average_burn_month_zone3 = [average_burn_month_zone3;
numel(fire_list(index,9))];
end

average_burn_month_zone4=[];
for month = 1:12
    index =fire_list(:,3)<=-140 & fire_list(:,3)>=-170 & fire_list(:,9)==month;
    average_burn_month_zone4 = [average_burn_month_zone4;
numel(fire_list(index,9))];
end
%%

average_burn_month_eachyear_zone1=[];
for year= 2001:2021
    index =fire_list(:,3)<=-46 & fire_list(:,3)>=-80 & fire_list(:,7)==year;
    average_burn_month_eachyear_zone1 =[average_burn_month_eachyear_zone1;
mean(fire_list(index,9))];
end

average_burn_month_eachyear_zone2=[];
for year= 2001:2021
    index =fire_list(:,3)<=-80 & fire_list(:,3)>=-115 & fire_list(:,7)==year;
    average_burn_month_eachyear_zone2 =[average_burn_month_eachyear_zone2;
mean(fire_list(index,9))];
end

average_burn_month_eachyear_zone3=[];
for year= 2001:2021
    index =fire_list(:,3)<=-115 & fire_list(:,3)>=-140 & fire_list(:,7)==year;
    average_burn_month_eachyear_zone3 =[average_burn_month_eachyear_zone3;
mean(fire_list(index,9))];
end
average_burn_month_eachyear_zone4=[];
for year= 2001:2021
    index =fire_list(:,3)<=-140 & fire_list(:,3)>=-170 & fire_list(:,7)==year;
    average_burn_month_eachyear_zone4 =[average_burn_month_eachyear_zone4;
mean(fire_list(index,9))];
end

%%
```

Appendix C

The MATLAB script used to generate analyses for the first subregion in the study called the Quebec and Labrador Peninsula (QLP).

```matlab
x = 1:21;

% Calculate the combined sum of all four zones
sum_fires1 = fires_permafrost_zone1 + fires_non_permafrost_zone1;
all_fires1=sum(sum_fires1);

% Normalize the data for all four zones to the range [0,100] for the whole
% sum
norm_sum_fires1 = 100*sum_fires1./all_fires1;
norm_permafrost1 = 100*fires_permafrost_zone1./all_fires1;
norm_continuous1 = 100*fires_continuous_zone1./all_fires1;
norm_discontinuous1 = 100*fires_discontinuous_zone1./all_fires1;
norm_sporadic1 = 100*fires_sporadic_zone1./all_fires1;
norm_isolated1 = 100*fires_isolated_zone1./all_fires1;
norm_non_permafrost1 = 100*fires_non_permafrost_zone1./all_fires1;


% Calculate linear regression lines for each zone
P_permafrost1 = polyfit(x, norm_permafrost1, 1);
P_continuous1 = polyfit(x, norm_continuous1, 1);
P_discontinuous1 = polyfit(x, norm_discontinuous1, 1);
P_sporadic1 = polyfit(x, norm_sporadic1, 1);
P_isolated1 = polyfit(x, norm_isolated1, 1);
P_non_permafrost1 = polyfit(x, norm_non_permafrost1, 1);

y_permafrost1=polyval(P_permafrost1,x);
y_continuous1=polyval(P_continuous1,x);
y_discontinuous1=polyval(P_discontinuous1,x);
y_sporadic1=polyval(P_sporadic1,x);
y_isolated1=polyval(P_isolated1,x);
y_non_permafrost1=polyval(P_non_permafrost1,x);


% Plot the normalized data and the linear regression lines for each zone
hfig = figure;

subplot('Position',[0.08 0.63 0.61 0.32]) %[left bottom width height]

plot(norm_non_permafrost1,'Marker','o','LineWidth',1.5)
hold on
plot(norm_isolated1,'Marker','o','LineWidth',1.5)
plot(norm_sporadic1, 'Marker','o','LineWidth',1.5)
plot(norm_discontinuous1,'Marker','o','LineWidth',1.5)
plot(norm_continuous1,'Marker','o','LineWidth',1.5)
plot(x,y_isolated1,'Color',[0.850980392156863 0.325490196078431
0.0980392156862745],...
    'LineStyle','--','LineWidth',1.5);
plot(x,y_sporadic1,'Color',[0.929411764705882 0.694117647058824
0.125490196078431],...
```

```
    'LineStyle','--','LineWidth',1.5);
plot(x,y_non_permafrost1,'Color',[0 0.447058823529412
0.741176470588235],'LineStyle','--','LineWidth',1.5);


% Add legend, title and axis labels
legend('Non Permafrost', 'Isolated
patches','Sporadic','Disontinuous','Continuous', 'Location', 'northeast')
% xlabel('Time (Year)')
ylabel('Fire pixels total (%)','FontName','Times New Roman')
title('(a)')
% Set axis limits and tick marks
xlim([1 21])
% yticks(0:10:100)
% yticklabels({'0', '10', '20', '30', '40', '50', '60', '70', '80', '90','100'})
% ylim([0  100])
xticks(1:21)
xticklabels({'2001', '2002', '2003', '2004', '2005', '2006', '2007', '2008',
'2009', '2010',...
    '2011', '2012', '2013', '2014', '2015', '2016', '2017', '2018',
'2019','2020','2021'})
set(findall(hfig,'-property','XMinorTick'),'XMinorTick','on')
xl = xlim;
xAx = get(gca,'XAxis');
xAx.MinorTickValues=linspace(xl(1),xl(2),21);
set(findall(hfig,'-property','XMinorGrid'),'XMinorGrid','on')
grid on




% Normalize the data for all four zones to the range [0,100] yearly
norm_yr_permafrost1 = 100*fires_permafrost_zone1./sum_fires1;
norm_yr_continuous1 = 100*fires_continuous_zone1./sum_fires1;
norm_yr_discontinuous1 = 100*fires_discontinuous_zone1./sum_fires1;
norm_yr_sporadic1 = 100*fires_sporadic_zone1./sum_fires1;
norm_yr_isolated1 = 100*fires_isolated_zone1./sum_fires1;
norm_yr_non_permafrost1 = 100*fires_non_permafrost_zone1./sum_fires1;

% Calculate linear regression lines for each zone
P_yr_permafrost1 = polyfit(x, norm_yr_permafrost1, 1);
P_yr_continuous1 = polyfit(x, norm_yr_continuous1, 1);
P_yr_discontinuous1 = polyfit(x, norm_yr_discontinuous1, 1);
P_yr_sporadic1 = polyfit(x, norm_yr_sporadic1, 1);
P_yr_isolated1 = polyfit(x, norm_yr_isolated1, 1);
P_yr_non_permafrost1 = polyfit(x, norm_yr_non_permafrost1, 1);

y_yr_permafrost1=polyval(P_yr_permafrost1,x);
y_yr_continuous1=polyval(P_yr_continuous1,x);
y_yr_discontinuous1=polyval(P_yr_discontinuous1,x);
y_yr_sporadic1=polyval(P_yr_sporadic1,x);
y_yr_isolated1=polyval(P_yr_isolated1,x);
y_yr_non_permafrost1=polyval(P_yr_non_permafrost1,x);


subplot('Position',[0.08 0.12 0.61 0.32]) %[left bottom width height]

plot(norm_yr_non_permafrost1,'Marker','o','LineWidth',1.5)
hold on
plot(norm_yr_isolated1,'Marker','o','LineWidth',1.5)
```

```matlab
plot(norm_yr_sporadic1, 'Marker','o','LineWidth',1.5)
plot(norm_yr_discontinuous1,'Marker','o','LineWidth',1.5)
plot(norm_yr_continuous1,'Marker','o','LineWidth',1.5)
plot(x,y_yr_isolated1,'Color',[0.850980392156863 0.325490196078431
0.0980392156862745],...
    'LineStyle','--','LineWidth',1.5);
plot(x,y_yr_sporadic1,'Color',[0.929411764705882 0.694117647058824
0.125490196078431],...
    'LineStyle','--','LineWidth',1.5);
plot(x,y_yr_non_permafrost1,'Color',[0 0.447058823529412
0.741176470588235],'LineStyle','--','LineWidth',1.5);


% Add legend, title and axis labels
% legend('Non Permafrost', 'Isolated
patches','Sporadic','Disontinuous','Continuous', 'Location', 'northeast')
xlabel('Time (Year)')
ylabel('Fire pixels year (%)','FontName','Times New Roman')
title('(b)')
% Set axis limits and tick marks
xlim([1 21])
% yticks(0:10:100)
% yticklabels({'0', '10', '20', '30', '40', '50', '60', '70', '80', '90','100'})
% ylim([0  100])
xticks(1:21)
xticklabels({'2001', '2002', '2003', '2004', '2005', '2006', '2007', '2008',
'2009', '2010',...
    '2011', '2012', '2013', '2014', '2015', '2016', '2017', '2018',
'2019','2020','2021'})
set(findall(hfig,'-property','XMinorTick'),'XMinorTick','on')
xl = xlim;
xAx = get(gca,'XAxis');
xAx.MinorTickValues=linspace(xl(1),xl(2),21);
set(findall(hfig,'-property','XMinorGrid'),'XMinorGrid','on')
grid on


sum_continuous1 = sum(fires_continuous_zone1);
sum_discontinuous1 = sum(fires_discontinuous_zone1);
sum_sporadic1 = sum(fires_sporadic_zone1);
sum_isolated1 = sum(fires_isolated_zone1);
sum_non_permafrost1 = sum(fires_non_permafrost_zone1);

subplot('Position',[0.8 0.10 0.13 0.85]); %[left bottom width height]

title('(b)')
x=1:5;
y=[sum_non_permafrost1 sum_isolated1 sum_sporadic1 sum_discontinuous1
sum_continuous1];
bar(x,y,'stacked')

b = bar(x,y,'FaceColor','flat');
b.CData(2,:) = [0.850980392156863 0.325490196078431 0.0980392156862745];
b.CData(3,:) = [0.929411764705882 0.694117647058824 0.125490196078431];
b.CData(4,:) = [0.494117647058824 0.184313725490196 0.556862745098039];
b.CData(5,:) = [0.466666666666667 0.674509803921569 0.188235294117647];

percent = 100 *y ./ sum(y);
for k = 1:length(percent)
```

```matlab
        text(x(k),y(k),sprintf('%0.1f%%',percent(k)),...
            'HorizontalAlignment','center','VerticalAlignment','bottom','FontSize',
15,'FontName','Times New Roman')
end

title('(c)')
ylim('padded')
yticks([0 10000 20000 30000 40000])
ylabel('Fire pixels')
yticklabels({'0','10000','20000','30000','40000'})
xticks([1 2 3 4 5])
xticklabels({'','','','',''})
xlabel({'2001-2021'})
set(findall(hfig,'-property','Interpreter'),'Interpreter', 'latex')
set(findall(hfig,'-property','TickLabelInterpreter'),'TickLabelInterpreter',
'latex','FontSize', 22)
grid on


%%

x = 1:21;
y1 = average_burn_latitude_zone1;
P1 = polyfit(x,y1,1);
yfit1 = polyval(P1,x);


hfig = figure;
subplot('Position',[0.08 0.63 0.48 0.32]) %[left bottom width height]

plot(average_burn_latitude_zone1,'Color',[0.850980392156863 0.325490196078431
0.0980392156862745],...
    'MarkerEdgeColor',[0 0 0],'Marker','o','LineWidth',1.5)
hold on;
plot(x,yfit1,'Color',[0.501960784313725 0.501960784313725
0.501960784313725],'LineStyle','--','LineWidth',1);
% eqn = string(" Linear: y = " + P1(1)) + "x + " + string(P1(2));
%
text(min(x),max(y1),eqn,"HorizontalAlignment","left","VerticalAlignment","top",'Fo
ntSize', 15)
title('(a)')
% xlabel({'Time (Year)'},'HorizontalAlignment','center')
ylabel(['Latitude ' '$^{\circ} C$'],'HorizontalAlignment','center','Interpreter',
'latex')
xlim([1 21])
ylim("padded")
% yticks([0 50000 100000 150000 200000 250000])
% yticklabels({'0','50000','10000','150000','200000','250000'})
xticks(1:21)
xticklabels({'2001', '2002', '2003', '2004', '2005', '2006', '2007', '2008',
'2009', '2010',...
    '2011', '2012', '2013', '2014', '2015', '2016', '2017', '2018',
'2019','2020','2021'})
xl = xlim;
xAx = get(gca,'XAxis');
xAx.MinorTickValues=linspace(xl(1),xl(2),21);
legend('Mean latitude','Linear','Location','northeast','FontSize', 15)
grid on
```

```matlab
y3 = average_burn_month_eachyear_zone1;
P3 = polyfit(x,y3,1);
yfit3 = polyval(P3,x);

subplot('Position',[0.08 0.12 0.48 0.32]) %[left bottom width height]

plot(average_burn_month_eachyear_zone1,'Color',[0.494117647058824
0.184313725490196 0.556862745098039],...
    'MarkerEdgeColor',[0 0 0],'Marker','o','LineWidth',1.5)
hold on
plot(x,yfit3,'Color',[0.501960784313725 0.501960784313725
0.501960784313725],'LineStyle','--','LineWidth',1)
title('(b)')
% eqn = string(" Linear: y = " + P3(1)) + "x + " + string(P3(2));
%
text(min(x),max(y3),eqn,"HorizontalAlignment","left","VerticalAlignment","top",'Fo
ntSize', 15)
xlabel({'Time (Year)'},'HorizontalAlignment','center')
ylabel({'Time (Month)'},'HorizontalAlignment','center')
xticks(1:21)
xticklabels({'2001', '2002', '2003', '2004', '2005', '2006', '2007', '2008',
'2009', '2010',...
    '2011', '2012', '2013', '2014', '2015', '2016', '2017', '2018',
'2019','2020','2021'})
xlim([1 21])
ylim("padded")
xl = xlim;
xAx = get(gca,'XAxis');
xAx.MinorTickValues=linspace(xl(1),xl(2),21);
yticks([5 6 7 8])
yticklabels({'May','Jun','Jul','Aug'})
legend('Mean date','Linear','Location','best','FontSize', 15)
grid on




subplot('Position',[0.66 0.12 0.30 0.83]); %[left bottom width height]

bar(average_burn_month_zone1, 'b')

x=1:12;
y=average_burn_month_zone1;
bar(x,y)
percent = 100 *y ./ sum(y);
for k = 1:length(percent)
    text(x(k),y(k),sprintf('%0.1f%%',percent(k)),...
        'HorizontalAlignment','center','VerticalAlignment','bottom','FontSize',
15,'FontName','Times New Roman')
end

% ylabel({'Fire pixels'},'HorizontalAlignment','center')
xlabel('Time (Month)')
ylabel('Fire pixels')
set(gca, 'XTick', 1:12, 'Xticklabel', ...
    {'Jan','Feb','Mar','Apr','May','Jun','Jul','Aug','Sep','Oct','Nov','Dec'})
```

```matlab
title('(c)')
ylim(([0 22000]))
yticks([0 5000 10000 15000 20000])
yticklabels({'0','5000','10000','15000','20000'})
picturewidth = 20;
hw_ratio = 0.65;
set(findall(hfig,'-property','XMinorTick'),'XMinorTick','on')
% xl = xlim;
% xAx = get(gca,'XAxis');
% xAx.MinorTickValues=linspace(xl(1),xl(2),21);
% set(findall(hfig,'-property','XMinorGrid'),'XMinorGrid','on')
% set(findall(hfig,'-property','FontSize'),'FontSize', 22)
legend('Fire pixels 2001-2021','Linear','FontSize', 15)
set(findall(hfig,'-property','Interpreter'),'Interpreter', 'latex')
set(findall(hfig,'-property','TickLabelInterpreter'),'TickLabelInterpreter',
'latex','FontSize', 22)
grid on
```

Appendix D

The MATLAB script used to generate analyses for the second subregion in the study otherwise known as the Central Canada (CC).

```matlab
x = 1:21;

% Calculate the combined sum of all four zones
sum_fires2 = fires_permafrost_zone2 + fires_non_permafrost_zone2;
all_fires2=sum(sum_fires2);

% Normalize the data for all four zones to the range [0,100] for the whole
% sum
norm_sum_fires2 = 100*sum_fires2./all_fires2;
norm_permafrost2 = 100*fires_permafrost_zone2./all_fires2;
norm_continuous2 = 100*fires_continuous_zone2./all_fires2;
norm_discontinuous2 = 100*fires_discontinuous_zone2./all_fires2;
norm_sporadic2 = 100*fires_sporadic_zone2./all_fires2;
norm_isolated2 = 100*fires_isolated_zone2./all_fires2;
norm_non_permafrost2 = 100*fires_non_permafrost_zone2./all_fires2;


% Calculate linear regression lines for each zone
P_permafrost2 = polyfit(x, norm_permafrost2, 1);
P_continuous2 = polyfit(x, norm_continuous2, 1);
P_discontinuous2 = polyfit(x, norm_discontinuous2, 1);
P_sporadic2 = polyfit(x, norm_sporadic2, 1);
P_isolated2 = polyfit(x, norm_isolated2, 1);
P_non_permafrost2 = polyfit(x, norm_non_permafrost2, 1);

y_permafrost2=polyval(P_permafrost2,x);
y_continuous2=polyval(P_continuous2,x);
y_discontinuous2=polyval(P_discontinuous2,x);
y_sporadic2=polyval(P_sporadic2,x);
y_isolated2=polyval(P_isolated2,x);
y_non_permafrost2=polyval(P_non_permafrost2,x);


% Plot the normalized data and the linear regression lines for each zone
hfig = figure;

subplot('Position',[0.08 0.63 0.61 0.32]) %[left bottom width height] [0.75 0.10
0.15 0.85]

plot(norm_non_permafrost2,'Marker','o','LineWidth',1.5)
hold on
plot(norm_isolated2,'Marker','o','LineWidth',1.5)
plot(norm_sporadic2, 'Marker','o','LineWidth',1.5)
plot(norm_discontinuous2,'Marker','o','LineWidth',1.5)
plot(norm_continuous2,'Marker','o','LineWidth',1.5)
% plot(norm_sum_fires2,'Marker','o','LineWidth',1.5)
plot(x,y_isolated2,'Color',[0.850980392156863 0.325490196078431
0.0980392156862745],...
    'LineStyle','--','LineWidth',1.5);
```

```matlab
plot(x,y_sporadic2,'Color',[0.929411764705882 0.694117647058824
0.125490196078431],...
    'LineStyle','--','LineWidth',1.5);
plot(x,y_non_permafrost2,'Color',[0 0.447058823529412
0.741176470588235],'LineStyle','--','LineWidth',1.5);
plot(x,y_discontinuous2,'Color',[0.494117647058824 0.184313725490196
0.556862745098039],'LineStyle','--','LineWidth',1.5);
plot(x,y_continuous2,'Color',[0.466666666666667 0.674509803921569
0.188235294117647],'LineStyle','--','LineWidth',1.5);


% Add legend, title and axis labels
legend('Non Permafrost', 'Isolated
patches','Sporadic','Disontinuous','Continuous', 'Location', 'northeast')
xlabel('Time (Year)')
ylabel('Fire pixels total (%)','FontName','Times New Roman')
title('(a)')
% Set axis limits and tick marks
xlim([1 21])
% yticks(0:10:100)
% yticklabels({'0', '10', '20', '30', '40', '50', '60', '70', '80', '90','100'})
% ylim([0  100])
xticks(1:21)
xticklabels({'2001', '2002', '2003', '2004', '2005', '2006', '2007', '2008',
'2009', '2010',...
    '2011', '2012', '2013', '2014', '2015', '2016', '2017', '2018',
'2019','2020','2021'})
set(findall(hfig,'-property','XMinorTick'),'XMinorTick','on')
xl = xlim;
xAx = get(gca,'XAxis');
xAx.MinorTickValues=linspace(xl(1),xl(2),21);
set(findall(hfig,'-property','XMinorGrid'),'XMinorGrid','on')
grid on



% Normalize the data for all four zones to the range [0,100] yearly
norm_yr_permafrost2 = 100*fires_permafrost_zone2./sum_fires2;
norm_yr_continuous2 = 100*fires_continuous_zone2./sum_fires2;
norm_yr_discontinuous2 = 100*fires_discontinuous_zone2./sum_fires2;
norm_yr_sporadic2 = 100*fires_sporadic_zone2./sum_fires2;
norm_yr_isolated2 = 100*fires_isolated_zone2./sum_fires2;
norm_yr_non_permafrost2 = 100*fires_non_permafrost_zone2./sum_fires2;

% Calculate linear regression lines for each zone
P_yr_permafrost2 = polyfit(x, norm_yr_permafrost2, 1);
P_yr_continuous2 = polyfit(x, norm_yr_continuous2, 1);
P_yr_discontinuous2 = polyfit(x, norm_yr_discontinuous2, 1);
P_yr_sporadic2 = polyfit(x, norm_yr_sporadic2, 1);
P_yr_isolated2 = polyfit(x, norm_yr_isolated2, 1);
P_yr_non_permafrost2 = polyfit(x, norm_yr_non_permafrost2, 1);

y_yr_permafrost2=polyval(P_yr_permafrost2,x);
y_yr_continuous2=polyval(P_yr_continuous2,x);
y_yr_discontinuous2=polyval(P_yr_discontinuous2,x);
y_yr_sporadic2=polyval(P_yr_sporadic2,x);
y_yr_isolated2=polyval(P_yr_isolated2,x);
y_yr_non_permafrost2=polyval(P_yr_non_permafrost2,x);
```

84

```matlab
subplot('Position',[0.08 0.12 0.61 0.32]) %[left bottom width height]

plot(norm_yr_non_permafrost2,'Marker','o','LineWidth',1.5)
hold on
plot(norm_yr_isolated2,'Marker','o','LineWidth',1.5)
plot(norm_yr_sporadic2, 'Marker','o','LineWidth',1.5)
plot(norm_yr_discontinuous2,'Marker','o','LineWidth',1.5)
plot(norm_yr_continuous2,'Marker','o','LineWidth',1.5)
plot(x,y_yr_isolated2,'Color',[0.850980392156863 0.325490196078431
0.0980392156862745],...
    'LineStyle','--','LineWidth',1.5);
plot(x,y_yr_sporadic2,'Color',[0.929411764705882 0.694117647058824
0.125490196078431],...
    'LineStyle','--','LineWidth',1.5);
plot(x,y_yr_non_permafrost2,'Color',[0 0.447058823529412
0.741176470588235],'LineStyle','--','LineWidth',1.5);


% Add legend, title and axis labels
legend('Non Permafrost', 'Isolated
patches','Sporadic','Disontinuous','Continuous', 'Location', 'northeast')
xlabel('Time (Year)')
ylabel('Fire pixels year (%)','FontName','Times New Roman')
title('(b)')
% Set axis limits and tick marks
xlim([1 21])
% yticks(0:10:100)
% yticklabels({'0', '10', '20', '30', '40', '50', '60', '70', '80', '90','100'})
% ylim([0  100])
xticks(1:21)
xticklabels({'2001', '2002', '2003', '2004', '2005', '2006', '2007', '2008',
'2009', '2010',...
    '2011', '2012', '2013', '2014', '2015', '2016', '2017', '2018',
'2019','2020','2021'})
set(findall(hfig,'-property','XMinorTick'),'XMinorTick','on')
xl = xlim;
xAx = get(gca,'XAxis');
xAx.MinorTickValues=linspace(xl(1),xl(2),21);
set(findall(hfig,'-property','XMinorGrid'),'XMinorGrid','on')
grid on


sum_continuous2 = sum(fires_continuous_zone2);
sum_discontinuous2 = sum(fires_discontinuous_zone2);
sum_sporadic2 = sum(fires_sporadic_zone2);
sum_isolated2 = sum(fires_isolated_zone2);
sum_non_permafrost2 = sum(fires_non_permafrost_zone2);

subplot('Position',[0.8 0.10 0.13 0.85]); %[left bottom width height]

x=1:5;
y=[sum_non_permafrost2 sum_isolated2 sum_sporadic2 sum_discontinuous2
sum_continuous2];
bar(x,y,'grouped')

b = bar(x,y,'FaceColor','flat');
b.CData(2,:) = [0.850980392156863 0.325490196078431 0.0980392156862745];
b.CData(3,:) = [0.929411764705882 0.694117647058824 0.125490196078431];
```

```matlab
b.CData(4,:) = [0.494117647058824 0.184313725490196 0.556862745098039];
b.CData(5,:) = [0.46666666666667 0.674509803921569 0.188235294117647];

percent = 100 *y ./ sum(y);
for k = 1:length(percent)
    text(x(k),y(k),sprintf('%0.0f%%',percent(k)),...
        'HorizontalAlignment','center','VerticalAlignment','bottom','FontSize',
15,'FontName','Times New Roman')
end


title('(c)')
ylim('padded')
yticks([0 50000 100000 150000])
ylabel('Fire pixels')
yticklabels({'0','50000','100000','150000'})
xticks([1 2 3 4 5])
xticklabels({'','','','',''})
xlabel({'2001-2021'});
set(findall(hfig,'-property','Interpreter'),'Interpreter', 'latex')
set(findall(hfig,'-property','TickLabelInterpreter'),'TickLabelInterpreter',
'latex','FontSize', 22)
grid on


%%


x = 1:21;
y1 = average_burn_latitude_zone2;
P1 = polyfit(x,y1,1);
yfit1 = polyval(P1,x);


hfig = figure;
subplot('Position',[0.08 0.63 0.48 0.32]) %[left bottom width height]

plot(average_burn_latitude_zone2,'Color',[0.850980392156863 0.325490196078431
0.0980392156862745],...
    'MarkerEdgeColor',[0 0 0],'Marker','o','LineWidth',1.5)
hold on;
plot(x,yfit1,'Color',[0.501960784313725 0.501960784313725
0.501960784313725],'LineStyle','--','LineWidth',1);
% eqn = string(" Linear: y = " + P1(1)) + "x + " + string(P1(2));
%
text(min(x),max(y1),eqn,"HorizontalAlignment","left","VerticalAlignment","top",'Fo
ntSize', 15)
title('(a)')
% xlabel({'Time (Year)'},'HorizontalAlignment','center')
ylabel(['Latitude ' '$^{\circ} C$'],'HorizontalAlignment','center','Interpreter',
'latex')
xlim([1 21])
ylim("padded")
% yticks([0 50000 100000 150000 200000 250000])
% yticklabels({'0','50000','10000','150000','200000','250000'})
xticks(1:21)
xticklabels({'2001', '2002', '2003', '2004', '2005', '2006', '2007', '2008',
'2009', '2010',...
```

86

```matlab
    '2011', '2012', '2013', '2014', '2015', '2016', '2017', '2018',
'2019','2020','2021'})
xl = xlim;
xAx = get(gca,'XAxis');
xAx.MinorTickValues=linspace(xl(1),xl(2),21);
legend('Mean latitude','Linear','Location','northeast','FontSize', 15)
grid on




y3 = average_burn_month_eachyear_zone2;
P3 = polyfit(x,y3,1);
yfit3 = polyval(P3,x);

subplot('Position',[0.08 0.12 0.48 0.32]) %[left bottom width height]

plot(average_burn_month_eachyear_zone2,'Color',[0.494117647058824
0.184313725490196 0.556862745098039],...
    'MarkerEdgeColor',[0 0 0],'Marker','o','LineWidth',1.5)
hold on
plot(x,yfit3,'Color',[0.501960784313725 0.501960784313725
0.501960784313725],'LineStyle','--','LineWidth',1)
title('(b)')
% eqn = string(" Linear: y = " + P3(1)) + "x + " + string(P3(2));
%
text(min(x),max(y3),eqn,"HorizontalAlignment","left","VerticalAlignment","top",'Fo
ntSize', 15)
xlabel({'Time (Year)'},'HorizontalAlignment','center')
ylabel({'Time (Month)'},'HorizontalAlignment','center')
xticks(1:21)
xticklabels({'2001', '2002', '2003', '2004', '2005', '2006', '2007', '2008',
'2009', '2010',...
    '2011', '2012', '2013', '2014', '2015', '2016', '2017', '2018',
'2019','2020','2021'})
xlim([1 21])
ylim("padded")
xl = xlim;
xAx = get(gca,'XAxis');
xAx.MinorTickValues=linspace(xl(1),xl(2),21);
yticks([5 6 7 8])
yticklabels({'May','Jun','Jul','Aug'})
legend('Mean date','Linear','Location','best','FontSize', 15)
grid on




subplot('Position',[0.66 0.12 0.30 0.83]); %[left bottom width height]

bar(average_burn_month_zone2, 'b')

x=1:12;
y=average_burn_month_zone2;
bar(x,y)
percent = 100 *y ./ sum(y);
for k = 1:length(percent)
    text(x(k),y(k),sprintf('%0.0f%%',percent(k)),...
```

```matlab
        'HorizontalAlignment','center','VerticalAlignment','bottom','FontSize',
15,'FontName','Times New Roman')
end

% ylabel({'Fire pixels'},'HorizontalAlignment','center')
xlabel('Time (Month)')
ylabel('Fire pixels')
set(gca, 'XTick', 1:12, 'Xticklabel', ...
    {'Jan','Feb','Mar','Apr','May','Jun','Jul','Aug','Sep','Oct','Nov','Dec'})
title('(c)')
ylim(([0 135000]))
yticks([0 30000 60000 90000 120000])
yticklabels({'0','30000','60000','90000','120000'})
picturewidth = 20;
hw_ratio = 0.65;
set(findall(hfig,'-property','XMinorTick'),'XMinorTick','on')
% xl = xlim;
% xAx = get(gca,'XAxis');
% xAx.MinorTickValues=linspace(xl(1),xl(2),21);
% set(findall(hfig,'-property','XMinorGrid'),'XMinorGrid','on')
% set(findall(hfig,'-property','FontSize'),'FontSize', 22)
legend('Fire pixels 2001-2021','Linear','FontSize', 15)
set(findall(hfig,'-property','Interpreter'),'Interpreter', 'latex')
set(findall(hfig,'-property','TickLabelInterpreter'),'TickLabelInterpreter',
'latex','FontSize', 22)
grid on
```

Appendix E

The MATLAB script used to generate analyses for the third subregion in the study otherwise known as the Western Cordillera (WC).

```matlab
x = 1:21;

% Calculate the combined sum of all four zones
sum_fires3 = fires_permafrost_zone3 + fires_non_permafrost_zone3;
all_fires3=sum(sum_fires3);

% Normalize the data for all four zones to the range [0,100] for the whole
% sum
norm_sum_fires3 = 100*sum_fires3./all_fires3;
norm_permafrost3 = 100*fires_permafrost_zone3./all_fires3;
norm_continuous3 = 100*fires_continuous_zone3./all_fires3;
norm_discontinuous3 = 100*fires_discontinuous_zone3./all_fires3;
norm_sporadic3 = 100*fires_sporadic_zone3./all_fires3;
norm_isolated3 = 100*fires_isolated_zone3./all_fires3;
norm_non_permafrost3 = 100*fires_non_permafrost_zone3./all_fires3;


% Calculate linear regression lines for each zone
P_permafrost3 = polyfit(x, norm_permafrost3, 1);
P_continuous3 = polyfit(x, norm_continuous3, 1);
P_discontinuous3= polyfit(x, norm_discontinuous3, 1);
P_sporadic3 = polyfit(x, norm_sporadic3, 1);
P_isolated3 = polyfit(x, norm_isolated3, 1);
P_non_permafrost3 = polyfit(x, norm_non_permafrost3, 1);

y_permafrost3=polyval(P_permafrost3,x);
y_continuous3=polyval(P_continuous3,x);
y_discontinuous3=polyval(P_discontinuous3,x);
y_sporadic3=polyval(P_sporadic3,x);
y_isolated3=polyval(P_isolated3,x);
y_non_permafrost3=polyval(P_non_permafrost3,x);


% Plot the normalized data and the linear regression lines for each zone
hfig = figure;

subplot('Position',[0.08 0.63 0.61 0.32]) %[left bottom width height] [0.75 0.10
0.15 0.85]

plot(norm_non_permafrost3,'Marker','o','LineWidth',1.5)
hold on
plot(norm_isolated3,'Marker','o','LineWidth',1.5)
plot(norm_sporadic3, 'Marker','o','LineWidth',1.5)
plot(norm_discontinuous3,'Marker','o','LineWidth',1.5)
plot(norm_continuous3,'Marker','o','LineWidth',1.5)
% plot(norm_sum_fires2,'Marker','o','LineWidth',1.5)
plot(x,y_isolated3,'Color',[0.850980392156863 0.325490196078431
0.0980392156862745],...
    'LineStyle','--','LineWidth',1.5);
```

```matlab
plot(x,y_sporadic3,'Color',[0.929411764705882 0.694117647058824
0.125490196078431],...
    'LineStyle','--','LineWidth',1.5);
plot(x,y_non_permafrost3,'Color',[0 0.447058823529412
0.741176470588235],'LineStyle','--','LineWidth',1.5);
plot(x,y_discontinuous3,'Color',[0.494117647058824 0.184313725490196
0.556862745098039],'LineStyle','--','LineWidth',1.5);
plot(x,y_continuous3,'Color',[0.466666666666667 0.674509803921569
0.188235294117647],'LineStyle','--','LineWidth',1.5);


% Add legend, title and axis labels
legend('Non Permafrost', 'Isolated
patches','Sporadic','Disontinuous','Continuous', 'Location', 'northeast')
xlabel('Time (Year)')
ylabel('Fire pixels total (%)','FontName','Times New Roman')
title('(a)')
% Set axis limits and tick marks
xlim([1 21])
% yticks(0:10:100)
% yticklabels({'0', '10', '20', '30', '40', '50', '60', '70', '80', '90','100'})
% ylim([0  100])
xticks(1:21)
xticklabels({'2001', '2002', '2003', '2004', '2005', '2006', '2007', '2008',
'2009', '2010',...
    '2011', '2012', '2013', '2014', '2015', '2016', '2017', '2018',
'2019','2020','2021'})
set(findall(hfig,'-property','XMinorTick'),'XMinorTick','on')
xl = xlim;
xAx = get(gca,'XAxis');
xAx.MinorTickValues=linspace(xl(1),xl(2),21);
set(findall(hfig,'-property','XMinorGrid'),'XMinorGrid','on')
grid on



% Normalize the data for all four zones to the range [0,100] yearly
norm_yr_permafrost3 = 100*fires_permafrost_zone3./sum_fires3;
norm_yr_continuous3 = 100*fires_continuous_zone3./sum_fires3;
norm_yr_discontinuous3 = 100*fires_discontinuous_zone3./sum_fires3;
norm_yr_sporadic3 = 100*fires_sporadic_zone3./sum_fires3;
norm_yr_isolated3 = 100*fires_isolated_zone3./sum_fires3;
norm_yr_non_permafrost3 = 100*fires_non_permafrost_zone3./sum_fires3;

% Calculate linear regression lines for each zone
P_yr_permafrost3 = polyfit(x, norm_yr_permafrost3, 1);
P_yr_continuous3 = polyfit(x, norm_yr_continuous3, 1);
P_yr_discontinuous3 = polyfit(x, norm_yr_discontinuous3, 1);
P_yr_sporadic3 = polyfit(x, norm_yr_sporadic3, 1);
P_yr_isolated3 = polyfit(x, norm_yr_isolated3, 1);
P_yr_non_permafrost3 = polyfit(x, norm_yr_non_permafrost3, 1);

y_yr_permafrost3=polyval(P_yr_permafrost3,x);
y_yr_continuous3=polyval(P_yr_continuous3,x);
y_yr_discontinuous3=polyval(P_yr_discontinuous3,x);
y_yr_sporadic3=polyval(P_yr_sporadic3,x);
y_yr_isolated3=polyval(P_yr_isolated3,x);
y_yr_non_permafrost3=polyval(P_yr_non_permafrost3,x);
```

90

```matlab
subplot('Position',[0.08 0.12 0.61 0.32]) %[left bottom width height]

plot(norm_yr_non_permafrost3,'Marker','o','LineWidth',1.5)
hold on
plot(norm_yr_isolated3,'Marker','o','LineWidth',1.5)
plot(norm_yr_sporadic3, 'Marker','o','LineWidth',1.5)
plot(norm_yr_discontinuous3,'Marker','o','LineWidth',1.5)
plot(norm_yr_continuous3,'Marker','o','LineWidth',1.5)
plot(x,y_yr_isolated3,'Color',[0.850980392156863 0.325490196078431
0.0980392156862745],...
    'LineStyle','--','LineWidth',1.5);
plot(x,y_yr_sporadic3,'Color',[0.929411764705882 0.694117647058824
0.125490196078431],...
    'LineStyle','--','LineWidth',1.5);
plot(x,y_yr_non_permafrost3,'Color',[0 0.447058823529412
0.741176470588235],'LineStyle','--','LineWidth',1.5);


% Add legend, title and axis labels
legend('Non Permafrost', 'Isolated
patches','Sporadic','Disontinuous','Continuous', 'Location', 'northeast')
xlabel('Time (Year)')
ylabel('Fire pixels year (%)','FontName','Times New Roman')
title('(b)')
% Set axis limits and tick marks
xlim([1 21])
% yticks(0:10:100)
% yticklabels({'0', '10', '20', '30', '40', '50', '60', '70', '80', '90','100'})
% ylim([0  100])
xticks(1:21)
xticklabels({'2001', '2002', '2003', '2004', '2005', '2006', '2007', '2008',
'2009', '2010',...
    '2011', '2012', '2013', '2014', '2015', '2016', '2017', '2018',
'2019','2020','2021'})
set(findall(hfig,'-property','XMinorTick'),'XMinorTick','on')
xl = xlim;
xAx = get(gca,'XAxis');
xAx.MinorTickValues=linspace(xl(1),xl(2),21);
set(findall(hfig,'-property','XMinorGrid'),'XMinorGrid','on')
grid on


sum_continuous3 = sum(fires_continuous_zone3);
sum_discontinuous3 = sum(fires_discontinuous_zone3);
sum_sporadic3 = sum(fires_sporadic_zone3);
sum_isolated3 = sum(fires_isolated_zone3);
sum_non_permafrost3 = sum(fires_non_permafrost_zone3);

subplot('Position',[0.8 0.10 0.13 0.85]); %[left bottom width height]

x=1:5;
y=[sum_non_permafrost3 sum_isolated3 sum_sporadic3 sum_discontinuous3
sum_continuous3];
bar(x,y,'grouped')

b = bar(x,y,'FaceColor','flat');
b.CData(2,:) = [0.850980392156863 0.325490196078431 0.0980392156862745];
b.CData(3,:) = [0.929411764705882 0.694117647058824 0.125490196078431];
```

```matlab
b.CData(4,:) = [0.494117647058824 0.184313725490196 0.556862745098039];
b.CData(5,:) = [0.466666666666667 0.674509803921569 0.188235294117647];

percent = 100 *y ./ sum(y);
for k = 1:length(percent)
    text(x(k),y(k),sprintf('%0.0f%%',percent(k)),...
        'HorizontalAlignment','center','VerticalAlignment','bottom','FontSize',
15,'FontName','Times New Roman')
end


title('(c)')
ylim('padded')
yticks([0 50000 100000 150000 200000])
ylabel('Fire pixels')
yticklabels({'0','50000','100000','150000','200000'})
xticks([1 2 3 4 5])
xticklabels({'','','','',''})
xlabel({'2001-2021'});
set(findall(hfig,'-property','Interpreter'),'Interpreter', 'latex')
set(findall(hfig,'-property','TickLabelInterpreter'),'TickLabelInterpreter',
'latex','FontSize', 22)
grid on



%%


x = 1:21;
y1 = average_burn_latitude_zone3;
P1 = polyfit(x,y1,1);
yfit1 = polyval(P1,x);


hfig = figure;
subplot('Position',[0.08 0.63 0.48 0.32]) %[left bottom width height]

plot(average_burn_latitude_zone3,'Color',[0.850980392156863 0.325490196078431
0.0980392156862745],...
    'MarkerEdgeColor',[0 0 0],'Marker','o','LineWidth',1.5)
hold on;
plot(x,yfit1,'Color',[0.501960784313725 0.501960784313725
0.501960784313725],'LineStyle','--','LineWidth',1);
% eqn = string(" Linear: y = " + P1(1)) + "x + " + string(P1(2));
%
text(min(x),max(y1),eqn,"HorizontalAlignment","left","VerticalAlignment","top",'Fo
ntSize', 15)
title('(a)')
% xlabel({'Time (Year)'},'HorizontalAlignment','center')
ylabel(['Latitude ' '$^{\circ} C$'],'HorizontalAlignment','center','Interpreter',
'latex')
xlim([1 21])
ylim("padded")
% yticks([0 50000 100000 150000 200000 250000])
% yticklabels({'0','50000','10000','150000','200000','250000'})
xticks(1:21)
xticklabels({'2001', '2002', '2003', '2004', '2005', '2006', '2007', '2008',
'2009', '2010',...
```

92

```matlab
    '2011', '2012', '2013', '2014', '2015', '2016', '2017', '2018',
'2019','2020','2021'})
xl = xlim;
xAx = get(gca,'XAxis');
xAx.MinorTickValues=linspace(xl(1),xl(2),21);
legend('Mean latitude','Linear','Location','northeast','FontSize', 15)
grid on




y3 = average_burn_month_eachyear_zone3;
P3 = polyfit(x,y3,1);
yfit3 = polyval(P3,x);

subplot('Position',[0.08 0.12 0.48 0.32]) %[left bottom width height]

plot(average_burn_month_eachyear_zone3,'Color',[0.494117647058824
0.184313725490196 0.556862745098039],...
    'MarkerEdgeColor',[0 0 0],'Marker','o','LineWidth',1.5)
hold on
plot(x,yfit3,'Color',[0.501960784313725 0.501960784313725
0.501960784313725],'LineStyle','--','LineWidth',1)
title('(b)')
% eqn = string(" Linear: y = " + P3(1)) + "x + " + string(P3(2));
%
text(min(x),max(y3),eqn,"HorizontalAlignment","left","VerticalAlignment","top",'Fo
ntSize', 15)
xlabel({'Time (Year)'},'HorizontalAlignment','center')
ylabel({'Time (Month)'},'HorizontalAlignment','center')
xticks(1:21)
xticklabels({'2001', '2002', '2003', '2004', '2005', '2006', '2007', '2008',
'2009', '2010',...
    '2011', '2012', '2013', '2014', '2015', '2016', '2017', '2018',
'2019','2020','2021'})
xlim([1 21])
ylim("padded")
xl = xlim;
xAx = get(gca,'XAxis');
xAx.MinorTickValues=linspace(xl(1),xl(2),21);
yticks([5 6 7 8])
yticklabels({'May','Jun','Jul','Aug'})
legend('Mean date','Linear','Location','best','FontSize', 15)
grid on




subplot('Position',[0.66 0.12 0.30 0.83]); %[left bottom width height]

bar(average_burn_month_zone3, 'b')

x=1:12;
y=average_burn_month_zone3;
bar(x,y)
percent = 100 *y ./ sum(y);
for k = 1:length(percent)
    text(x(k),y(k),sprintf('%0.1f%%',percent(k)),...
```

```matlab
        'HorizontalAlignment','center','VerticalAlignment','bottom','FontSize',
15,'FontName','Times New Roman')
end

% ylabel({'Fire pixels'},'HorizontalAlignment','center')
xlabel('Time (Month)')
ylabel('Fire pixels')
set(gca, 'XTick', 1:12, 'Xticklabel', ...
    {'Jan','Feb','Mar','Apr','May','Jun','Jul','Aug','Sep','Oct','Nov','Dec'})
title('(c)')
ylim('padded')
yticks([0 30000 60000 90000 120000])
yticklabels({'0','30000','60000','90000','120000'})
picturewidth = 20;
hw_ratio = 0.65;
set(findall(hfig,'-property','XMinorTick'),'XMinorTick','on')
% xl = xlim;
% xAx = get(gca,'XAxis');
% xAx.MinorTickValues=linspace(xl(1),xl(2),21);
% set(findall(hfig,'-property','XMinorGrid'),'XMinorGrid','on')
% set(findall(hfig,'-property','FontSize'),'FontSize', 22)
legend('Fire pixels 2001-2021','Linear','FontSize', 15)
set(findall(hfig,'-property','Interpreter'),'Interpreter', 'latex')
set(findall(hfig,'-property','TickLabelInterpreter'),'TickLabelInterpreter',
'latex','FontSize', 22)
grid on
```

Appendix F

The MATLAB script used to generate analyses for the fourth and last subregion in the study otherwise known as the Alaska (AL).

```matlab
x = 1:21;

% Calculate the combined sum of all four zones
sum_fires4 = fires_permafrost_zone4 + fires_non_permafrost_zone4;
all_fires4 = sum(sum_fires4);

% Calculate precentage of total amount of fires for every zone
all_fires_all_zones = all_fires1+all_fires2+all_fires3+all_fires4;
norm_all_fires1=100*all_fires1./all_fires_all_zones;
norm_all_fires2=100*all_fires2./all_fires_all_zones;
norm_all_fires3=100*all_fires3./all_fires_all_zones;
norm_all_fires4=100*all_fires4./all_fires_all_zones;


% Normalize the data for all four zones to the range [0,100] for the whole
% sum
norm_sum_fires4 = 100*sum_fires4./all_fires4;
norm_permafrost4 = 100*fires_permafrost_zone4./all_fires4;
norm_continuous4 = 100*fires_continuous_zone4./all_fires4;
norm_discontinuous4 = 100*fires_discontinuous_zone4./all_fires4;
norm_sporadic4 = 100*fires_sporadic_zone4./all_fires4;
norm_isolated4 = 100*fires_isolated_zone4./all_fires4;
norm_non_permafrost4 = 100*fires_non_permafrost_zone4./all_fires4;


% Calculate linear regression lines for each zone
P_permafrost4 = polyfit(x, norm_permafrost4, 1);
P_continuous4 = polyfit(x, norm_continuous4, 1);
P_discontinuous4= polyfit(x, norm_discontinuous4, 1);
P_sporadic4 = polyfit(x, norm_sporadic4, 1);
P_isolated4 = polyfit(x, norm_isolated4, 1);
P_non_permafrost4 = polyfit(x, norm_non_permafrost4, 1);

y_permafrost4=polyval(P_permafrost4,x);
y_continuous4=polyval(P_continuous4,x);
y_discontinuous4=polyval(P_discontinuous4,x);
y_sporadic4=polyval(P_sporadic4,x);
y_isolated4=polyval(P_isolated4,x);
y_non_permafrost4=polyval(P_non_permafrost4,x);


% Plot the normalized data and the linear regression lines for each zone
hfig = figure;

subplot('Position',[0.08 0.63 0.61 0.32]) %[left bottom width height] [0.75 0.10
0.15 0.85]

plot(norm_non_permafrost4,'Marker','o','LineWidth',1.5)
```

```matlab
hold on
plot(norm_isolated4,'Marker','o','LineWidth',1.5)
plot(norm_sporadic4, 'Marker','o','LineWidth',1.5)
plot(norm_discontinuous4,'Marker','o','LineWidth',1.5)
plot(norm_continuous4,'Marker','o','LineWidth',1.5)
% plot(norm_sum_fires2,'Marker','o','LineWidth',1.5)
plot(x,y_isolated4,'Color',[0.850980392156863 0.325490196078431
0.0980392156862745],...
    'LineStyle','--','LineWidth',1.5);
plot(x,y_sporadic4,'Color',[0.929411764705882 0.694117647058824
0.125490196078431],...
    'LineStyle','--','LineWidth',1.5);
plot(x,y_non_permafrost4,'Color',[0 0.447058823529412
0.741176470588235],'LineStyle','--','LineWidth',1.5);
plot(x,y_discontinuous4,'Color',[0.494117647058824 0.184313725490196
0.556862745098039],'LineStyle','--','LineWidth',1.5);
plot(x,y_continuous4,'Color',[0.466666666666667 0.674509803921569
0.188235294117647],'LineStyle','--','LineWidth',1.5);


% Add legend, title and axis labels
legend('Non Permafrost', 'Isolated
patches','Sporadic','Disontinuous','Continuous', 'Location', 'northeast')
xlabel('Time (Year)')
ylabel('Fire pixels total (%)','FontName','Times New Roman')
title('(a)')
% Set axis limits and tick marks
xlim([1 21])
% yticks(0:10:100)
% yticklabels({'0', '10', '20', '30', '40', '50', '60', '70', '80', '90','100'})
% ylim([0  100])
xticks(1:21)
xticklabels({'2001', '2002', '2003', '2004', '2005', '2006', '2007', '2008',
'2009', '2010',...
    '2011', '2012', '2013', '2014', '2015', '2016', '2017', '2018',
'2019','2020','2021'})
set(findall(hfig,'-property','XMinorTick'),'XMinorTick','on')
xl = xlim;
xAx = get(gca,'XAxis');
xAx.MinorTickValues=linspace(xl(1),xl(2),21);
set(findall(hfig,'-property','XMinorGrid'),'XMinorGrid','on')
grid on



% Normalize the data for all four zones to the range [0,100] yearly
norm_yr_permafrost4 = 100*fires_permafrost_zone4./sum_fires4;
norm_yr_continuous4 = 100*fires_continuous_zone4./sum_fires4;
norm_yr_discontinuous4 = 100*fires_discontinuous_zone4./sum_fires4;
norm_yr_sporadic4 = 100*fires_sporadic_zone4./sum_fires4;
norm_yr_isolated4 = 100*fires_isolated_zone4./sum_fires4;
norm_yr_non_permafrost4 = 100*fires_non_permafrost_zone4./sum_fires4;

% Calculate linear regression lines for each zone
P_yr_permafrost4 = polyfit(x, norm_yr_permafrost4, 1);
P_yr_continuous4 = polyfit(x, norm_yr_continuous4, 1);
P_yr_discontinuous4 = polyfit(x, norm_yr_discontinuous4, 1);
P_yr_sporadic4 = polyfit(x, norm_yr_sporadic4, 1);
P_yr_isolated4 = polyfit(x, norm_yr_isolated4, 1);
```

```matlab
P_yr_non_permafrost4 = polyfit(x, norm_yr_non_permafrost4, 1);

y_yr_permafrost4=polyval(P_yr_permafrost4,x);
y_yr_continuous4=polyval(P_yr_continuous4,x);
y_yr_discontinuous4=polyval(P_yr_discontinuous4,x);
y_yr_sporadic4=polyval(P_yr_sporadic4,x);
y_yr_isolated4=polyval(P_yr_isolated4,x);
y_yr_non_permafrost4=polyval(P_yr_non_permafrost4,x);


subplot('Position',[0.08 0.12 0.61 0.32]) %[left bottom width height]

plot(norm_yr_non_permafrost4,'Marker','o','LineWidth',1.5)
hold on
plot(norm_yr_isolated4,'Marker','o','LineWidth',1.5)
plot(norm_yr_sporadic4, 'Marker','o','LineWidth',1.5)
plot(norm_yr_discontinuous4,'Marker','o','LineWidth',1.5)
plot(norm_yr_continuous4,'Marker','o','LineWidth',1.5)
plot(x,y_yr_isolated4,'Color',[0.850980392156863 0.325490196078431
0.0980392156862745],...
    'LineStyle','--','LineWidth',1.5);
plot(x,y_yr_sporadic4,'Color',[0.929411764705882 0.694117647058824
0.125490196078431],...
    'LineStyle','--','LineWidth',1.5);
plot(x,y_yr_non_permafrost4,'Color',[0 0.447058823529412
0.741176470588235],'LineStyle','--','LineWidth',1.5);


% Add legend, title and axis labels
legend('Non Permafrost', 'Isolated
patches','Sporadic','Disontinuous','Continuous', 'Location', 'northeast')
xlabel('Time (Year)')
ylabel('Fire pixels year (%)','FontName','Times New Roman')
title('(b)')
% Set axis limits and tick marks
xlim([1 21])
% yticks(0:10:100)
% yticklabels({'0', '10', '20', '30', '40', '50', '60', '70', '80', '90','100'})
% ylim([0  100])
xticks(1:21)
xticklabels({'2001', '2002', '2003', '2004', '2005', '2006', '2007', '2008',
'2009', '2010',...
    '2011', '2012', '2013', '2014', '2015', '2016', '2017', '2018',
'2019','2020','2021'})
set(findall(hfig,'-property','XMinorTick'),'XMinorTick','on')
xl = xlim;
xAx = get(gca,'XAxis');
xAx.MinorTickValues=linspace(xl(1),xl(2),21);
set(findall(hfig,'-property','XMinorGrid'),'XMinorGrid','on')
grid on


sum_continuous4 = sum(fires_continuous_zone4);
sum_discontinuous4 = sum(fires_discontinuous_zone4);
sum_sporadic4 = sum(fires_sporadic_zone4);
sum_isolated4 = sum(fires_isolated_zone4);
sum_non_permafrost4 = sum(fires_non_permafrost_zone4);


subplot('Position',[0.8 0.10 0.13 0.85]); %[left bottom width height]
```

```
x=1:5;
y=[sum_non_permafrost4 sum_isolated4 sum_sporadic4 sum_discontinuous4
sum_continuous4];
bar(x,y,'grouped')

b = bar(x,y,'FaceColor','flat');
b.CData(2,:) = [0.850980392156863 0.325490196078431 0.0980392156862745];
b.CData(3,:) = [0.929411764705882 0.694117647058824 0.125490196078431];
b.CData(4,:) = [0.494117647058824 0.184313725490196 0.556862745098039];
b.CData(5,:) = [0.466666666666667 0.674509803921569 0.188235294117647];

percent = 100 *y ./ sum(y);
for k = 1:length(percent)
    text(x(k),y(k),sprintf('%0.0f%%',percent(k)),...
        'HorizontalAlignment','center','VerticalAlignment','bottom','FontSize',
15,'FontName','Times New Roman')
end


title('(c)')
ylim('padded')
yticks([0 20000 40000 60000 80000])
ylabel('Fire pixels')
yticklabels({'0','20000','40000','60000','80000'})
xticks([1 2 3 4 5])
xticklabels({'','','','',''})
xlabel({'2001-2021'});
set(findall(hfig,'-property','Interpreter'),'Interpreter', 'latex')
set(findall(hfig,'-property','TickLabelInterpreter'),'TickLabelInterpreter',
'latex','FontSize', 22)
grid on




%%


x = 1:21;
y1 = average_burn_latitude_zone4;
P1 = polyfit(x,y1,1);
yfit1 = polyval(P1,x);


hfig = figure;
subplot('Position',[0.08 0.63 0.48 0.32]) %[left bottom width height]

plot(average_burn_latitude_zone4,'Color',[0.850980392156863 0.325490196078431
0.0980392156862745],...
    'MarkerEdgeColor',[0 0 0],'Marker','o','LineWidth',1.5)
hold on;
plot(x,yfit1,'Color',[0.501960784313725 0.501960784313725
0.501960784313725],'LineStyle','--','LineWidth',1);
% eqn = string(" Linear: y = " + P1(1)) + "x + " + string(P1(2));


98
```

```matlab
%
text(min(x),max(y1),eqn,"HorizontalAlignment","left","VerticalAlignment","top",'Fo
ntSize', 15)
title('(a)')
% xlabel({'Time (Year)'},'HorizontalAlignment','center')
ylabel(['Latitude ' '$^{\circ} C$'],'HorizontalAlignment','center','Interpreter',
'latex')
xlim([1 21])
ylim("padded")
% yticks([0 50000 100000 150000 200000 250000])
% yticklabels({'0','50000','10000','150000','200000','250000'})
xticks(1:21)
xticklabels({'2001', '2002', '2003', '2004', '2005', '2006', '2007', '2008',
'2009', '2010',...
    '2011', '2012', '2013', '2014', '2015', '2016', '2017', '2018',
'2019','2020','2021'})
xl = xlim;
xAx = get(gca,'XAxis');
xAx.MinorTickValues=linspace(xl(1),xl(2),21);
legend('Mean latitude','Linear','Location','northeast','FontSize', 15)
grid on


y3 = average_burn_month_eachyear_zone4;
P3 = polyfit(x,y3,1);
yfit3 = polyval(P3,x);

subplot('Position',[0.08 0.12 0.48 0.32]) %[left bottom width height]

plot(average_burn_month_eachyear_zone4,'Color',[0.494117647058824
0.184313725490196 0.556862745098039],...
    'MarkerEdgeColor',[0 0 0],'Marker','o','LineWidth',1.5)
hold on
plot(x,yfit3,'Color',[0.501960784313725 0.501960784313725
0.501960784313725],'LineStyle','--','LineWidth',1)
title('(b)')
% eqn = string(" Linear: y = " + P3(1)) + "x + " + string(P3(2));
%
text(min(x),max(y3),eqn,"HorizontalAlignment","left","VerticalAlignment","top",'Fo
ntSize', 15)
xlabel({'Time (Year)'},'HorizontalAlignment','center')
ylabel({'Time (Month)'},'HorizontalAlignment','center')
xticks(1:21)
xticklabels({'2001', '2002', '2003', '2004', '2005', '2006', '2007', '2008',
'2009', '2010',...
    '2011', '2012', '2013', '2014', '2015', '2016', '2017', '2018',
'2019','2020','2021'})
xlim([1 21])
ylim("padded")
xl = xlim;
xAx = get(gca,'XAxis');
xAx.MinorTickValues=linspace(xl(1),xl(2),21);
yticks([5 6 7 8])
yticklabels({'May','Jun','Jul','Aug'})
legend('Mean date','Linear','Location','best','FontSize', 15)
grid on
```

```matlab
subplot('Position',[0.66 0.12 0.30 0.83]); %[left bottom width height]

bar(average_burn_month_zone4, 'b')

x=1:12;
y=average_burn_month_zone4;
bar(x,y)
percent = 100 *y ./ sum(y);
for k = 1:length(percent)
    text(x(k),y(k),sprintf('%0.0f%%',percent(k)),...
        'HorizontalAlignment','center','VerticalAlignment','bottom','FontSize',
15,'FontName','Times New Roman')
end

% ylabel({'Fire pixels'},'HorizontalAlignment','center')
xlabel('Time (Month)')
ylabel('Fire pixels')
set(gca, 'XTick', 1:12, 'Xticklabel', ...
    {'Jan','Feb','Mar','Apr','May','Jun','Jul','Aug','Sep','Oct','Nov','Dec'})
title('(c)')
ylim('padded')
yticks([0 20000 40000 60000 80000])
yticklabels({'0','20000','40000','60000','80000'})
picturewidth = 20;
hw_ratio = 0.65;
set(findall(hfig,'-property','XMinorTick'),'XMinorTick','on')
% xl = xlim;
% xAx = get(gca,'XAxis');
% xAx.MinorTickValues=linspace(xl(1),xl(2),21);
% set(findall(hfig,'-property','XMinorGrid'),'XMinorGrid','on')
% set(findall(hfig,'-property','FontSize'),'FontSize', 22)
legend('Fire pixels 2001-2021','Linear','FontSize', 15)
set(findall(hfig,'-property','Interpreter'),'Interpreter', 'latex')
set(findall(hfig,'-property','TickLabelInterpreter'),'TickLabelInterpreter',
'latex','FontSize', 22)
grid on
```